DISTORTION ANALYSIS OF ANALOG ELECTRONIC CIRCUITS USING MODULATED SIGNALS

Author | ***Adam Cooman***
Promotor | ***Gerd Vandersteen***

THESIS SUBMITTED IN FULFILMENT OF THE REQUIREMENTS FOR THE DEGREE OF DOCTOR IN ENGINEERING

VUB VRIJE UNIVERSITEIT BRUSSEL
DEPARTMENT ELEC

FACULTY OF ENGINEERING

Department of
Fundamental Electricity
and Instrumentation (ELEC)

Thesis submitted in fulfilment of the requirements for the degree of
Doctor in Engineering (Doctor in de Ingenieurswetenschappen) by

ir. Adam Cooman

Distortion Analysis of Analog Electronic Circuits Using Modulated Signals

PROMOTOR

Prof. Dr. ir. Gerd Vandersteen

JURY

Prof. Dr. ir. Heidi Ottevaere (VUB - B-PHOT) president
Prof. Dr. ir. Roger Vounckx (VUB - ETRO) vice-president
Prof. Dr. ir. Piet Wambacq (VUB - ETRO) secretary
Dr. ir. Fabien Seyfert (INRIA - APICS)
Prof. Dr. ir. Fabio Filicori (Università di Bologna)
Prof. Dr. ir Raymond Quéré (Université de Limoges - XLIM)

Academic year 2016-2017

isbn: 978-94-6197-473-0
doi: 10.13140/RG.2.2.30684.39049

University Press
Leegstraat 15, 9060 Zelzate, Belgium
http://www.universitypress.be

Vrije Universiteit Brussel, dept. ELEC
Pleinlaan 2, 1050 Brussels, Belgium
http://vubirelec.be/

This work is sponsored by the Institute for the Promotion of Innovation through Science and Technology in Flanders (IWT-Vlaanderen) and the Strategic Research Program of the VUB (SRP-19)

Lay-out advice and cover design by Lennert Gavel

Contents

1. Introduction

Many of the electronic devices we use today still contain a significant amount of analog electronic circuits. Typically, the analog circuitry is used as the interface between the digital heart of the device and the outside world. Take a smartphone for example: The phone contains analog circuits responsible for reading out sensor data, like the microphone and the pixels in the camera. There are analog electronic circuits to drive actuators in the system, like the speakers or the battery charging module. Finally and most importantly, analog circuits are responsible for the wireless communication of the phone.

In all these applications, the circuits should behave as linearly as possible to maintain a high signal quality. Non-linear behaviour in the circuit will distort the signals. The designer of the circuit needs good tools to be able to design very linear circuits and it is the goal of this thesis to develop such tools. Specifically, we focus on an analysis that allows the designer to pinpoint the main cause of non-linear distortion in his or her circuit. With this information, the designer can effectively reduce the distortion generated by the circuit.

In this introductory chapter, we will first define what we mean by linear and non-linear circuits and systems. Then we will give an overview of the commonly used techniques to quantify non-linear distortion in electronic circuits (Section 1.1) and discuss existing analysis tools which deal with the non-linear distortion in those circuits (Section 1.2). We end the chapter by discussing the need for a new analysis tool for wideband excitation signals (Section 1.3) and summarise the structure of the thesis (Section 1.4).

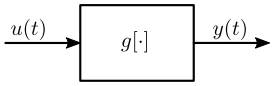

Figure 1.1.: Representation of a circuit with input $u(t)$ and output $y(t)$

For now, we will consider an analog electronic circuit as a (non-)linear system with input $u(t)$ and output $y(t)$ (Figure 1.1). The behaviour of the system is represented by the function $g[\cdot]$ which maps $u(t)$ onto $y(t)$. First, we will always assume that the systems described in this thesis are causal and time-invariant.

Time-invariant: The behaviour of the system doesn't change over time:

$$\text{when } y(t) = g[u(t)] \text{ then } g[u(t+\tau)] = y(t+\tau) \ \forall \tau \in \mathbb{R}$$

Causal: the output of the system at a time instance t_1 only depends on the input signal at times $t \leq t_0$.

When a system's output depends only on the current value of the input signal, the system will be called *static*. When the system is not static it is called *dynamic* and it is said to have memory, because it "remembers" past values of the input signal.

A system is Linear Time-Invariant (LTI) when it is time-invariant and when it satisfies the linear *superposition principle*, which requires the two following properties:

Additivity when two signals $u_1(t)$ and $u_2(t)$ are sent through the linear system $g[\cdot]$, the output of the system is the sum of the outputs when $u_1(t)$ and $u_2(t)$ are sent through the system separately:

$$g[u_1(t) + u_2(t)] = g[u_1(t)] + g[u_2(t)]$$

Homogeneity when the input signal $u(t)$ is amplified by a factor α, the output of the system is also multiplied by the same factor α:

$$g[\alpha u(t)] = \alpha g[u(t)]$$

The behaviour of an LTI system is perfectly represented by its Frequency Response Function (FRF) $G(j\omega)$ in the frequency domain. When a single-tone signal at frequency ω with an amplitude A is applied to an LTI system, the resulting output signal is a tone at the same frequency, but with a modified amplitude and phase:

$$u(t) = A\sin(\omega t) \ \text{ then } \ y(t) = |G(j\omega)| \cdot A\sin(\omega t + \angle G(j\omega))$$

where $|\cdot|$ indicates the magnitude and $\angle\cdot$ is the phase. This input-output relation is independent of the amplitude A.

No real-life system is truly linear: there will always be an amplitude for which the system will start deviating from its linear behaviour. Designers however still prefer to work with LTI models, even in the non-linear case, because the linear framework is simpler and more understandable than a full non-linear framework.

To obtain a linear model from a non-linear system, designers use a process called *linearisation*. We will use several different types of linearisation throughout this thesis but for now we will start with the most commonly used form: *small-signal linearisation*.

When the input signal has a DC offset u_{DC}, the small-signal linearisation of the system is obtained by calculating the derivative of the non-linear function(s) around that DC value. In case of a static non-linear system, the small-signal linearisation equals

$$g\left[u_{DC}+u(t)\right] \cong g\left[u_{DC}\right] + \underbrace{\left.\frac{\partial g\left[x\right]}{\partial x}\right|_{x=u_{DC}}}_{\text{linearisation}} u(t)$$

In a weakly non-linear system[1], the behaviour for small-amplitude signals will be well described by the LTI system obtained with a small-signal linearisation. Any deviation the system makes from the linearised system is usually considered as non-linear distortion[2]. The different non-linear effects, which include inter-modulation, compression, expansion and desensitisation are discussed in detail in [Maas 88, Wamb 98].

As an example of how non-linearity can affect the performance of a device, consider a modern transceiver as shown in Figure 1.2. The transceiver consists of a lot of sub-circuits, each with a distinct function in the transceiver. All the sub-circuits in the transceiver should act linearly to avoid distorting the received or transmitted signal. Linearity is therefore a key specification in most of the blocks in the transceiver.

[1] From [Wamb 98]: *A circuit behaves weakly nonlinearly if, for the applied input signal, it can be accurately described by the first three terms of its (converging) Volterra series.*

[2] We will use a different definition for non-linear distortion outside of this introduction which also works for strongly non-linear systems. Our definition for distortion is given in chapter 2

We will consider the following blocks of the transceiver in this thesis:

Low Noise Amplifiers (LNAs) The LNA is the first amplifier in the receiver. Its job is to amplify the small signals picked up by the antenna without adding too much noise. The small signals in the band of interest will not cause a lot of non-linear distortion, but possibly strong signals in neighbouring frequency bands might influence the received signals through the non-linear effects in the LNA. Usually, the bandpass filter in front of the LNA is added to remove the out-of-band interferers. In systems where compactness is critical, or in wideband receivers, this bandpass filter might not be present. This has large implications on the required linearity of the LNA.

Power Amplifiers (PAs) are the amplifiers responsible to generate the transmitted signal. Linearity of the PA is essential because non-linear effects will create spectral regrowth which may cause interference for signals in neighbouring frequency bands. Also, the non-linear effects will distort the transmitted signals, which can introduce errors in the communication link. Besides the linearity, the power efficiency of the PA is important in modern systems. The need for a higher power efficiency is pushing the designs into strongly non-linear operating modes. Guaranteeing a high linearity while simultaneously maintaining high power efficiency makes the PA the most challenging block to design in a transmitter [Crip 06, McCu 15].

Filters are used throughout the transceiver to make the circuit frequency selective. Both bandpass and lowpass filters are used in our example. When the filters in a system are built using passive components, non-linearity is not an issue. However, passive filters are costly and often impossible to integrate on a chip. To save cost and space, active filters are preferred over passive filters in many transceivers [Pact 07]. The anti-alias filters, for example, are usually integrated active filters. The drawback of these filters is that they consume power and that they introduce non-linear distortion.

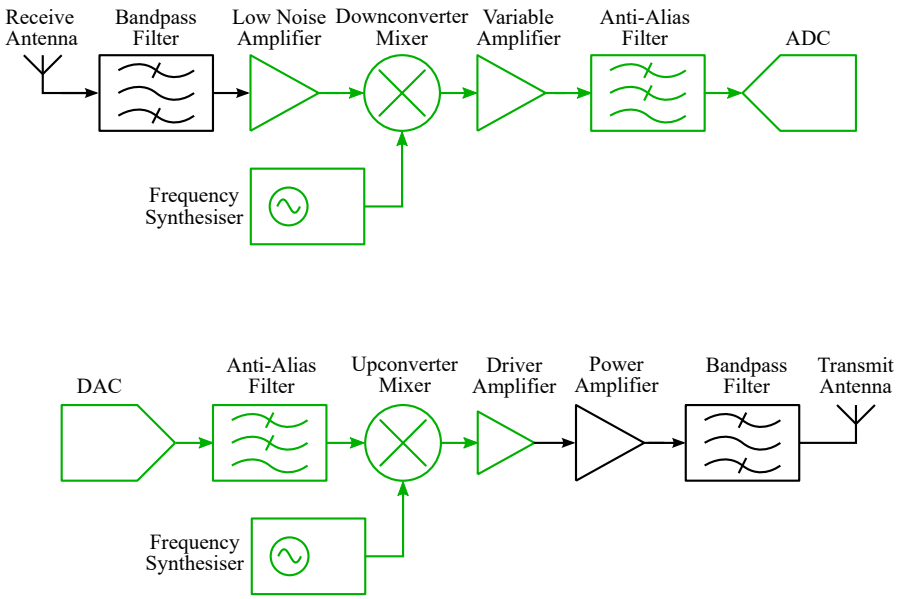

Figure 1.2.: Example of a modern transceiver. The receiver is shown on the top, the transmitter is shown on the bottom. The blocks that can easily be integrated on-chip these days are indicated in green.

Non-linear distortion will also be detrimental to the performance of the other blocks in the transceiver, but we will not consider the following sub-circuits in this thesis.

Analog to Digital Convertors (ADCs) and DACs are the interface between the digital and analog worlds of the transceiver. The techniques introduced in this thesis can be extended to mixed-signal circuits as is shown in [Vand 09, Bos 08].

Mixers are the circuit blocks that are responsible for the up- and down-conversion to and from baseband in the transceiver [Maas 86]. A mixer can be considered as a circuit element which multiplies the incoming signal with the tone generated by the frequency synthesiser. Multiplication is an inherently non-linear operation, so it may be weird to discuss the linearity of a mixer. However, when the transfer from RF to baseband or vice versa is considered, the linearity of the mixer can be defined [Maas 86]. The techniques introduced in this thesis can be generalised to work for mixers [Vand 07, Vand 10, Thor 11b], but this is considered to be outside of the scope of this thesis.

Frequency synthesisers are not considered in this thesis, but the linearity of the components with which the synthesiser is built is also key to its correct operation [Cran 98, Peum 16].

It is clear that linearity is an important design specification of each of the blocks in the transceiver. More and more of these blocks are being integrated on-chip to obtain cheap and compact transceivers. All blocks that are currently integrated in most transceivers are indicated in green in Figure 1.2.

The continued push towards integration has placed more and more emphasis on the non-linear distortion generated by the circuits over the years. The decrease of supply voltages in aggressively scaled technologies even results in non-linear distortion to become one of the main limiting factors for the dynamic range of the different blocks in modern electronic circuits.

Building a prototype to test the circuit performance is expensive and time-consuming. This is why most of the design and verification of the performance of a circuit is done first in a circuit simulator. The designers of the circuits need good simulation tools to be able to predict, analyse and decrease the amount of non-linear distortion generated by a circuit. It is the goal of this thesis to create such a simulation tool.

1.1. Classic methods to quantify distortion

A first test to determine the linearity of a system is to apply a single-tone test signal to the input of the system

$$u(t) = A\sin(\omega t)$$

The frequency ω and amplitude A are chosen by the designer such that the test signal is in the same frequency and amplitude range as the signals which will excite the circuit in its application. When this signal is applied to the system, the output signal will contain tones at the original frequency ω and harmonics at integer multiples of that base frequency[3] (Figure 1.3). We will use $Y(k\omega)$ to indicate the phasor of the output signal at a frequency $k\omega$.

To indicate the amount of non-linear distortion added to the output signal, the Total Harmonic Distortion (THD) is commonly used. The THD is the ratio of the sum of the amplitudes of all in the output signal harmonics to the amplitude of the fundamental of the output signal:

$$THD = \sqrt{\frac{\sum_{k=2}^{\infty} |Y(k\omega)|}{|Y(\omega)|}}$$

Usually, the THD is expressed as a percentage. The THD varies with both the amplitude and frequency of the input signal.

In a second test to quantify the non-linear distortion, the amplitude of the input signal is swept while its frequency is kept constant. The amplitude of the tones in the output signal is then visualised in a log-log plot shown on the left in Figure 1.5. In a weakly non-linear system, the fundamental has a linear slope of $1:1$ for small amplitudes. The second and third harmonic have $2:1$ and $3:1$ slopes on the log-log scale respectively. From the swept amplitude data, the 1dB compression point ($P_{-1\text{dB}}$), and harmonic intercept points (IP_{2h} and IP_{3h}) are obtained as shown in the figure.

The harmonics of the input signal can be filtered out by the system, so using the harmonics to determine non-linear behaviour can result in optimistic results. This is the case in most RF circuits, where the harmonics of a single tone placed in the circuit band are filtered. To quantify the in-band non-linear distortion, a two-tone signal is applied

$$u(t) = \frac{A}{2}\sin(2\pi\omega_1 t) + \frac{A}{2}\sin(2\pi\omega_2 t)$$

[3] We assume here that the system is Period-In Same Period-Out (PISPO), which will be defined rigorously in chapter 2

where the two frequencies ω_1 and ω_2 are usually placed close together. When a two-tone is applied to a non-linear system, both harmonics and intermodulation products appear at the output of the circuit (Figure 1.4). The third-order non-linearity in the circuit will create tones at $2\omega_1 - \omega_2$ and $2\omega_2 - \omega_1$, which are frequencies right next to the original set of tones. They will therefore not be filtered out and can be used to get a reliable estimate of the amount of non-linear distortion generated by the circuit (IM_3 as shown on the right in Figure 1.5).

In high-frequency PAs, it is common to plot the gain of the amplifier $|Y(j\omega)/U(j\omega)|$ as a function of its input signal in an AM-AM plot. This will give an indication of the amount of amplitude distortion the PA will add to a modulated signal. The phase distortion introduced by a PA is visualised in an AM-PM plot [Crip 06].

It is important to notice that all measures for non-linear distortion presented above depend on the frequency at which the experiment is carried out. A second important detail here is that these measures for non-linear distortion will fail to predict the distortion when a wideband signal is applied to the system. We will discuss this last point in a lot more detail in Section 1.3.

1.2. Distortion Contribution Analysis

All the measures for non-linear distortion discussed above only give an indication of the total distortion without providing in-depth insight into its origin. When we take a look inside one of the blocks of the transceiver, we will find that each of the blocks consists of many different sub-circuits.

Figure 1.6 shows an active filter as an example. The filter contains four Operational Transconductance Amplifiers (OTAs), placed in a feedback configuration. Each of these transconductors can still be sub-divided into two amplifying stages and a common-mode feedback amplifier as shown on the lower part of the figure. Each of the amplifying stages in the transconductor is made up of several transistors. It is clear from this example that this circuit consists of a hierarchy of sub-circuits.

Each of the sub-circuits will introduce some non-linear distortion. Some of the sub-circuits will contribute a lot to the total distortion of the circuit while others might contribute little. To reduce the total distortion generated by the circuit, the designer should get an indication of which part of the circuit is causing the problem. This is where a Distortion Contribution Analysis (DCA) can be used.

The aim of the Distortion Contribution Analysis (DCA) is to split the total distortion into contributions of each sub-circuit [Nara 67]. Comparing the different contributions allows the designer to pinpoint the dominant sources of non-linear distortion and hereby effectively reduce the total distortion [Aiki 11]. Note

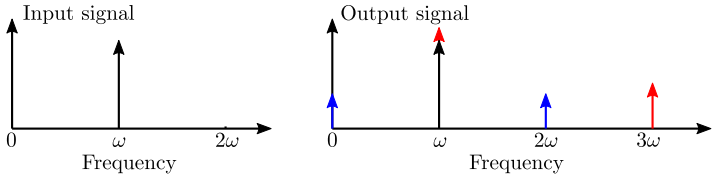

Figure 1.3.: When a single-tone excitation signal is applied to a non-linear circuit, harmonics appear at the output

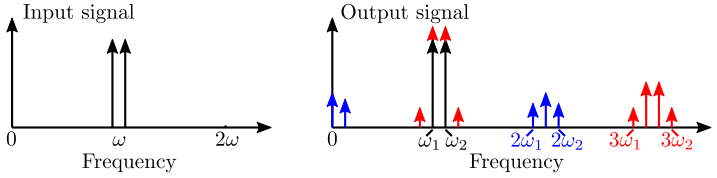

Figure 1.4.: With a two-tone excitation, intermodulation creates contributions close to the original tones

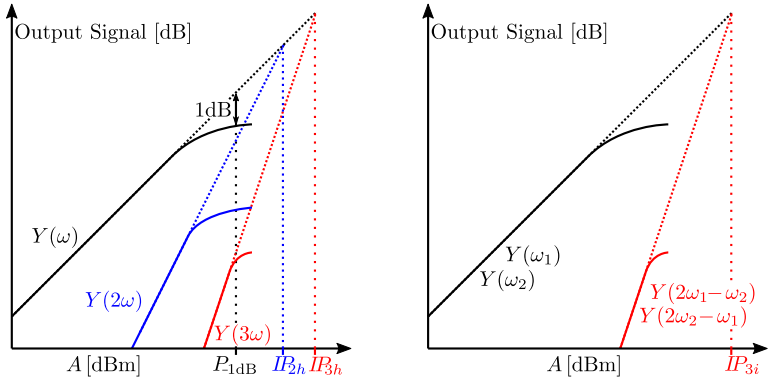

Figure 1.5.: When plotting the different tones of the output signal versus the amplitude of the input signal, both on a logarithmic scale, the plot shown above is obtained. On the left, we show this plot for a single-tone excitation applied to a weakly non-linear circuit, on the right a two-tone experiment is shown. From these plots, measures for the linearity, like the intercept points and compression points can be obtained.

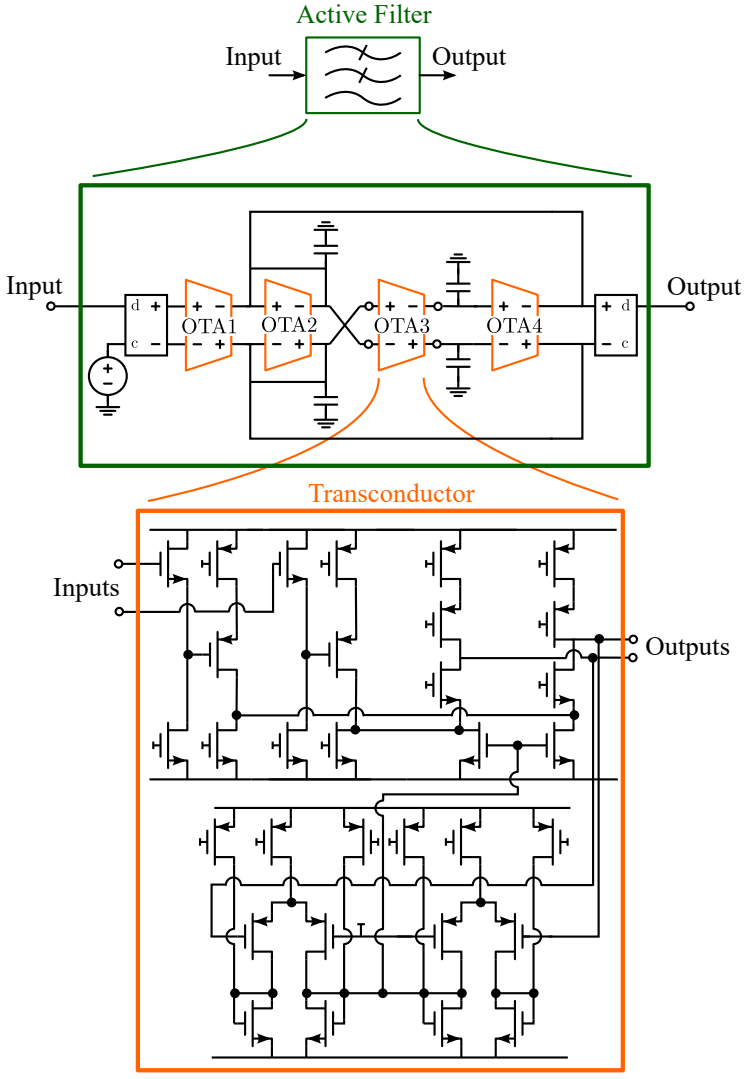

Figure 1.6.: An active filter is an intricate interconnection of a number of sub-circuits. Each of the sub-circuits will introduce some non-linear distortion and it is difficult to locate the main source of distortion.

that, taken from a birds-eye view, the DCA closely resembles a noise analysis [Engb 95, Dobr 89]. The difference is that it is now applied to non-linear distortion sources.

The classical way to perform a distortion analysis consists of calculating the circuit response using a Volterra series [Wamb 98]. Over the years, many different distortion analyses have been developed to calculate the distortion contributions to single and two-tone excitation signals. The main difference in how the distortion contributions are calculated in these different methods lies in the way they model the non-linear sub-blocks during this Volterra series development.

Some of the methods use heavily simplified behavioural models to predict the distortion contributions for specific classes of circuits. Well studied classes of circuits are feedback amplifiers [Cann 06a, Cann 06b, Palu 03] and operational amplifiers [Cann 06a, Hern 03, Hern 05]. These distortion analysis studies provide some general insight and design rules for low distortion, but they are too restricted to be used in general. Because they only analyse one specific circuit they will not be able to predict distortion contributions in more complex circuits like a full transceiver.

Other DCA methods rely on known transistor models and either simplify these transistor models [Groe 94] or use symbolic analysis to calculate the distortion contributions [Wamb 98, Wamb 99]. More recently, these methods have been improved such that the symbolic calculation is no longer needed [Dobr 03] and that the methods can work with any transistor model [Li 03]. These general methods are perfectly suited for the analysis of circuits that contain a small number of transistors. However, the amount of distortion contributions rises quickly in more complex circuits.

All the DCA techniques described assume that the underlying circuit is weakly non-linear, which makes them unsuited for the distortion analysis of PAs. The DCA described in [Aiki 05, Aiki 09, Aiki 12] has extended the methods such that they can deal with strongly non-linear effects as well.

1.3. Distortion under modulated signals

We have shown that most of the testing for non-linear distortion is performed using very simple excitation signals like two-tones. However, in their application, the circuits will not be excited by such simple signals. A transceiver, for example, processes signals which carry information. They occupy a certain bandwidth around a carrier frequency ω_{center}:

$$u(t) = A(t)\sin\left(\omega_{\text{center}}t + \phi(t)\right)$$

The information in the signal is contained in the time-variation of the amplitude and phase of the signal, both $A(t)$ and $\phi(t)$ are random signals because the content of the data which is being sent is not known in advance.

Due to the modulation with random signals, the exact excitation signal $u(t)$ cannot be known. However, the statistical information, like the Power Spectral Density (PSD) and Probability Density Function (PDF) are known and specified in the communication standard. A wireless Local Area Network (LAN) signal, for example, uses Orthogonal Frequency Domain Multiplexing (OFDM) modulated signals which occupy a bandwidth of 20MHz around the carrier frequency of 2.4GHz. Due to the properties of OFDM modulation, the PDF of the signal resembles a Gaussian.

The situation is similar in low-frequency electronic circuits: instead of single sines and two-tones, the circuits usually have to process noise-like signals in their real-world applications. We cannot predict the exact signals that will pass through the circuit, but we get a good idea of their PSD and PDF. We will also refer these noise-like low-frequency signals as modulated signals throughout the thesis, even though they are not represented by a modulated carrier frequency.

When the circuit is static, the results of a single-tone or two-tone test can be used to predict the distortion under modulated excitation signals [Crip 06]. In dynamic circuits and systems, the amount of non-linear distortion added to a modulated signal can differ strongly from the distortion added to a two-tone test signal. In [De L 07], intermodulation distortion of an amplifier was characterised with both a two-tone excitation signal and with a modulated signal. The results obtained for the intermodulation differ strongly, as shown in Figure 1.7. The same author has also demonstrated that the results obtained with load-pull measurements also depend on strongly on the input signal [De L 06]. The same problem is discussed in [Crip 06] and [Rola 13].

To get a correct representation of the non-linear distortion generated by a circuit, it should be excited by the modulated signals it encounters in its application, not by artificial test signals like two-tones. In this thesis, we explore how to deal with

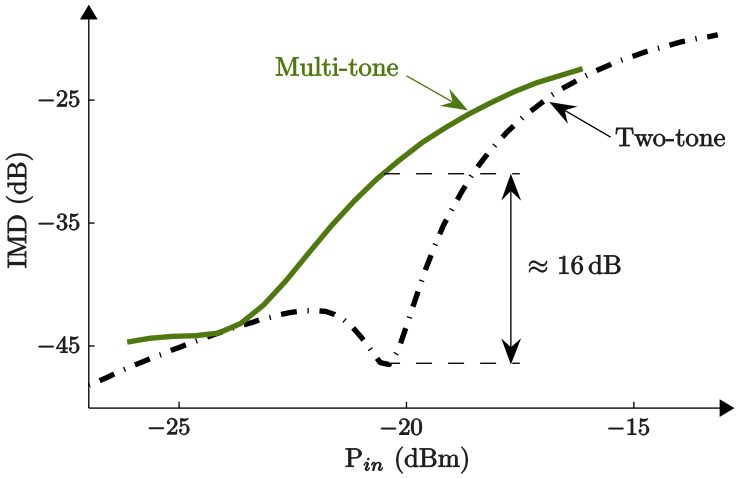

Figure 1.7.: When modulated signals are used, the measured intermodulation distortion can differ strongly from the intermodulation distortion observed with a two-tone excitation signal (Figure taken from [De L 07])

the complexity which is added to the distortion analysis by moving away from a simple excitation signal to a modulated signal.

1.4. Goals and outline

We have shown that modulated excitation signals have to be used to correctly determine the amount of non-linear distortion which is generated by a circuit. The goal of this thesis is to develop a DCA that can calculate the distortion contributions in electronic circuits under modulated excitation signals.

To be of any use in practice, we impose the following constraints on the DCA we develop:

No special simulations or custom models The DCA needs to work in a commercial simulator, which implies that it can only use the basic simulation tools and that it has no access to the internals of the simulator nor to the transistor models.

Hierarchy We have shown that electronic circuits are hierarchical. The user should be able to use DCA hierarchically: from the highest level of abstraction all the way down to the transistor level.

Generally applicable The DCA needs to be general. It should be able to handle both weakly and strongly dynamic non-linear circuits.

Minimum user interaction A minimum of user interaction should be required. Ideally, the DCA should work fully automatically without the need for the user to set a lot of parameters.

To be able to satisfy these goals, we needed an approach to distortion analysis which is very different from the techniques described above. The cornerstone of the DCA introduced in this thesis is the Best Linear Approximation (BLA). The BLA-based DCA differs from the classical approach in the following ways:

Fix the class of excitation signals The BLA only predicts the behaviour of the circuit for the class of input signals the circuit will encounter in its application and it will only be valid for those signals. When another type of signal is applied to the circuit, the BLA changes and another analysis will need to be performed.

Approximate modelling The BLA models the average behaviour of the circuit when it is excited by modulated excitation signals from the fixed class. Because the modulated signals are inherently random, we cannot predict the input and output signals of the circuits exactly.

Black box modelling The BLA is a black box model: it only takes input and output signals into account. No knowledge of the internals of the subcircuit blocks is required. This makes the BLA ideally suited to be applied hierarchically.

As its name suggests, the BLA is an approximate linear model. It will not be able to predict the input output behaviour of the circuit perfectly, but it will be "best" in least squares sense. Everything that cannot be explained by the BLA is the non-linear distortion introduced by the circuit. In the BLA-framework, the non-linear distortion acts as a noise disturbance. The BLA-based DCA then becomes a noise analysis.

In the remainder of this thesis, we detail how to use the BLA to analyse the distortion in an electronic circuit. The BLA is introduced in chapters 2 and 3. In chapter 2, we focus on the BLA of Single-Input Single-Output (SISO) systems. Chapter 3 extends the techniques to Multiple-Input Multiple-Output (MIMO) systems to be of use in the analysis of electronic circuits, which are inherently MIMO.

Once the tools are available to determine the BLA of a circuit, we can use the BLA to find the dominant source of non-linear distortion. Chapter 4 details how a DCA can be performed with the BLA, both on the system level and on the circuit level.

The fifth chapter of the thesis is different from the previous chapters. It deals with stability analysis instead of distortion analysis.

2. The Best Linear Approximation

The approach we will follow throughout this thesis is one of simplification and approximation: Instead of constructing a non-linear model that can predict the output signal exactly for any input signal, we construct an approximate model that works only for the of input signals for which the circuit was built.

This signal dependent approximate model is the Best Linear Approximation (BLA). As its name implies, the BLA is a Linear Time-Invariant (LTI) model, so, with some care, most of the concepts from linear circuit theory can be extended to non-linear circuits when the BLA is used. In chapter 4, the BLA will be used extensively in distortion analysis of electronic circuits. In this chapter, the fundamental concepts behind the BLA are introduced.

This chapter summarises the formal definitions and properties of the BLA. In Section 2.1, the BLA is introduced. Then, the multisine is proposed as the excitation signal which makes estimation of the BLA of a non-linear system the easiest (Section 2.2). Finally Section 2.3 details the procedure to estimate the BLA in a feedback configuration.

The work presented in this chapter is not new and has mainly been developed at the ELEC department of the VUB over many years. More details about the BLA, extra references, and its theoretical background can be found in [Pint 12].

2.1. The Best Linear Approximation

The non-linear systems we will consider in this thesis are assumed to be causal and time-invariant. Additionally, during chapters 2-4 we assume that the non-linear systems are in the Wiener class of systems as defined in [Sche 80].

Definition A non-linear system is in the Wiener class of systems when its input-output behaviour can be approximated in least-squares sense by a Volterra series.

When an input signal with a certain period P is applied to a non-linear system in the Wiener class, the output signal has the same periodicity as the input signal. This period-maintaining principle is called the Period-In Same Period-Out (PISPO) principle [Rola 13, Pint 12]. The Wiener class of systems includes systems with strongly non-linear behaviour like switching, clipping or dead-zones. Systems that generate sub-harmonics or chaos are not in the Wiener class because they don't satisfy the PISPO principle.

Consider that the input signal of the non-linear system is a random signal generated by a stationary process. The input signal is indicated by $u(t)$ and the output signal by $y(t)$. Both signals are defined around their average operating point, such that their mean value equals zero:

$$\mathbb{E}\{u(t)\} = 0 \qquad \mathbb{E}\{y(t)\} = 0$$

where $\mathbb{E}\{\cdot\}$ indicates the expected value.

The Best Linear Approximation (BLA) for a non-linear system is the LTI model g^{BLA} which minimises the mean-square error between the input $u(t)$ and the output $y(t)$. When the BLA is a stable LTI system, we can express this in the time domain:

$$g^{\text{BLA}} = \underset{g[\cdot]\in\mathscr{G}}{\operatorname{argmin}}\ \mathbb{E}\left\{\left(y(t) - g[u(t)]\right)^2\right\} \tag{2.1}$$

where $\mathscr{G}$ indicates the class of all stable LTI models. In general, the BLA should not be a stable linear system, which is why it is best defined in the frequency domain as [Pint 12]

$$G^{\text{BLA}}_{U\to Y}(j\omega) = \frac{S_{yu}(j\omega)}{S_{uu}(j\omega)} \tag{2.2}$$

where $G^{\text{BLA}}_{U\to Y}(j\omega)$ is the Frequency Response Function (FRF) of an LTI system g^{BLA}. $S_{yu}(j\omega)$ is the cross-power spectrum between the input and output signals and

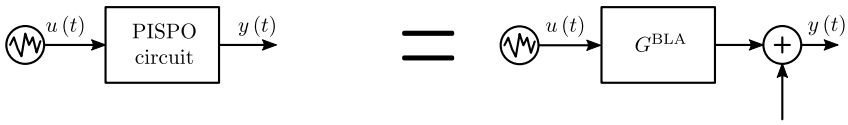

Figure 2.1.: A non-linear circuit excited by a random signal can be approximated by its BLA. The distortion term $d(t)$ then looks like noise.

$S_{uu}(j\omega)$ is the auto-power spectrum of the input signal. They are defined as:

$$S_{yu}(j\omega) = \mathcal{F}\left\{R_{yu}(\tau)\right\}(j\omega) \qquad R_{yu}(\tau) = \mathbb{E}\left\{y(t)\,u(t-\tau)\right\} = \int_{-\infty}^{+\infty} y(t)\,u(t-\tau)\,dt$$

$$S_{uu}(j\omega) = \mathcal{F}\left\{R_{uu}(\tau)\right\}(j\omega) \qquad R_{uu}(\tau) = \mathbb{E}\left\{u(t)\,u(t-\tau)\right\} = \int_{-\infty}^{+\infty} u(t)\,u(t-\tau)\,dt$$

where $\mathcal{F}\{\cdot\}$ indicates the Fourier transform.

The BLA of a circuit will depend on the input signal. It has been shown that for input signals with the same Power Spectral Density (PSD) and Probability Density Function (PDF), the BLA is the same [Pint 12].

The residual of the approximation by the BLA is the non-linear distortion generated by the circuit. Throughout this thesis, the distortion will be indicated with the letter d. When the BLA is a stable system, the non-linear distortion introduced by the non-linear system can be defined as:

$$d(t) = y(t) - g^{\mathrm{BLA}}[u(t)]$$

The distortion has the following properties [Pint 12]:

- $d(t)$ has zero mean: $\mathbb{E}\{d(t)\} = 0$
- $d(t)$ is uncorrelated with the input signal $u(t)$: $\mathbb{E}\{d(t)\,u(t-\tau)\} = 0$.
- $d(t)$ depends on the input power spectrum.
- The autopower spectrum of the distortion $S_{dd}(j\omega)$ is a continuous function of the frequency.

These properties indicate that $d(t)$ is a noise-like signal. We will use this key observation throughout this thesis.

Example 2.1: The BLA of a static non-linear system

As an example system to show some of the properties of the BLA, we consider a simple static non-linear system with the following input-output relation

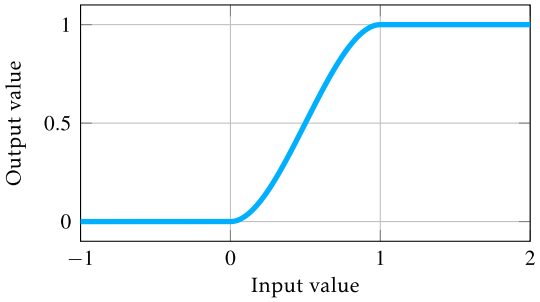

The non-linearity is chosen such that it resembles the relation between the gate voltage and drain current of a transistor, as described in [Crip 06]. It is a continuous piecewise function defined as

$$y = g(u) \text{ where } \begin{cases} u < 0 & y = 0 \\ u \in [0,1] & y = 3u^2 - 2u^3 \\ u > 1 & y = 1 \end{cases}$$

The input signal $u(t)$ is a filtered Gaussian i.i.d noise signal around a DC offset of 0.05. Due to the small DC offset, the system behaves as an amplifier biased on the edge of class-B. The root mean square (rms) value of the signal is 0.1 and most of the power of the noise signal is lies in the frequency band between 0Hz and 1Hz. Note that the frequency of the signals doesn't matter for a static system like the one we are studying here. The input signal is shown below:

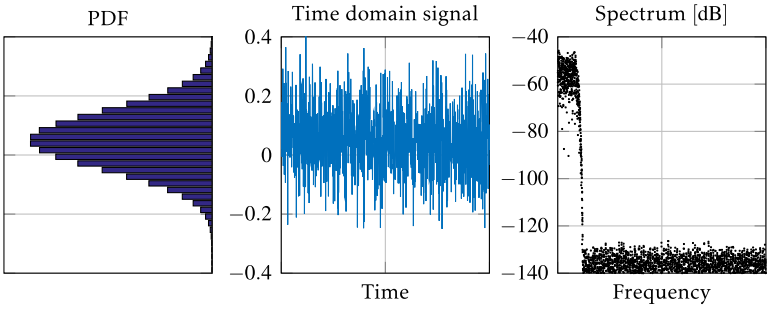

The output signal $y(t)$ of the static non-linear system is easily obtained by applying the function above to each input sample. The system acts strongly non-linear and adds a lot of distortion to the signal. The obtained output signal is shown below:

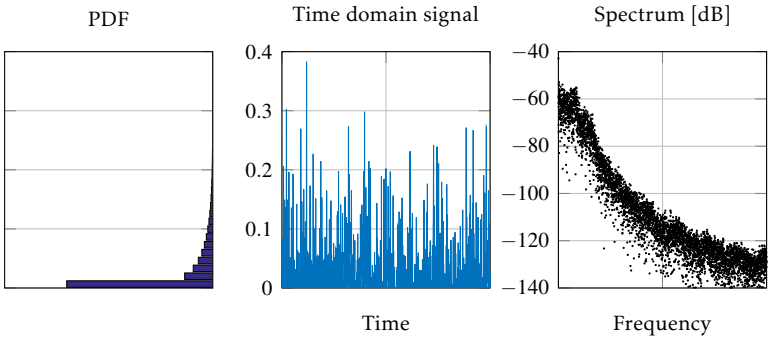

The BLA of this system is calculated using the techniques detailed in [Pint 12]. Throughout this thesis, we will use a different excitation signal and estimation technique to obtain the BLA, they are both detailed later in this chapter. We will not go in detail here on how the BLA is obtained with these noise excitations, the interested reader is referred to [Pint 12]. The BLA and its uncertainty are shown below:

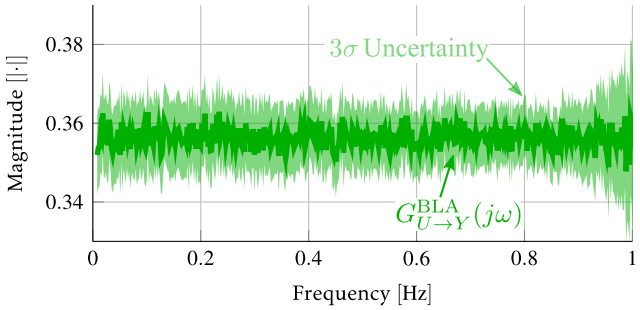

It is clear that the BLA is static for this circuit. This is due to the Gaussian distribution of the input signal. If the input signal were to have another PDF, the BLA obtained for this static circuit would not be static [Enqv 05]. The increase of the uncertainty at the end of the frequency band is due to the lower level of the input signal there.
As a final test on this simple example, we show how the BLA changes as a function of the rms of the input signal. The above procedure is repeated

for different rms values of the input signal. For each rms value, magnitude of the BLA at 0.5Hz and its uncertainty are plotted.

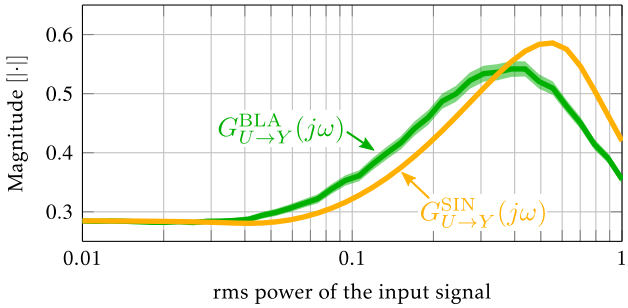

It is clear that the BLA varies strongly as a function of the rms of the input signal. As a form of comparison, we applied a single tone signal with the same rms and DC offset as the noise to the test system:

$$u(t) = \mathrm{rms} \cdot \sqrt{2}\sin(\omega t) + 0.05$$

We then calculated resulting output signal $y(t)$ and the large-signal gain of the system

$$G^{\mathrm{SIN}}_{U\to Y} = \frac{Y(j\omega)}{U(j\omega)}$$

and plotted this as a function of the amplitude. The resulting curve is shown in orange on the same figure as the BLA. It is clear that the large-signal linearisation depends on the class of input signals.

2.2. Multisine excitation signals

Using random, non-deterministic signals as input $u(t)$ for the non-linear system is not always convenient from a practical point of view. In measurement set-ups and simulations, it is preferred to work with periodic excitation signals [Pint 12]. The main reason for this lies in the fact that we can determine the steady-state response of the circuit, which makes it easier to determine the FRF and BLA in the frequency domain. Additionally, when random signals are transformed to the frequency domain, spectral leakage is unavoidable, which complicates the analysis.

For two random excitation signals with the same PSD and PDF, the BLA of a circuit is equal [Pint 12]. So, to determine the BLA in practice, we will construct periodic signals with the same PSD and PDF as the excitation signals the circuit encounters in its application and use those periodic signals to determine the BLA.

The periodic excitation signal we will use throughout this thesis is a sum of a very large number[1] of harmonically related sines called a *multisine*:

$$u(t) = \sum_{k=1}^{k_{\max}} A_k \sin\left(2\pi k f_{\text{res}} t + \phi_k\right) \tag{2.3}$$

f_{res} is the frequency resolution of the multisine. A_k is the amplitude of the k^{th} tone in the multisine and ϕ_k is the phase of that tone. The phases ϕ_k are used to control the PDF of the multisine as will be discussed later. The amplitudes A_k are used to set the PSD of the multisine. A tone in the multisine with zero amplitude will be called a non-excited frequency line, the excited frequency lines have a non-zero A_k.

In a *lowpass multisine*, the excited frequency lines start from $k = 1$. Some of the frequency lines can be left unexcited to obtain information about the in-band distortion, we will discuss this in more detail later. In a *bandpass multisine*, all frequency lines up to a large number $k_{\min}$ are non-excited. Bandpass multisines will be used to represent modulated signals around a carrier frequency.

The multisine will strongly resemble a filtered noise signal in the time domain when the total amount of tones in the multisine is very large ($k_{\max} \to \infty$) and the phases of the different tones are chosen randomly. The PDF will resemble a Gaussian when the phase of the tones in the multisine is selected independently from a uniform distribution $[0, 2\pi[$. With the algorithm described in [Scho 98], the phases ϕ_k can be set to give the multisine an arbitrary PDF.

[1] Theoretically, we need an infinite amount of tones, in practice, we will use at least 50 tones to get good results.

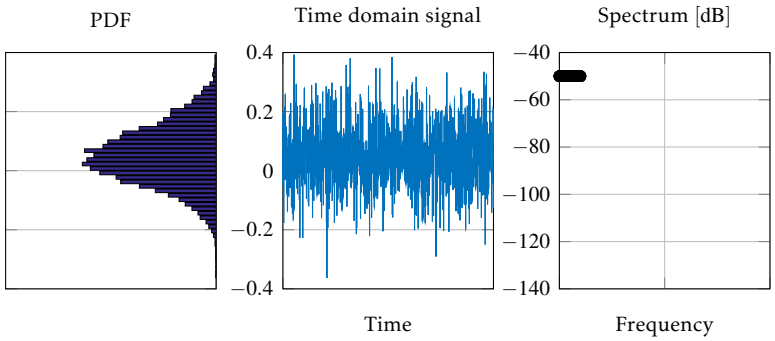

Figure 2.2.: A random-phase multisine with a large number of tones resembles a filtered Gaussian noise signal in the time domain, but its PSD can be precisely controlled in the frequency domain.

With a single set of random phases, a multisine signal is not a random signal, but deterministic and periodic. The randomness is introduced by considering many different phase realisations: In each of the phase realisations, only the phases ϕ_k are changed. The base frequency f_{res}, number of tones $k_{\max}$ and amplitude of the tones A_k are left unchanged.

The BLA is then equal to the average frequency response of the system over the phase realisations of the multisine. A robust way to determine the BLA is by applying M phase realisations of the multisine one-by-one to the system. The steady-state response of the system to each of the phase realisations is then determined and saved. In Appendix A, we explain in detail how the steady-state response of a circuit excited by a multisine can be obtained in commercial circuit simulators.

The input signal of the system, measured in steady-state when the circuit is excited by the m^{th} phase realisation of the multisine will be indicated with $u^{\{m\}}(t)$. The output signal $y^{\{m\}}(t)$ is defined in the same way.

For PISPO systems, both the input signal and output signal can be written as a Fourier series with base frequency f_{res}:

$$u^{\{m\}}(t) = \sum_{k=0}^{\infty} U^{\{m\}}(k)\, e^{j2\pi k f_{\text{res}} t} + \overline{U^{\{m\}}(k)} e^{-j2\pi k f_{\text{res}} t}$$

$$y^{\{m\}}(t) = \sum_{k=0}^{\infty} Y^{\{m\}}(k)\, e^{j2\pi k f_{\text{res}} t} + \overline{Y^{\{m\}}(k)} e^{-j2\pi k f_{\text{res}} t}$$

The BLA of the system can now be determined as the average frequency response of the system:

$$G_{U\to Y}^{\mathrm{BLA}}(j\omega_k) = \mathbb{E}\left\{\frac{Y^{\{m\}}(k)}{U^{\{m\}}(k)}\right\} \cong \frac{1}{M}\sum_{m=1}^{M}\frac{Y^{\{m\}}(k)}{U^{\{m\}}(k)}$$

Note that the BLA can only be determined on excited frequency lines of the multisine, otherwise, a division by zero is performed. The approximation will be very good when the amount of phase realisations M is very large. In practice, we look to the variance on the BLA-estimate to determine whether more phase realisations are needed to obtain a more accurate estimate. The variance on the BLA-estimate is given by

$$\sigma^2_{G_{U\to Y}^{\mathrm{BLA}}}(j\omega_k) = \frac{1}{M(M-1)}\sum_{m=1}^{M}\left|\frac{Y^{\{m\}}(k)}{U^{\{m\}}(k)} - G_{U\to Y}^{\mathrm{BLA}}(j\omega_k)\right|^2$$

The distortion introduced by the circuit as the response to a single phase realisation will be denoted $D^{\{m\}}(k)$ and is defined as:

$$D^{\{m\}}(k) = Y^{\{m\}}(k) - G_{U\to Y}^{\mathrm{BLA}}(j\omega_k)\,U^{\{m\}}(k) \tag{2.4}$$

When the average behaviour of the distortion signal over many different phase realisations is considered, its noise-like properties appear

- The average distortion at every frequency line is zero mean $\mathbb{E}\{D(k)\} = 0$
- The distortion is uncorrelated to the input signal: $\mathbb{E}\left\{D(k)\overline{U(k)}\right\} = 0$
- The average power of the distortion signal $\mathbb{E}\left\{D(k)\overline{D(k)}\right\}$ is a continuous function of frequency.

In the properties listed above, the expected value is always taken over the different phase realisations of the multisine. In practice, we can easily determine the power of the distortion introduced by the system as:

$$\mathbb{E}\left\{D(k)\overline{D(k)}\right\} = \frac{1}{M-1}\sum_{m=1}^{M}\left|\frac{Y^{\{m\}}(k)}{U^{\{m\}}(k)} - G_{U\to Y}^{\mathrm{BLA}}(j\omega_k)\right|^2$$

Example 2.2: Estimating the BLA with a multisine

The same static non-linear system as before is now excited by a multisine to determine its BLA. To obtain the same results as before, the multisine needs to resemble the filtered Gaussian noise signal that was used earlier. A lowpass multisine with a flat PSD between 0Hz and 1Hz is used. The base frequency of the multisine is set to $f_{\text{res}} = 2\text{mHz}$, which results in $k_{\max} = 500$ excited frequency lines in the band of the multisine. The rms value of the multisine is set to 0.1. The resulting multisine was already shown before in Figure 2.2. The output signal of the system obtained with this multisine excitation is shown below:

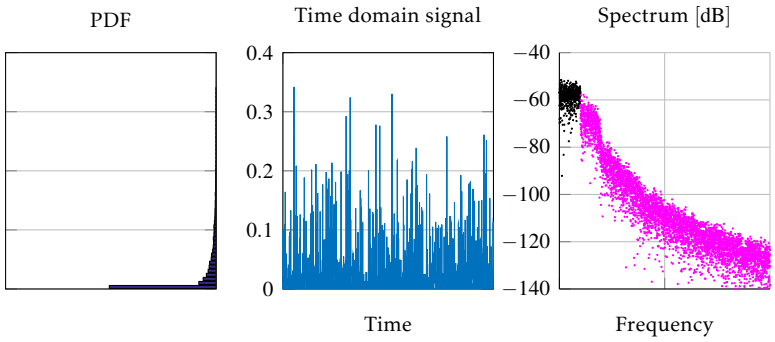

The excited frequency lines of the multisine are shown in black on the plot above. The non-excited frequency lines are shown in magenta. The non-excited frequency lines contain only non-linear distortion and it is clear that the distortion there closely resembles noise.
$M = 2000$ phase realisations of the multisine were used in the averaging to obtain the BLA and its uncertainty:

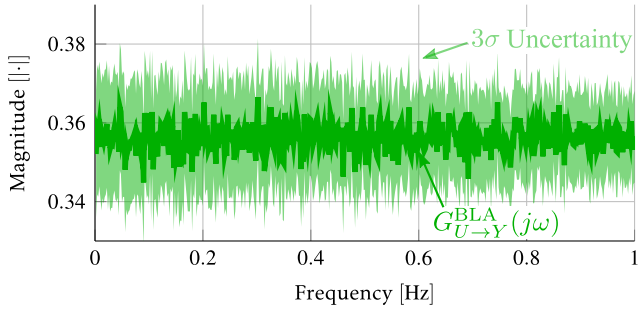

The BLA obtained with a multisine is clearly equal to the BLA obtained before with the real Gaussian noise signal, which supports the use of multisines to determine the BLA of a non-linear system.

Special multisines for detection of non-linearities

The greatest benefit of working with periodic signals it that they can be modified easily to gain more insight into the non-linear distortion generated by the non-linear system. By carefully choosing the non-excited lines in the excitation signal, the distortion generated by a system can be determined just by inspection of the steady-state spectra without needing to determine the BLA of the circuit [De L 07].

An even non-linearity in a system mixes the input signal an even amount of times, so an even amount of tones from the input signal are combined to obtain the even contributions. When the multisine excites only odd frequency bins, all even-order distortion will only appear on even frequency bins, separating the even and odd non-linear distortion contributions. This multisine, which excites only odd frequency bins ($A_k = 0$ for all even k) will be called an *odd multisine*. Note that DC ($k=0$) should not be excited since $k = 0$ is even.

The odd frequency bins in response of a system to an odd multisine contains the excited frequency lines and the odd-order non-linear distortion. To determine the statistics of the odd-order distortion at an excited line, we can calculate the BLA using multiple phase realisations of the multisine and subtract the contribution due to the BLA as in (2.4). Alternatively, some of the odd frequencies can be left unexcited as well, to obtain detection lines in the multisine. These odd detection lines only contain contributions due to odd-order non-linear distortion. To avoid disturbing the noise-like properties of the non-linear distortion, the detection lines are chosen randomly out of groups of 4 excited lines in the odd multisine [Vanh 00]. The resulting odd multisine with randomly spaced detection lines will be called *random-odd multisine*.

Another advantage of using an odd multisine is that, because even-order distortion only falls on even frequency lines, there is less distortion on the estimate of the BLA, which can reduce the amount of phase realisations needed to obtain a low uncertainty.

Note that these special multisines are only useful in lowpass multisines for base-band circuits. In narrow-band bandpass multisines, the even and odd non-linear contributions are automatically split. Detection lines can still be used there to allow quick inspection of the in-band odd-order distortion.

Example 2.3: Using random-odd multisines

As an illustration, we will apply a random-odd multisine to the static non-linear system we have used as an example throughout this chapter. The same multisine with $f_{\text{res}} = 2\text{mHz}$ as before was used, but now the amplitude of every even tone was set to zero and some of the odd tones were also left out. The amplitude of the remaining tones was rescaled such that the rms of the multisine remained 0.1. The output spectrum obtained with this random-odd multisine excitation signal is shown below:

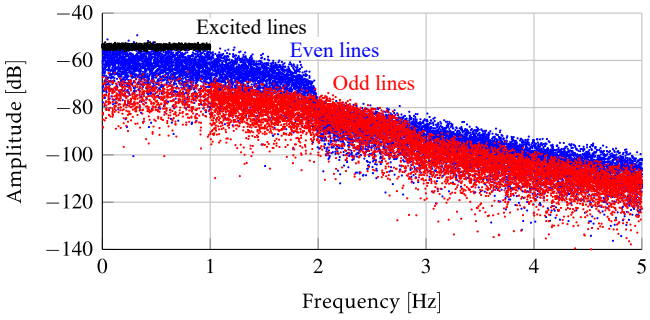

The excited frequency lines are shown in black, the even frequency lines are shown in blue and the non-excited odd frequency lines are shown in red. It is clear that the even and odd non-linear distortion generated by the circuit are separated and the distortion levels in the circuit can be determined quickly by just looking at the different colours in the plot.
The colour scheme used here to plot the steady-state spectrum of a non-linear system under a multisine excitation will be used throughout this thesis. The legend for the colour scheme is:

Colour	Explanation
Black	Frequency lines which are excited by the multisine
Blue	Even frequency lines with only even-order distortion
Red	Non-excited odd lines with only odd-order distortion
Magenta	Frequency lines with both even- and odd-order distortion
Grey	Frequency lines which contain only simulation noise

When a full multisine is used instead of an odd multisine, the non-excited frequency lines contain both even and odd-order distortion. In that case, the non-excited lines are coloured magenta. This was the case in the previous example where a full multisine was applied to the non-linear test system.

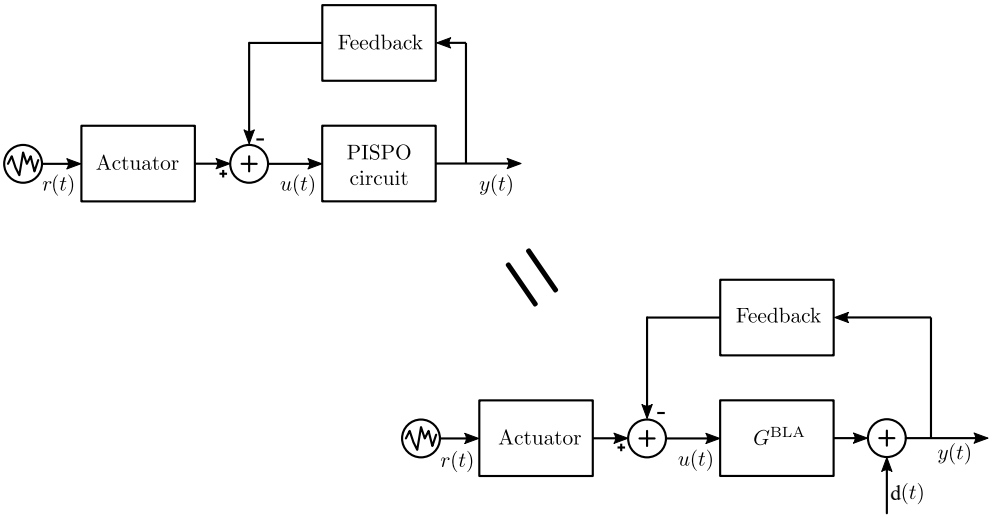

Figure 2.3.: In closed loop, the BLA can still be used. Instead of working directly from input $u(t)$ to output $y(t)$, the known reference signal $r(t)$ is used to obtain an unbiased estimate. The distortion introduced by the system in closed loop ($d(t)$) retains its noise-like properties, but it will now be uncorrelated to the reference signal instead of to the input signal.

2.3. The BLA in feedback

All previous techniques to estimate the BLA are only valid when the input signal $u(t)$is not disturbed by neither non-linear distortion, nor noise (This is commonly referred to as the *output error* framework). When the non-linear system is placed in a feedback configuration as shown in Figure 2.3, we should not use the estimator described before, because it will be biased in the closed-loop case [Pint 13].

Note that this “identification in feedback" is extremely important in the context of electronic circuits because most circuits will be placed, implicitly or explicitly, in a feedback configuration. An identification tool that can not deal with input errors is hence not very useful in the context of electronic circuits.

To correctly estimate the BLA of a system in feedback, the reference signal $r(t)$ is required. The reference signal is the signal which drives the complete closed-loop system and is exactly known. The BLA of the system in feedback is then defined as

$$G^{\mathrm{BLA}}_{U\to Y}(j\omega) = \frac{G^{\mathrm{BLA}}_{R\to Y}(j\omega)}{G^{\mathrm{BLA}}_{R\to U}(j\omega)} \tag{2.5}$$

This BLA now depends on the system, the feedback around the system and the properties of the reference signal.

The reference signal $r(t)$ will be chosen preferably as a multisine shaped to represent the random signals which the closed-loop system will encounter in its application. M different phase realisations of the multisine are applied to the closed-loop system and the steady-state spectra of the reference ($r^{\{m\}}(t)$), input signal ($u^{\{m\}}(t)$) and output signal ($y^{\{m\}}(t)$) are saved.

The BLA is now estimated in two steps: first, the BLA from the reference signal to the input and output of the system in feedback is determined with the techniques described before. Second, the two BLAs are combined to obtain the BLA of the system in feedback. This method does not introduce a bias on the BLA-estimate [Pint 13]

Step 1: Determine the BLA from the reference to input/output The signals and distortion at the input signal $u(t)$ and output signal $y(t)$ are strongly linked due to the feedback around the system. Therefore, the two signals are treated together as a signal vector. In literature, this vector of stacked output-input signals is usually denoted with $\mathbf{Z}(k)$ [Pint 13]

$$\mathbf{Z}^{\{m\}}(k) = \begin{bmatrix} Y^{\{m\}}(k) \\ U^{\{m\}}(k) \end{bmatrix}$$

In the first step of estimating the BLA of the system in feedback consists of estimating the Single-Input Multiple-Output (SIMO) BLA from the reference signal to the $\mathbf{Z}$-vector:

$$\mathbf{G}^{\text{BLA}}_{R\to\mathbf{Z}}(j\omega_k) = \mathbb{E}\left\{\mathbf{Z}^{\{m\}}(k)\left(R^{\{m\}}(k)\right)^{-1}\right\} \cong \frac{1}{M}\sum_{m=1}^{M}\mathbf{Z}^{\{m\}}(k)\left(R^{\{m\}}(k)\right)^{-1}$$

$\mathbf{G}^{\text{BLA}}_{R\to\mathbf{Z}}(j\omega_k) \in \mathbb{C}^{2\times 1}$ contains both the BLA from the reference signal to the input signal of the system in feedback and the BLA from the reference signal to its output signal:

$$\mathbf{G}^{\text{BLA}}_{R\to\mathbf{Z}}(j\omega_k) = \begin{bmatrix} G^{\text{BLA}}_{R\to Y}(j\omega_k) \\ G^{\text{BLA}}_{R\to U}(j\omega_k) \end{bmatrix}$$

The difference between $\mathbf{Z}^{\{m\}}(k)$ and the signals predicted by the BLA represent the non-linear distortion measured at the input and output nodes of the system. We will indicate this distortion vector with $\mathbf{D}_\mathbf{Z}$

$$\mathbf{D}^{\{m\}}_\mathbf{Z} = \mathbf{Z}^{\{m\}}(k) - \mathbf{G}^{\text{BLA}}_{R\to\mathbf{Z}}(j\omega_k)R^{\{m\}}(k)$$

The signals in $\mathbf{D}_{\mathbf{Z}}^{\{m\}}$ are noise-like and uncorrelated to the reference signal. They are however not uncorrelated among each other. The covariance matrix of the distortion measured at both nodes will be indicated with $\mathbf{C}_{\mathbf{D}_\mathbf{Z}}$ and can be calculated as

$$\mathbf{C}_{\mathbf{D}_\mathbf{Z}}(j\omega_k) \cong \frac{1}{M-1}\sum_{m=1}^{M} \mathbf{D}_{\mathbf{Z}}^{\{m\}} \left(\mathbf{D}_{\mathbf{Z}}^{\{m\}}\right)^{\mathsf{H}}$$

The uncertainty on the estimate for $\mathbf{G}_{R\to\mathbf{Z}}^{\mathrm{BLA}}(j\omega_k)$ is obtained from this covariance matrix as:

$$\mathbf{C}_{\mathbf{G}_{R\to\mathbf{Z}}^{\mathrm{BLA}}}(j\omega_k) \cong \frac{1}{M}\mathbf{C}_{\mathbf{D}_\mathbf{Z}}(j\omega_k)$$

Step 2: Determine the BLA from input to output Once the BLAs from the reference signal to the input and output of the system in feedback have been determined, the BLA of the system in feedback is calculated as the ratio between both:

$$G_{U\to Y}^{\mathrm{BLA}}(j\omega_k) = \frac{G_{R\to Y}^{\mathrm{BLA}}(j\omega_k)}{G_{R\to U}^{\mathrm{BLA}}(j\omega_k)}$$

The uncertainty on this final BLA-estimate is calculated as [Pint 13]

$$\sigma^2_{G_{U\to Y}^{\mathrm{BLA}}}(j\omega_k) = \frac{1}{M}\left|\frac{1}{G_{R\to U}^{\mathrm{BLA}}(j\omega_k)}\right|^2 \mathbf{V}(j\omega_k)\,\mathbf{C}_{\mathbf{D}_\mathbf{Z}}(j\omega_k)\,\mathbf{V}^{\mathsf{H}}(j\omega_k)$$
$$\mathbf{V}(j\omega_k) = \begin{bmatrix} 1 & -G_{U\to Y}^{\mathrm{BLA}}(j\omega_k) \end{bmatrix}$$

Determining the distortion introduced by the system in feedback To determine the distortion introduced by the system in the feedback configuration, we start from $\mathbf{C}_{\mathbf{D}_\mathbf{Z}}$ which represents the distortion covariance matrix of the output-input signals in closed loop. The power of the distortion introduced by the system in closed-loop is then

$$\mathbb{E}\left\{D(k)D^{\mathsf{H}}(k)\right\} = \begin{bmatrix} 1 & -G_{U\to Y}^{\mathrm{BLA}}(j\omega_k) \end{bmatrix} \mathbf{C}_{\mathbf{D}_\mathbf{Z}} \begin{bmatrix} 1 & -G_{U\to Y}^{\mathrm{BLA}}(j\omega_k) \end{bmatrix}^{\mathsf{H}}$$

Example 2.4: Estimating the BLA in feedback

As an example, consider an Operational Amplifier (op-amp) placed in an inverting feedback configuration. The op-amp is a two-stage Miller op-amp designed in a commercial 0.18μm technology with a Gain-Bandwidth product of 10MHz for a load capacitance of 10pF.

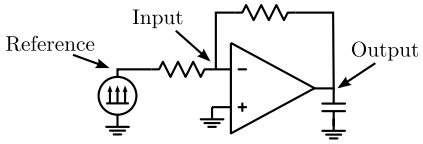

The reference signal is a random-odd multisine with $f_{\text{res}} = 0.1\text{kHz}$ which excites frequencies up to $f_{\text{max}} = 100\text{kHz}$. The amplitude spectrum of the multisine is chosen to be flat as a function of frequency and such that the rms voltage equals 50mV. The spectrum of the reference signal is shown below:

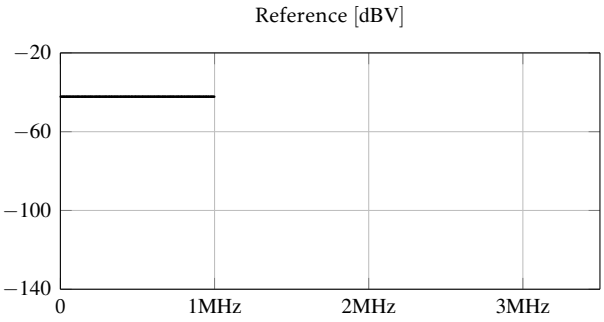

The input and output voltages of the op-amp are obtained with a Harmonic Balance (HB) simulation. The steady-state spectra are shown below. Both input and output spectra clearly contain non-linear distortion, as there is energy appearing at non-excited frequency lines. Like before, the even frequency bins are coloured blue and the non-excited odd frequency bins are indicated in red.

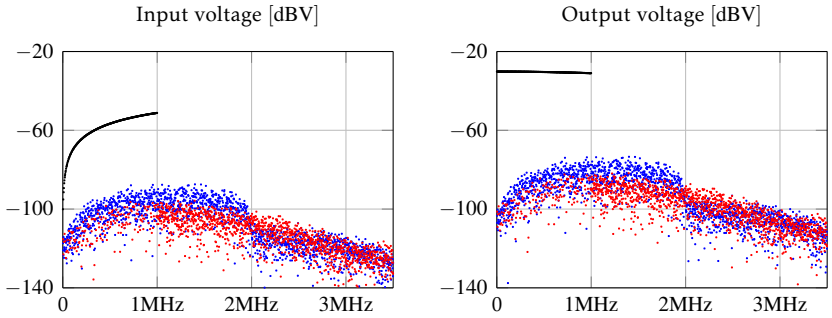

To determine the BLA of the op-amp from its input voltage to its output voltage, the step for identification in feedback should be used. First, the BLA from the reference signal to the input and output voltage of the op-amp is determined. The results obtained by averaging over $M = 6$ realisations of the input multisine are shown below. We can use this small number of phase realisations because the circuit is weakly non-linear.

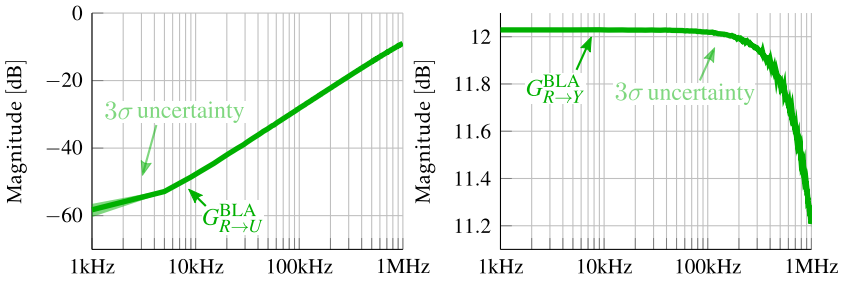

The BLA of the op-amp in feedback is then obtained by using (2.5):

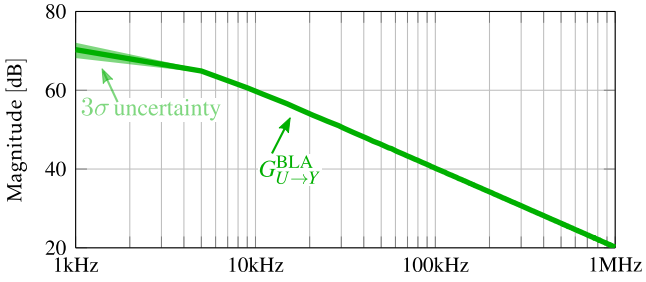

Summary

In this chapter, we have introduced the Best Linear Approximation (BLA), a powerful tool which allows us to describe the behaviour of both weakly and strongly non-linear systems. The BLA is a black box model of the system, so no information about the internals of the system are required, only the input-output behaviour is taken into consideration by the BLA.

The BLA is the linear model which describes the input-output behaviour of the system best in least-squares sense, it depends on both the system and on the PSD and PDF of the input signal. The residual of the approximation of the system by the BLA defines the distortion introduced by the system. This distortion has noise-like properties: it is zero mean, is uncorrelated to the input signal of the circuit and has a smooth power spectrum. This is why we will combine the BLA with a noise analysis in chapter 4 to be able to calculate the distortion contributions in a circuit which is excited by modulated signals.

When the non-linear system is placed in a (non-)linear feedback configuration, the properties of the BLA and the distortion remain, but they are translated to the reference signal $r(t)$ which drives the closed-loop system. The BLA of the closed loop system depends on the system itself and on the properties of the reference signal, just like the BLA of an open-loop system. However, in a feedback configuration, the BLA also depends on the feedback around the circuit.

Every system described in this chapter has a single input signal and a single output signal (Single-Input Single-Output (SISO)). Electronic circuits are rarely SISO, they normally need to be described by a Multiple-Input Multiple-Output (MIMO) BLA. The estimation of the MIMO BLA in simulations of electronic circuits is the topic of the next chapter.

3. Determining the MIMO BLA of circuits

The results of this chapter are obtained through close collaboration with Ebrahim Louarroudi and Piet Bronders. The work is mainly based on previous work by Ludwig De Locht [De L 07] and Rik Pintelon [Pint 11]

In the previous chapter, we introduced the Best Linear Approximation (BLA) and showed that it can be used to describe the behaviour of Single-Input Single-Output (SISO) non-linear systems under wideband excitation signals.

Only idealised electronic circuits can be modelled adequately with a SISO representation. To describe circuits with finite input and output impedance, reverse gain, and differential systems (with two inputs and/or outputs) a Multiple-Input Multiple-Output (MIMO) representation should be used. In this chapter, we extend the BLA framework to such MIMO non-linear systems.

This chapter focuses on the techniques needed for the estimation of the MIMO BLA in circuit simulations. In the next chapter, we will detail how to determine the non-linear distortion introduced by such MIMO systems. The estimation technique described here is one out of many possibilities to perform a MIMO BLA estimation. For more information on the alternative estimation techniques, the interested reader is referred to [Pint 12] and [Pint 11].

First, the open-loop MIMO identification procedure is detailed (Section 3.1). Then, the closed-loop case is discussed (Section 3.2). Finally, we adapt the identification techniques specifically to the identification of electronic circuits and apply the techniques to a class-C amplifier (Section 3.3).

3.1. Identification of MIMO systems

Consider a Period-In Same Period-Out (PISPO) non-linear system with n_u input signals and n_y output signals as shown in Figure 3.1. For now, assume that the inputs are perfectly known. The system is excited by a set of multisine excitation signals (2.3) with a common frequency resolution f_{res}. The Power Spectral Density (PSD) and Probability Density Function (PDF) of the multisines are shaped such that they resemble the signals the system will encounter in its application.

The output of the system can then be described as the sum of the response of the $n_u \times n_y$ Best Linear Approximation (BLA) and a distortion term $\mathbf{D}(k)$ [Pint 11]:

$$\mathbf{Y}(k) = \mathbf{G}^{\text{BLA}}_{\mathbf{U}\to\mathbf{Y}}(j\omega_k)\,\mathbf{U}(k) + \mathbf{D}(k)$$

where $\mathbf{U}(k)$ and $\mathbf{Y}(k)$ are the vectors of stacked input and output signals respectively

$$\mathbf{U}(k) = \begin{bmatrix} U_1(k) \\ \vdots \\ U_{n_u}(k) \end{bmatrix} \in \mathbb{C}^{n_u \times 1} \qquad \mathbf{Y}(k) = \begin{bmatrix} Y_1(k) \\ \vdots \\ Y_{n_y}(k) \end{bmatrix} \in \mathbb{C}^{n_y \times 1}$$

The distortion term $\mathbf{D}(k) \in \mathbb{C}^{n_y \times 1}$ has the properties of an additive noise signal: it is zero mean ($\mathbb{E}\{\mathbf{D}(k)\} = 0$), uncorrelated to the input signals, and has a smooth power spectrum $\mathbb{E}\left\{\mathbf{D}\mathbf{D}^{\mathsf{H}}\right\}$.

If the system were linear, its $n_y \times n_u$ Frequency Response Matrix (FRM) could be estimated by running n_u independent experiments. In the first experiment, the multisine is applied to the first input of the circuit while all other inputs are set to zero. The steady-state response of the circuit in this first experiment is indicated as $\mathbf{Y}^{(1)}(k)$. The first column of the $\mathbf{G}_{\mathbf{U}\to\mathbf{Y}}$ is now simply obtained as

$$\left[\mathbf{G}_{\mathbf{U}\to\mathbf{Y}}(j\omega_k)\right]_{1..n_y,1} = \mathbf{G}_{U_1\to\mathbf{Y}}(j\omega_k) = \frac{\mathbf{Y}^{(1)}(k)}{U_1(k)}$$

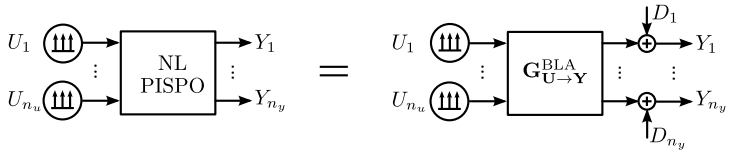

Figure 3.1.: When a PISPO non-linear system with n_u input signals and n_y output signals is excited by signals with a specified PSD and PDF, the system can be approximated by its BLA $\mathbf{G}^{\text{BLA}}_{\mathbf{U}\to\mathbf{Y}}$. There are then n_y non-linear distortion sources D_i.

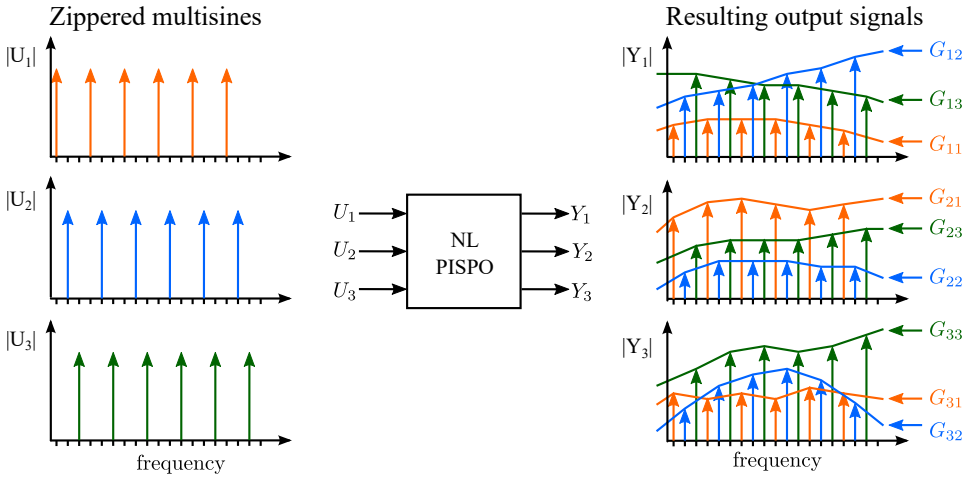

Figure 3.2.: When zippered multisine excitations are used, the input multisines are placed on non-overlapping frequency grids. With this kind of excitation, the MIMO BLA of a system can be determined by just looking at the correct frequency lines.

In the second experiment, only the second input is excited while all others are zero, this allows to obtain the second row of the FRM. This process is repeated for all inputs to obtain the full FRM $\mathbf{G}_{\mathbf{U}\to\mathbf{Y}}$.

When determining the MIMO BLA of a non-linear system, the PSD and PDF of all the input signals should be equal in every experiment of the circuit, so we cannot use the simple strategy described above. Instead of exciting the inputs one-by-one in different experiments however, we apply all random-phase multisines simultaneously to the MIMO system and use an interleaved frequency grid. With these *zippered multisines*, we can determine the BLA of a MIMO non-linear system [Verb 99, De L 07, Rive 09].

In a set of zippered multisines, the frequency lines in the different random-phase multisines are chosen such that they don't overlap (Figure 3.2). This turns the MIMO estimation problem into a set of SISO problems: Each column of the MIMO BLA is simply determined by looking at the correct frequency lines (Figure 3.2).

M different realisations of the zippered multisines are simulated. In each of the realisations all multisines are given a new random phase realisation. Each column of the MIMO BLA can then be estimated at the frequency grid of each of the different inputs by averaging over the phase realisations. For the n^{th} column of the

MIMO BLA, we calculate:

$$\left[\mathbf{G}^{\text{BLA}}_{\mathbf{U}\to\mathbf{Y}}(j\omega_k)\right]_{1..n_y,n} = \mathbf{G}^{\text{BLA}}_{U_n\to\mathbf{Y}}(j\omega_k) \cong \frac{1}{M}\sum_{m=1}^{M}\frac{\mathbf{Y}^{\{m\}}(k)}{U_n^{\{m\}}(k)} \text{ @ excited lines of input } U_n$$

The uncertainty on the estimate for the n^{th} column of the MIMO BLA is expressed by an $n_y \times n_y$ covariance matrix

$$\mathbf{C}_{\mathbf{G}^{\text{BLA}}_{U_n\to\mathbf{Y}}}(j\omega_k) = \frac{1}{M(M-1)}\sum_{m=1}^{M}\mathbf{E}^{\{m\}}(k)\left(\mathbf{E}^{\{m\}}(k)\right)^{\mathsf{H}}$$
$$\text{with } \mathbf{E}^{\{m\}}(k) = \mathbf{Y}^{\{m\}}(k) - \mathbf{G}^{\text{BLA}}_{U_n\to\mathbf{Y}}(j\omega_k)\,U_n^{\{m\}}(k)$$

This is repeated for each of the columns to obtain an estimate of the full MIMO BLA. Note that the different columns of the BLA are now known at different frequencies. A simple linear interpolation can be used to interpolate the BLA on the intermediate frequencies. After the interpolation, the different columns can finally be gathered to obtain the MIMO BLA

$$\mathbf{G}^{\text{BLA}}_{\mathbf{U}\to\mathbf{Y}}(j\omega_k) = \begin{bmatrix} \mathbf{G}^{\text{BLA}}_{U_1\to\mathbf{Y}}(j\omega_k) & \cdots & \mathbf{G}^{\text{BLA}}_{U_{nu}\to\mathbf{Y}}(j\omega_k) \end{bmatrix}$$

The uncertainty on the MIMO BLA is expressed by a block diagonal covariance matrix of size $n_y n_u \times n_y n_u$ which contains the uncertainty on the estimates of $\text{vec}\left(\mathbf{G}^{\text{BLA}}_{\mathbf{U}\to\mathbf{Y}}\right)$ where the vec operator stacks the columns of a matrix on top of each other [Brew 78].

$$\mathbf{C}_{\text{vec}\left(\mathbf{G}^{\text{BLA}}_{\mathbf{U}\to\mathbf{Y}}\right)}(j\omega_k) = \begin{bmatrix} \mathbf{C}_{G^{\text{BLA}}_{U_1\to\mathbf{Y}}}(j\omega_k) & \cdots & \mathbf{0} \\ \vdots & \ddots & \vdots \\ \mathbf{0} & \cdots & \mathbf{C}_{G^{\text{BLA}}_{U_{nu}\to\mathbf{Y}}}(j\omega_k) \end{bmatrix}$$

Many alternative techniques exist to zippered multisines exist to estimate the MIMO BLA [Pint 12]. Orthogonal multisine excitations [Pint 11], for example, could also be used to estimate the MIMO BLA. We opted to use zippered multisines because they simplify the MIMO estimation problem considerably and are easier to debug than the alternative methods. The drawback of using multisines on interleaved frequency grids is that the simulation time is considerably longer.

A considerable speed-up could be obtained when using orthogonal multisine excitations combined with state-of-the-art system identification techniques like the Local Polynomial Method (LPM) [Scho 09]. We opted to keep the used estimation techniques very simple which minimises the number of parameters that need to be set by the user of the techniques.

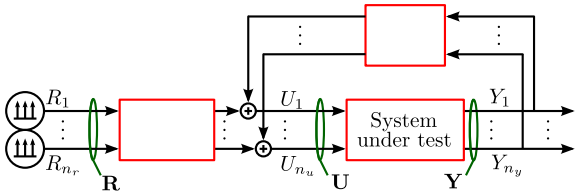

Figure 3.3.: A MIMO system in feedback.

3.2. Estimating the MIMO BLA in feedback

In the context of electronic circuits, the open-loop situation which we discussed in Section 3.1 is rarely encountered. Usually, a circuit is placed in a feedback configuration as shown in Figure 3.3. The closed-loop system is driven by n_r known reference signals. The complete circuit, which contains both the circuit under test and the elements around it is assumed to be PISPO.

The BLA of the system in feedback is defined as the MIMO extension of equation (2.5) [Pint 11]:

$$\mathbf{G}^{\text{BLA}}_{\mathbf{U}\to\mathbf{Y}}(j\omega_k) = \mathbf{G}^{\text{BLA}}_{\mathbf{R}\to\mathbf{Y}}(j\omega_k)\left(\mathbf{G}^{\text{BLA}}_{\mathbf{R}\to\mathbf{U}}(j\omega_k)\right)^{+} \tag{3.1}$$

where $\mathbf{G}^{\text{BLA}}_{\mathbf{R}\to\mathbf{Y}} \in \mathbb{C}^{n_y\times n_r}$ is the MIMO BLA from the reference signals to the output signals of the system and $\mathbf{G}^{\text{BLA}}_{\mathbf{R}\to\mathbf{U}} \in \mathbb{C}^{n_u\times n_r}$ is the MIMO BLA from the reference signals to the input signals of the system. $\cdot^{+}$ indicates the pseudo-inverse. To ensure that $\mathbf{G}^{\text{BLA}}_{\mathbf{R}\to\mathbf{A}}$ is invertible, at least n_u reference signals are needed in the circuit.

Similarly to the SISO case, the MIMO BLA of a system in feedback is determined in a two-step procedure. First, $\mathbf{G}^{\text{BLA}}_{\mathbf{R}\to\mathbf{Y}}$ and $\mathbf{G}^{\text{BLA}}_{\mathbf{R}\to\mathbf{U}}$ are estimated. Then, in the second step, $\mathbf{G}^{\text{BLA}}_{\mathbf{U}\to\mathbf{Y}}$ and its uncertainty are determined.

Step 1: Determine $\mathbf{G}^{\text{BLA}}_{\mathbf{R}\to\mathbf{Y}}$ and $\mathbf{G}^{\text{BLA}}_{\mathbf{R}\to\mathbf{U}}$ The MIMO BLA from the reference signals to the input and output signals can be obtained just as in the open-loop case by zippering the reference multisine signals. Because the distortion present at the input and output signals might be correlated due to the feedback around the system, $\mathbf{G}^{\text{BLA}}_{\mathbf{R}\to\mathbf{Z}}$ is calculated, where $\mathbf{Z}$ is the vector of stacked output-input signals:

$$\mathbf{G}^{\text{BLA}}_{\mathbf{R}\to\mathbf{Z}}(j\omega_k) = \begin{bmatrix} \mathbf{G}^{\text{BLA}}_{\mathbf{R}\to\mathbf{Y}}(j\omega_k) \\ \mathbf{G}^{\text{BLA}}_{\mathbf{R}\to\mathbf{U}}(j\omega_k) \end{bmatrix} \qquad \text{where } \mathbf{Z}(k) = \begin{bmatrix} \mathbf{Y}(k) \\ \mathbf{U}(k) \end{bmatrix} \in \mathbb{C}^{(n_y+n_u)\times 1}$$

$\mathbf{G}^{\text{BLA}}_{\mathbf{R}\to\mathbf{Z}}$ and its uncertainty is then determined using the open-loop techniques detailed in the previous section. Recall that the uncertainty on the estimate is expressed by a block diagonal covariance matrix $\mathbf{C}_{\text{vec}\left(\mathbf{G}^{\text{BLA}}_{\mathbf{R}\to\mathbf{Z}}\right)}$ of size $(n_y+n_u)n_r \times (n_y+n_u)n_r$.

Step 2: Determine $\mathbf{G}^{\text{BLA}}_{\mathbf{U}\to\mathbf{Y}}$ and its uncertainty Once $\mathbf{G}^{\text{BLA}}_{\mathbf{R}\to\mathbf{Z}}$ is estimated, the MIMO BLA of the system in feedback can be determined using (3.1). The uncertainty on this BLA-estimate is given by

$$\mathbf{C}_{\text{vec}\left(\mathbf{G}^{\text{BLA}}_{\mathbf{U}\to\mathbf{Y}}\right)}(j\omega_k) = \mathbf{T}\mathbf{C}_{\text{vec}\left(\mathbf{G}^{\text{BLA}}_{\mathbf{R}\to\mathbf{Z}}\right)}\mathbf{T}^{\mathsf{H}}$$
$$\text{with}\mathbf{T} = \left(\left(\mathbf{G}^{\text{BLA}}_{\mathbf{R}\to\mathbf{U}}\right)^{+}\right)^{\mathrm{T}} \otimes \begin{bmatrix} \mathbf{I}_{n_y} & -\mathbf{G}^{\text{BLA}}_{\mathbf{U}\to\mathbf{Y}} \end{bmatrix}$$

where $\cdot^{\mathrm{T}}$ indicates the matrix transpose and $\otimes$ is the Kronecker product of two matrices [Brew 78].

3.3. Estimating the MIMO BLA of electronic circuits

Now that we have elaborated on how to estimate the MIMO BLA of a general non-linear system, we will apply these techniques to determine the MIMO BLA of an electronic circuit.

The linear behaviour of a circuit with P ports is fully described by a $P \times P$ FRM. The MIMO BLA will therefore also be a $P \times P$ BLA. Depending on the choice of input and output signals, many different circuit representations, like the Y-parameters or Z-parameters, can be used to fully describe the behaviour of the circuit. It is the designer's freedom to choose the representation that best suits his application. In this thesis, we will use waves and S-parameters to describe the behaviour of circuits for reasons that will become clear in the next chapter.

S^{BLA}-parameters

The incident and reflected waves at the ports of the circuit are chosen as the input and output signals in all MIMO BLAs in the remainder of this thesis.

$$\mathbf{U}(k) = \mathbf{A}(k) = \begin{bmatrix} A_1(k) \\ \vdots \\ A_P(k) \end{bmatrix} \qquad \mathbf{Y}(k) = \mathbf{B}(k) = \begin{bmatrix} B_1(k) \\ \vdots \\ B_P(k) \end{bmatrix}$$

The incident wave A_p and reflected wave B_p at port p of the circuit are calculated using the port voltage V_p and port current I_p in the following way [Kuro 65, Mark 92]:

$$A_p(k) = \frac{1}{2\sqrt{50}}\left(V_p(k) + 50 \cdot I_p(k)\right) \qquad B_p(k) = \frac{1}{2\sqrt{50}}\left(V_p(k) - 50 \cdot I_p(k)\right)$$

We will always use a reference impedance of 50Ω as is clear from the formulae above.

The $P \times P$ MIMO BLA that describes the relation between the vectors of **A** and **B** waves at the ports of the circuit will be called the S^{BLA}-parameters in the remainder of the thesis.

$$\mathbf{B}(k) = \mathbf{S}^{\text{BLA}}_{\mathbf{A}\rightarrow\mathbf{B}}(j\omega_k)\,\mathbf{A}(k) + \mathbf{D}(k)$$

The distortion added by the circuit is represented by P outward radiating wave sources which are gathered in the distortion vector **D**. We will discuss how **D** is determined in the next chapter. Here, we focus on estimating $\mathbf{S}^{\text{BLA}}_{\mathbf{A}\rightarrow\mathbf{B}}$.

Estimating the S^{BLA}-parameters

To estimate the S^{BLA}-parameters of a circuit with P ports, there should be at least P reference signals present in the circuit. Most circuits are, however, only excited by a single reference signal R_1, as shown in Figure 3.4. With this main reference signal alone, it is impossible to estimate the MIMO BLA, so extra reference signals need to be added to the circuit. These added reference signals will be called *tickler* multisines [De L 07](Figure 3.4). Adding the tickler signals to the circuit is a difficult process to automate as many different constraints should be satisfied to allow a correct estimation of the MIMO BLA

Constraints on the tickler signals

1. The tickler signals should be added to the circuit without disturbing the BLA of the whole circuit. This implies that the tickler multisines should have a very small amplitude compared to the amplitude of the main multisine. At the same time, the amplitude of the tickler signals should be large enough to be able to obtain a good estimate of the BLA. Choosing the correct amplitude of the tickler signals usually requires some trial and error, as it depends on both the circuit and on the simulation settings. In low-frequency circuits, when the reverse gain of a circuit is very low, it can even be impossible to obtain a good estimate of this reverse gain without needing to push the amplitude of the ticker multisines to (too) high levels.

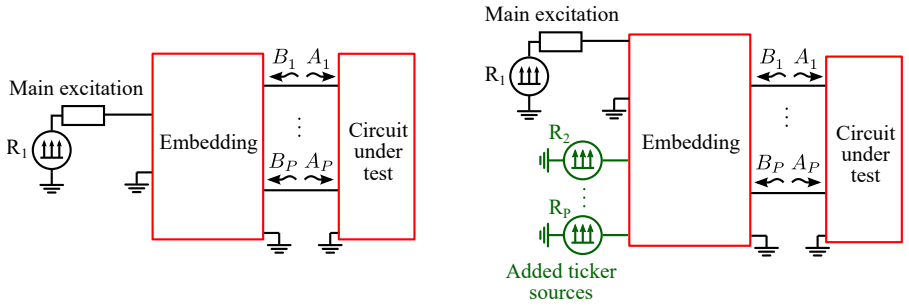

Figure 3.4.: To be able to estimate the MIMO BLA of a circuit, extra reference signals need to be added to the circuit such that the amount of reference signals is equal to the amount of ports of the sub-circuit. These added reference signals are called tickler multisines.

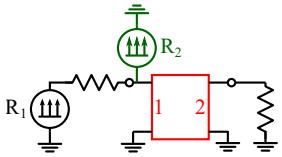

Figure 3.5.: Example of a bad choice for the location of the tickler multisine.

2. Choosing the location of the tickler signals in the circuit is the second difficulty. As we showed before, the BLA from the reference signals to the incident waves of the circuit ($\mathbf{G}^{\text{BLA}}_{\mathbf{R}\to\mathbf{A}}$) needs to be inverted to determine the MIMO BLA of the circuit in its feedback configuration. The location of the tickler signals should be chosen such that $\mathbf{G}^{\text{BLA}}_{\mathbf{R}\to\mathbf{A}}$ is well-conditioned. Consider the two-port in Figure 3.5 as an example. The tickler multisine is connected to the same port as the main multisine. Hence, $\mathbf{G}^{\text{BLA}}_{\mathbf{R}\to\mathbf{A}}$ will be very badly conditioned, which will result in a totally inaccurate estimate for the output impedance at the second port ($\left[\mathbf{S}^{\text{BLA}}\right]_{2,2}$). In this specific case, the tickler signal should be connected to a node close to the second port of the circuit.

Although it seems difficult to correctly set up these tickler multisines, we will use them to estimate the S^{BLA}-parameters of several circuits in the next chapter.

Example 3.1: S^{BLA}-parameters of a class-C amplifier

We will determine the S^{BLA}-parameters of the transistor in the class-C amplifier shown below.

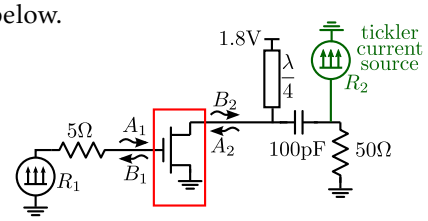

The transistor in the amplifier is placed in a common-source configuration, so it will be modelled by a 2×2 MIMO BLA.

The amplifier is excited by a random-phase multisine R_1 which excites 41 frequencies in a band of 40MHz around 1GHz, which corresponds to a frequency resolution $f_{\mathrm{res}} = 1\mathrm{MHz}$. The multisine has a flat PSD with a root mean square (rms) value is 0.2V, which results in an amplitude of 44mV for each of the tones of the multisine:

$$r_1(t) = \sum_{k=980}^{1020} (44\mathrm{mV}) \cdot \sin(2\pi k (1\mathrm{MHz}) t + \phi_k)$$

Because we want to estimate a 2-port circuit, one tickler multisine needs to be added to the circuit. To obtain a well-conditioned FRM from the reference signals to both A-waves at the ports of the transistor, the tickler current source is connected to the load of the circuit (R_2, shown in green in the figure).

The two reference signals R_1 and R_2 are zippered to allow easy estimation of the MIMO BLA. The excited lines of the tickler multisine are placed 1Hz away from the frequency grid of the main multisine. The amplitude of the tones of the tickler multisines is chosen to be $40\mu\mathrm{A}$, which results in the following multisine signal:

$$r_2(t) = \sum_{h=980}^{1020} (40\mu\mathrm{A}) \cdot \sin(2\pi (h (1\mathrm{MHz}) + 1\mathrm{Hz}) t + \phi_h)$$

Both multisines are given random phases ϕ_k and ϕ_h and are applied together to the circuit. The steady-state response of the circuit to $M = 20$ phase realisations was obtained with Harmonic Balance (HB) simulations. In a HB simulation, the tones for the tickler multisine are easily added to the frequency grid by including 1Hz in the list of fundamental frequencies of the HB simulation. When the 1Hz tone is given an order of 1, a frequency

line will appear at ±1Hz distance from the frequency lines of the main multisine. The tickler in this example multisine will only excite the lines at +1Hz, the other lines are left unexcited. The drawback of this approach is that the amount of frequency lines is three times larger than in the simulation with a single multisine. The simulation time is therefore very high in this kind of simulations.
The resulting B_2 wave for some of the phase realisations of the multisines is shown below

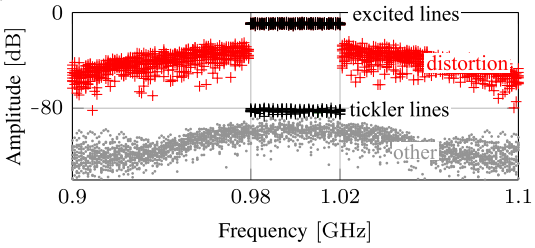

The excited lines of R_1 are shown in black +. The out-of-band odd-order distortion is shown red +. In between the frequency lines of R_1, the response to R_2 visible. The excited lines of R_2 are indicated with green +, while all remaining bins in the steady-state spectrum are grey ●. The amplitude of the tickler was chosen such that the tickler response was clearly visible above the numeric noise floor.
The obtained BLAs and their 3σ uncertainty interval are shown below:

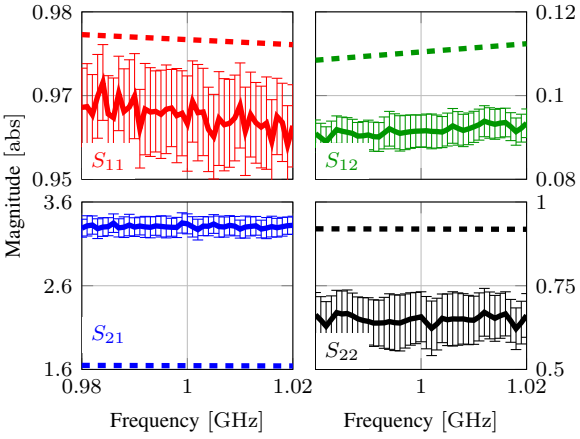

The dashed lines are the small-signal S-parameters. The largest differences are observed on S_{21} and S_{22}, which is to be expected for a class-C biased transistor.

4. Distortion Contribution Analysis with the BLA

An analog electronic circuit contains many different sources of non-linear distortion. Every transistor or sub-circuit can add some distortion to the signals that are being processed by the circuit and it is the job of the designer to ensure that the total distortion generated by the circuit remains within acceptable bounds. The Distortion Contribution Analysis (DCA) calculates the distortion contributions of each of the sub-circuits to the total distortion at the output of the circuit. This information about the main cause of non-linear distortion in his circuit enables the designer to effectively reduce the distortion generated.

The concept of the DCA is very old [Nara 67] and has attracted a lot of interest over the years [Wamb 98, Aiki 05]. However, to this day, a DCA is not readily available to many circuit designers. As was discussed in chapter 1, most of the described implementations of a DCA are based on the Volterra description of non-linear circuits. In Volterra-based methods, it is very hard to limit the amount of distortion contributions, which makes the Volterra-based DCA unsuitable to be used under modulated excitation signals. A simple miller op-amp, for example, gives rise to over 700 distortion contributions when analysed with a Volterra method [Wamb 98], which makes proper analysis of the results a difficult task.

In this chapter, we detail how to perform a distortion analysis with the Best Linear Approximation (BLA). In chapter 2, we have shown that the BLA can be used to describe the behaviour of non-linear circuits under modulated excitation signals. We have also shown that, in the BLA-framework, the distortion behaves like noise. This noise-like behaviour of the distortion allows to combine the BLA with a noise analysis to obtain a DCA that can determine the distortion contributions in a (strongly non-linear) circuit under modulated signals.

In the first part of the chapter (Section 4.1), the DCA on the system level is considered. In a system-level simulation, the interconnection of sub-bocks on a high abstraction level is studied. The circuit sub-systems are assumed to be Single-Input Single-Output (SISO) (non-linear) blocks in these system-level simulations.

In the second part of the chapter (Section 4.2), we descend from system-level simulations to the circuit level. When working on the circuit level, the sub-circuits have non-ideal input and output impedances and a reverse gain, so they have to be represented by their Multiple-Input Multiple-Output (MIMO) BLA. Techniques to estimate the MIMO BLA of a sub-circuit were detailed in the previous chapter.

Both the system-level and circuit-level BLA-based DCA are applied to several examples to demonstrate how they can be used in circuit analysis.

The idea for a BLA-based DCA was originally proposed in [De L 04], and was used to analyse basic circuits in [Bron 08, Bos 08, Vand 09, Vand 07]. All these previous implementations of the BLA-based DCA did not consider the correlation between the distortion sources in the circuit. We demonstrate in this chapter that it is very important to keep the correlation into account to be able to obtain correct results in the DCA.

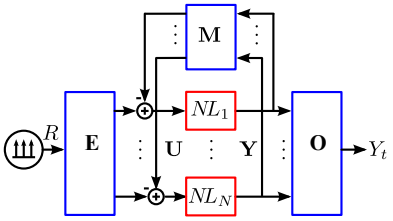

Figure 4.1.: The general circuit configuration under consideration consists of multiple non-linear systems NL_n which are placed in a feedback configuration. This configuration can represent any interconnection of non-linear blocks where **E**, **M** and **O** represent linear systems.

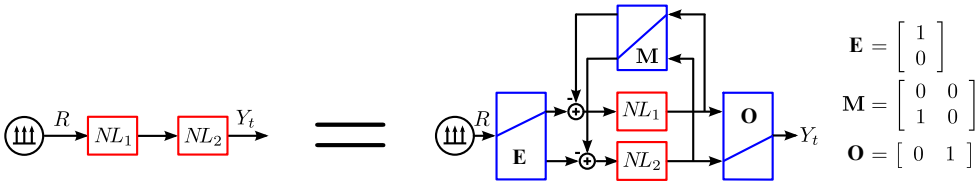

Figure 4.2.: Example of how the general structure can be used to represent a cascade of non-linear sub-circuits.

4.1. Distortion Contribution Analysis on the system level

Consider N Single-Input Single-Output (SISO) non-linear blocks embedded in a linear feedback structure as shown in Figure 4.1. The input of the n^{th} non-linear block is indicated with $U_{[n]}$, the output of the same sub-circuit is $Y_{[n]}$. The whole system is excited by a single modulated excitation signal $R(k)$ and the total circuit has an output signal which will be indicated with $Y_t(k)$. The complete system is assumed to the Period-In Same Period-Out (PISPO).

The linear feedback dynamics around the non-linear blocks are represented by a Frequency Response Matrix (FRM) $\mathbf{M}(j\omega_k) \in \mathbb{C}^{N\times N}$. The reference signal is interconnected to the inputs of the non-linear blocks through a linear system represented by the FRM $\mathbf{E}(j\omega_k) \in \mathbb{C}^{N\times 1}$. The outputs of the non-linear blocks are connected to the total output signal of the circuit through a linear system represented by the FRM $\mathbf{O}(j\omega_k) \in \mathbb{C}^{1\times N}$.

The feedback system proposed here can be made to resemble any interconnection of linear and SISO non-linear sub-circuits. As an example, it is shown in Figure 4.2 how a cascade of two non-linear blocks can be represented with the general structure.

The reference signal is a modulated signal with a fixed Power Spectral Density (PSD) and Probability Density Function (PDF). In all our tests, $r(t)$ will be a Random Phase Multisine (RPM) which is shaped such that the multisine has the same properties as the modulated signal.

Using the BLA framework, we can write the output of the system $Y_{\text{t}}(k)$ as

$$Y_{\text{t}}(k) = G^{\text{BLA}}_{R\to Y_{\text{t}}}(j\omega_k)R(k) + D_t(k) \tag{4.1}$$

where $G^{\text{BLA}}_{R\to Y_t}$ is the SISO BLA from the reference signal to the total output of the system. D_t is the non-linear distortion created by the system. D_t has noise-like properties, as was explained in Chapter 2. The distortion term D_t is uncorrelated to the reference signal and it has a continuous power spectrum $\mathbb{E}\left\{D_t D_t^{\text{H}}\right\}$. The goal of the DCA is to write the power of the distortion term as a sum of distortion contributions of the N non-linear sub-circuits in the circuit.

To determine the distortion contributions of each sub-circuit to the output, a three-step procedure is needed:

1. Determine the BLA of the non-linear sub-circuits ($G^{\mathrm{BLA}}_{U_{[n]}\to Y_{[n]}}$)
2. Determine the distortion added by each sub-circuit ($D_{[n]}$)
3. Refer the distortion of each non-linear sub-circuit to the output

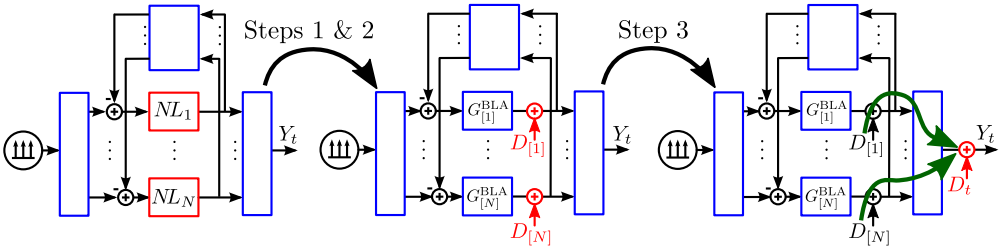

Figure 4.3.: Visual representation of the three-step procedure needed to determine the distortion contributions to the output signal.

Step 1: Determine the BLA of the non-linear sub-circuits

Each of the SISO BLAs of the N non-linear sub-blocks is determined using the two-step procedure described in Chapter 2. First, the BLAs from the reference signal (R) both to the output signal ($Y_{[n]}$) and to the input signal ($U_{[n]}$) of each sub-circuit is calculated by using the steady-state response of the circuit to M different phase realisations of the multisine:

$$G^{\mathrm{BLA}}_{R\to Y_{[n]}}(j\omega_k) = \frac{1}{M}\sum_{m=1}^{M}\frac{Y^{\{m\}}_{[n]}(k)}{R^{\{m\}}(k)} \qquad G^{\mathrm{BLA}}_{R\to U_{[n]}}(j\omega_k) = \frac{1}{M}\sum_{m=1}^{M}\frac{U^{\{m\}}_{[n]}(k)}{R^{\{m\}}(k)}$$

where the superscript $\cdot^{\{m\}}$ indicates the steady-state spectrum of the signal when the system is excited by the m^{th} phase realisation of the multisine. In the second step, the BLA of the sub-circuit itself is determined as:

$$G^{\mathrm{BLA}}_{U_{[n]}\to Y_{[n]}}(j\omega_k) = \frac{G^{\mathrm{BLA}}_{R\to Y_{[n]}}(j\omega_k)}{G^{\mathrm{BLA}}_{R\to U_{[n]}}(j\omega_k)}$$

This process is repeated for each of the non-linear sub-circuits.

Step 2: Determine the distortion added by each sub-circuit

The different distortion sources in the circuit are all uncorrelated to the reference signal. However, they can be correlated among each other. Later in this chapter, we will demonstrate that this correlation is key to obtaining a correct DCA. To deal with the correlation between the different non-linear blocks, their output and input signals are gathered in a vector of signals:

$$\mathbf{U}(k) = \begin{bmatrix} U_{[1]}(k) \\ \vdots \\ U_{[N]}(k) \end{bmatrix} \qquad \mathbf{Y}(k) = \begin{bmatrix} Y_{[1]}(k) \\ \vdots \\ Y_{[N]}(k) \end{bmatrix}$$

The BLA between $\mathbf{U}(k)$ and $\mathbf{Y}(k)$ is given by a MIMO BLA which is a diagonal matrix with the different SISO BLAs on its diagonal:

$$\mathbf{G}^{\text{BLA}}_{\mathbf{U}\to\mathbf{Y}}(j\omega_k) = \begin{bmatrix} G^{\text{BLA}}_{U_{[1]}\to Y_{[1]}}(j\omega_k) & \cdots & 0 \\ \vdots & \ddots & \vdots \\ 0 & \cdots & G^{\text{BLA}}_{U_{[N]}\to Y_{[N]}}(j\omega_k) \end{bmatrix}$$

The relation between the input and output vector of the gathered non-linear sub-circuits can now be written as:

$$\mathbf{Y}(k) = \mathbf{G}^{\text{BLA}}_{\mathbf{U}\to\mathbf{Y}}(j\omega_k)\,\mathbf{U}(k) + \mathbf{D}(k) \tag{4.2}$$

where $\mathbf{D}(k) \in \mathbb{C}^{N\times 1}$ contains the non-linear distortion introduced by the sub-circuits. The power of the distortion sources is expressed by the covariance matrix $\mathbf{C}_{\mathbf{D}}(j\omega_k) \in \mathbb{C}^{N\times N}$

$$\mathbf{C}_{\mathbf{D}}(j\omega_k) = \mathbb{E}\left\{\mathbf{D}(k)\,\mathbf{D}^{\mathsf{H}}(k)\right\} = \begin{bmatrix} \mathbb{E}\left\{D_{[1]}D^{\mathsf{H}}_{[1]}\right\} & \cdots & \mathbb{E}\left\{D_{[N]}D^{\mathsf{H}}_{[1]}\right\} \\ \vdots & \ddots & \vdots \\ \mathbb{E}\left\{D_{[1]}D^{\mathsf{H}}_{[N]}\right\} & \cdots & \mathbb{E}\left\{D_{[N]}D^{\mathsf{H}}_{[N]}\right\} \end{bmatrix}$$

where the expected value is, as usual, taken over the different phase realisations of the reference multisine. The diagonal elements of $\mathbf{C}_{\mathbf{D}}(j\omega_k)$ represent the power of each of the distortion sources in the circuit. The off-diagonal elements represent the co-variance or correlation between the distortion sources in the circuit.

Just like with the BLA itself, obtaining an unbiased estimate of $\mathbf{C}_{\mathbf{D}}$ is done in two steps. First, the distortion at the input and output of the different sub-blocks is determined using the Single-Input Multiple-Output (SIMO) BLAs from reference

R to $\mathbf{Y}$ and $\mathbf{U}$

$$\mathbf{D}_{\mathbf{Z}}^{\{m\}}(k) = \begin{bmatrix} Y_{[1]}^{\{m\}}(k) \\ \vdots \\ Y_{[N]}^{\{m\}}(k) \\ U_{[1]}^{\{m\}}(k) \\ \vdots \\ U_{[N]}^{\{m\}}(k) \end{bmatrix} - \begin{bmatrix} \mathbf{G}_{R\to Y_{[1]}}^{\mathrm{BLA}}(j\omega_k) \\ \vdots \\ \mathbf{G}_{R\to Y_{[N]}}^{\mathrm{BLA}}(j\omega_k) \\ \mathbf{G}_{R\to U_{[1]}}^{\mathrm{BLA}}(j\omega_k) \\ \vdots \\ \mathbf{G}_{R\to U_{[N]}}^{\mathrm{BLA}}(j\omega_k) \end{bmatrix} R^{\{m\}}(k)$$

$$\mathbf{C}_{\mathbf{D}_\mathbf{Z}}(j\omega_k) = \mathbb{E}\left\{\mathbf{D}_\mathbf{Z}\mathbf{D}_\mathbf{Z}^{\mathsf{H}}\right\}(k) \cong \frac{1}{M-1}\sum_{m=1}^{M} \mathbf{D}_\mathbf{Z}^{\{m\}}(k)\left(\mathbf{D}_\mathbf{Z}^{\{m\}}(k)\right)^{\mathsf{H}}$$

$\mathbf{C}_{\mathbf{D}_\mathbf{Z}}(j\omega_k) \in \mathbb{C}^{2N\times 2N}$ is the covariance matrix of the distortion signals present at the stacked output-input vector. To obtain a full-rank estimate of $\mathbf{C}_{\mathbf{D}_\mathbf{Z}}$, the response to at least $M = 2N$ phase realisations of the multisine must be simulated.

In the second step, the covariance matrix of the distortion sources $\mathbf{C}_\mathbf{D}(j\omega_k)$ is obtained from $\mathbf{C}_{\mathbf{D}_\mathbf{Z}}(j\omega_k)$ using

$$\mathbf{C}_\mathbf{D}(j\omega_k) = \begin{bmatrix} \mathbf{I}_N & -\mathbf{G}_{\mathbf{U}\to\mathbf{Y}}^{\mathrm{BLA}}(j\omega_k) \end{bmatrix} \mathbf{C}_{\mathbf{D}_\mathbf{Z}}(j\omega_k) \begin{bmatrix} \mathbf{I}_N & -\mathbf{G}_{\mathbf{U}\to\mathbf{Y}}^{\mathrm{BLA}}(j\omega_k) \end{bmatrix}^{\mathsf{H}}$$

where $\mathbf{I}_N$ is this expression is the identity matrix of size N.

Step 3: Refer the distortion of each sub-circuit to the output

In the third and last step of the BLA-based DCA, we look for the relation between the distortion sources at the output of every sub-circuit and the distortion at the output node of the circuit.

This step is identical to a classic noise analysis. In such a noise analysis, the noise power introduced by each source is determined first. Then the Frequency Response Function (FRF) between every noise source and the output signal of the circuit is determined. The noise contribution is then calculated as the product of the noise power and the square of the magnitude of the FRF.

In a noise analysis, the different noise sources are usually uncorrelated, resulting in a diagonal covariance matrix. Distortion sources on the other hand, can show a strong correlation, so the off-diagonal elements in $\mathbf{C}_\mathbf{D}$ cannot be ignored.

Because each non-linear sub-circuit can be replaced by its BLA, we can applying linear system theory to the circuit shown in Figure 4.1 to obtain an expression for the output signal Y_t as a function of the reference multisine R and the distortion sources $\mathbf{D}$. The following expressions are calculated for each of the frequencies ω_k

at which the BLA is known. For notational simplicity, we will omit the frequency indices (k) and $(j\omega_k)$ from now on. The following equations describe the system:

$$\begin{cases} \mathbf{U} = \mathbf{E}R - \mathbf{M}\mathbf{Y} \\ \mathbf{Y} = \mathbf{G}^{\text{BLA}}_{\mathbf{U}\to\mathbf{Y}}\mathbf{U} + \mathbf{D} \\ Y_t = \mathbf{O}\mathbf{Y} \end{cases}$$

Plugging the first equation into the second and solving for $\mathbf{Y}$, we obtain

$$\mathbf{Y} = \left(\mathbf{I}_N + \mathbf{G}^{\text{BLA}}_{\mathbf{U}\to\mathbf{Y}}\mathbf{M}\right)^{-1}\left(\mathbf{G}^{\text{BLA}}_{\mathbf{U}\to\mathbf{Y}}\mathbf{E}R + \mathbf{D}\right)$$

Using this expression in the third expression and grouping the terms in R and $\mathbf{D}$ yields:

$$\begin{aligned} Y_t = &\overbrace{\mathbf{O}\left[\mathbf{I}_N + \mathbf{G}^{\text{BLA}}_{\mathbf{U}\to\mathbf{Y}}\mathbf{M}\right]^{-1}\mathbf{G}^{\text{BLA}}_{\mathbf{U}\to\mathbf{Y}}\mathbf{E}}^{G^{\text{BLA}}_{R\to Y_t}}R \\ &+ \underbrace{\mathbf{O}\left[\mathbf{I}_N + \mathbf{G}^{\text{BLA}}_{\mathbf{U}\to\mathbf{Y}}\mathbf{M}\right]^{-1}\mathbf{D}}_{D_t} \end{aligned}$$

The second part of the equation yields the expression for the output distortion as a function of the distortion in the sub-systems:

$$D_t = \mathbf{O}\left[\mathbf{I}_N + \mathbf{G}^{\text{BLA}}_{\mathbf{U}\to\mathbf{Y}}\mathbf{M}\right]^{-1}\mathbf{D} = \mathbf{T}_{\text{out}}\mathbf{D}$$

$\mathbf{T}_{\text{out}} \in \mathbb{C}^{1\times N}$ contains the FRF from each distortion source to the output node. The elements of $\mathbf{T}_{\text{out}}$ will be denoted $T_{[i]}$:

$$\mathbf{T}_{\text{out}} = \begin{bmatrix} T_{[1]} & \cdots & T_{[i]} & \cdots & T_{[N]} \end{bmatrix}$$

So $T_{[i]}$ is the FRF from distortion source $D_{[i]}$ to the output of the whole circuit. When we consider the power of the distortion at the output node, we obtain:

$$\begin{aligned} \mathbb{E}\left\{D_t D_t^{\mathsf{H}}\right\} =& \mathbb{E}\left\{\mathbf{T}_{\text{out}}\mathbf{D}\left(\mathbf{T}_{\text{out}}\mathbf{D}\right)^{\mathsf{H}}\right\} \\ =& \mathbf{T}_{\text{out}}\mathbb{E}\left\{\mathbf{D}\mathbf{D}^{\mathsf{H}}\right\}\mathbf{T}_{\text{out}}^{\mathsf{H}} \\ =& \mathbf{T}_{\text{out}}\mathbf{C}_{\mathbf{D}}\mathbf{T}_{\text{out}}^{\mathsf{H}} \end{aligned}$$

this can be re-written as

$$\mathbb{E}\left\{D_t D_t^{\mathsf{H}}\right\} = \sum_{i=1}^{N}\sum_{j=1}^{N} T_{[i]}T_{[j]}^{\mathsf{H}}\left[\mathbf{C}_{\mathbf{D}}\right]_{i,j}$$

Here, we use the notation $[\mathbf{X}]_{i,j}$ to indicate the element on the i^{th} row and the j^{th} column of the matrix $\mathbf{X}$. This sum now contains all the distortion contributions and is the core of the DCA as it splits the power of the distortion at the output of the system into a sum of distortion contributions from each of the sub-blocks and some contributions due to the correlation between the distortion sources.

The contributions which are due to the diagonal elements of $\mathbf{C_D}$ will be called *direct distortion contributions*. The direct distortion contribution due to stage i will be indicated as $C_{[i]}$. The direct distortion contributions will always be positive real numbers:

$$C_{[i]} = T_{[i]} T_{[i]}^{\mathsf{H}} [\mathbf{C_D}]_{i,i} = \left|T_{[i]}\right|^2 [\mathbf{C_D}]_{i,i}$$

The contributions due to correlation between two distortion sources will be called *correlation distortion contributions*. We will indicate the correlation distortion contribution due to stages i and j as $C_{[i,j]}$.

$\mathbf{C_D}$ is a Hermitian matrix, so $[\mathbf{C_D}]_{i,j} = \left([\mathbf{C_D}]_{j,i}\right)^{\mathsf{H}}$. Due to this property, $C_{[i,j]}$ and $C_{[j,i]}$ can always be combined to obtain a single real-valued correlation contribution:

$$\begin{aligned} C_{[i,j]} &= T_{[i]} T_{[j]}^{\mathsf{H}} [\mathbf{C_D}]_{i,j} + T_{[j]} T_{[i]}^{\mathsf{H}} [\mathbf{C_D}]_{j,i} \\ &= 2\Re\left\{ T_{[i]} T_{[j]}^{\mathsf{H}} [\mathbf{C_D}]_{i,j} \right\} \end{aligned}$$

This makes that the correlation contributions are real numbers, which can be either positive or negative. Negative correlation contributions indicate that a certain distortion source is working to compensate the distortion introduced by another sub-block.

Combining the information about the direct and correlation contributions, we finally obtain

$$\begin{aligned} \mathbb{E}\left\{ D_t D_t^{\mathsf{H}} \right\} &= \sum_{i=1}^{N} \left|T_{[i]}\right|^2 [\mathbf{C_D}]_{i,i} + \sum_{i=2}^{N} \sum_{j=1}^{i-1} 2\Re\left\{ T_{[i]} T_{[j]}^{\mathsf{H}} [\mathbf{C_D}]_{i,j} \right\} \\ &= \sum_{i=1}^{N} C_{[i]} + \sum_{i=2}^{N} \sum_{j=1}^{i-1} 2\Re\left\{ C_{[i,j]} \right\} \end{aligned} \tag{4.3}$$

So in a circuit with N SISO sub-circuits, there will be $1/2N(N+1)$ distortion contributions of which N are direct contributions. The remaining $1/2N(N-1)$ contributions are correlation contributions.

Example 4.1: A non-linear stage followed by its inverse

This example analyses the cascade of two static non-linear blocks. The first non-linear block is an exponential function and the second its inverse: a logarithm. The cascade of both blocks results in a perfectly linear system.

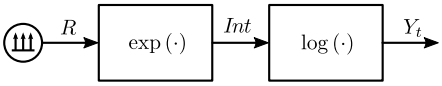

The system is excited by a random-phase multisine with a frequency resolution $f_{\text{res}} = 1\text{Hz}$ which excites all frequencies up to $f_{\text{max}} = 100\text{Hz}$. The root mean square (rms) of the multisine was set to 0.5V.
The steady-state spectrum for the signal measured between the two non-linear blocks is shown below.

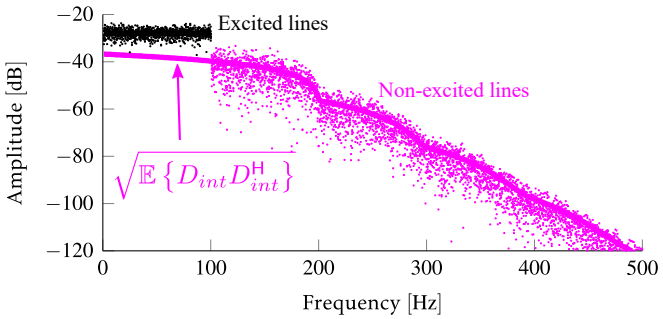

The frequency bins excited by the multisine are shown in black, the remaining frequency lines in magenta. The measured distortion power at the internal signal is shown with the magenta line in the plot. The amount of non-linear distortion at the intermediate signal in this cascade is very high (signal to distortion ratio of 10dB), but all the distortion is completely cancelled out by the second block, so that the input and output signals are exactly the same. We calculate the BLA of the two non-linear blocks using 10000 phase realisations of the multisine. The obtained result is shown below.

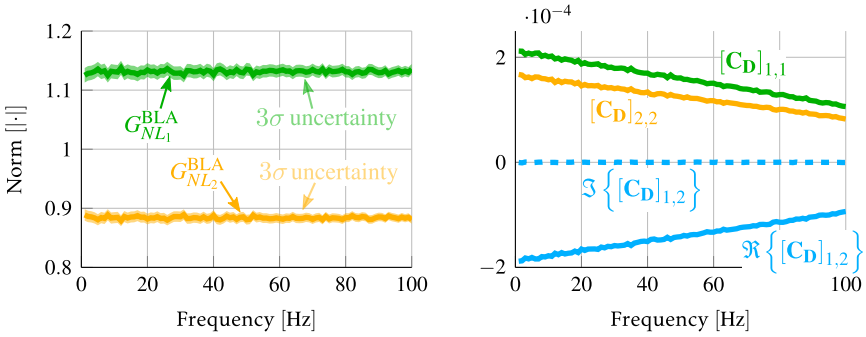

The plot on the right shows the elements of the obtained $\mathbf{C_D}$. The two diagonal elements express the power of the distortion added by each of the non-linear blocks. The off-diagonal element represents the correlation between the two distortion sources. The FRF from each distortion source to the output can easily be derived for this circuit:

$$T_{[1]} = G^{\text{BLA}}_{NL_2} \qquad T_{[2]} = 1$$

The three distortion contributions to the output can now be calculated. The direct contributions due to the first and second stage are

$$C_{[NL_1]} = \left|G^{\text{BLA}}_{NL_2}\right|^2 [\mathbf{C_D}]_{1,1} \qquad C_{[NL_2]} = [\mathbf{C_D}]_{2,2}$$

The correlation contribution is given by

$$C_{[NL_1,NL_2]} = G^{\text{BLA}}_{NL_2} [\mathbf{C_D}]_{1,2}$$

The obtained contributions are plotted below:

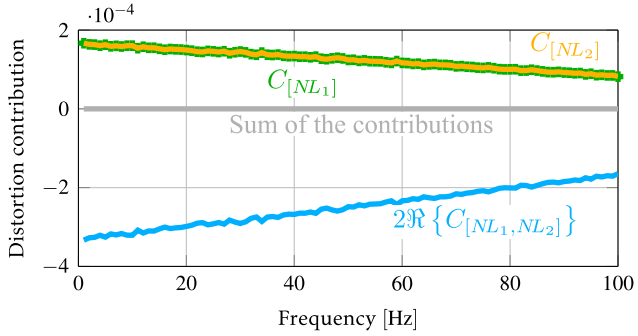

The two direct contributions are equal in amplitude. The correlation equal to the sum of the two direct contributions, but opposite in sign. The sum of all contributions (shown in gray on the plot above) therefore lies very close to zero.

The above example demonstrates how the BLA-based DCA would behave during the analysis of the non-linear distortion in an electronic system with pre-distortion. In modern high-frequency power amplifiers, the non-linear distortion added by the power amplifier is reduced by pre-distorting its input signal such that the distortion in the resulting output signal is minimal [Ghan 09].

In our proposed framework, both the power amplifier and the pre-distortion module will create direct contributions to the distortion at the output of the total circuit. The BLA-based method cannot distinguish between the wanted non-linear distortion generated by the pre-distortion module and additional unwanted non-linear distortion. When the pre-distortion module is working properly however, both direct contributions will be equal in size and the correlation contribution will cancel out both contributions perfectly, as is demonstrated in the above example.

With some further research, the proposed DCA could be used to assess the performance of pre-distortion systems, but this is considered outside the scope of this thesis. Initial steps towards using the BLA during the design of pre-distortion systems in combination with Iterative Learning Control as explained in [Scho 17].

Example 4.2: DCA of two non-linear stages in feedback

As a second example of a BLA-based DCA on the system level, consider two non-linear stages that are placed in a feedback configuration:

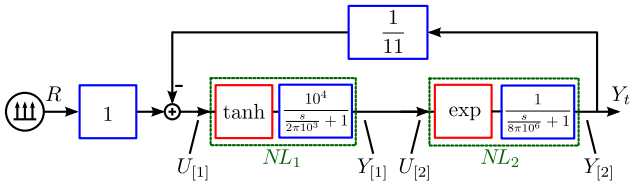

The first stage consists of a $\tanh(\cdot)$ non-linear block followed by a linear block with a single pole at 1kHz and a DC gain of 10000. The second non-linear block consists of an $\exp(\cdot)$ non-linear block followed by a linear block with a DC gain of 0dB and a single pole at 40MHz. The feedback block is a static linear block with a gain of $1/11$.
The circuit is excited by a random-phase multisine with a base frequency f_0 of 1kHz. The multisine excites all frequencies up to 1MHz. The output signal Y_t obtained under different phase realisations of the multisine is shown below. The rms of the distortion at the output of the circuit is indicated with the magenta line.

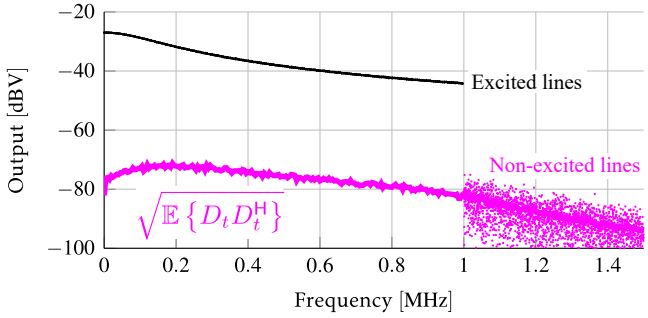

The BLA of the two non-linear stages is determined using the classic techniques to determine the BLA in feedback. 100 phase realisations of the input multisine were used in the averaging. The obtained BLAs and their uncertainties are shown below.

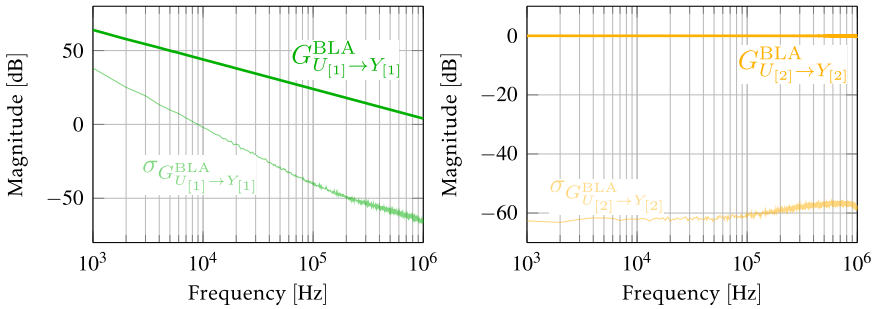

Because there are two SISO non-linear sub-circuits, the distortion matrix $\mathbf{C_D}$ is a 2×2 matrix. The frequency responses from the distortion sources to the output signal are given by

$$T_{[1]} = \frac{1}{L} G^{\mathrm{BLA}}_{U_{[2]}\to Y_{[2]}} \qquad T_{[2]} = \frac{1}{L} \qquad \text{with} \qquad L = 1 + \frac{G^{\mathrm{BLA}}_{U_{[1]}\to Y_{[1]}} G^{\mathrm{BLA}}_{U_{[2]}\to Y_{[2]}}}{11}$$

The distortion contributions to the output can be calculated using these FRFs. There are two direct distortion contributions

$$C_{[1]} = \left| \frac{G^{\mathrm{BLA}}_{U_{[2]}\to Y_{[2]}}}{L} \right|^2 [\mathbf{C_D}]_{1,1} \qquad C_{[2]} = \left| \frac{1}{L} \right|^2 [\mathbf{C_D}]_{2,2}$$

and a correlation contribution

$$C_{[1,2]} = \frac{G^{\mathrm{BLA}}_{U_{[2]}\to Y_{[2]}}}{|L|^2} [\mathbf{C_D}]_{1,2}$$

These three different contributions are plotted as a function of frequency below. The gray line that was added is the power of the distortion at the output node.

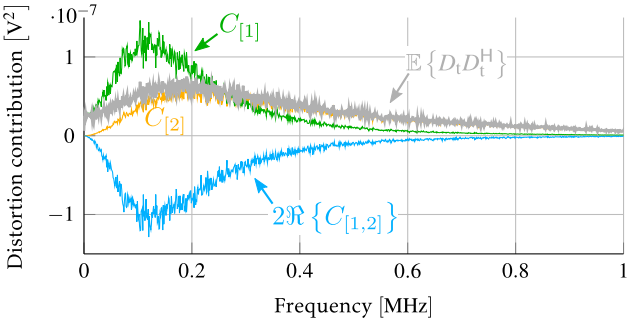

At low frequencies, the first stage is the dominant source of distortion. In the higher frequency range, the second stage contributes more.

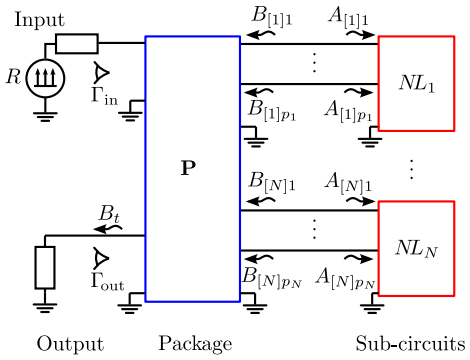

Figure 4.4.: The circuit under test will consist of N non-linear sub-circuits embedded in a linear package. The whole circuit is excited by a reference signal R. The goal of the DCA is split the distortion in the output wave B_t into its contributions.

4.2. Distortion Contribution Analysis on the circuit level

This section extends the DCA to determine the distortion contributions in a circuit-level simulation. Circuit level sub-circuits can have non-ideal input and output impedances and a significant reverse gain. A port-based representation is therefore needed to properly model the behaviour of the sub-circuits in circuit-level simulations.

In this thesis, S-parameters are used as the circuit representation of choice. We work with a wave-based representation because the S-parameters of interconnections, like a through or an open, still give rise to matrices which don't contain infinity as one of its parameters, unlike the Y or Z parameters in those special cases. Calculating the distortion contributions to the output signal then requires so a noise analysis based on S-parameters.

It was explained in chapter 3 that the BLA of a circuit multiple ports is a MIMO BLA. Herein lies the main difference for the DCA compared to the system-level DCA: The sub-circuits are MIMO blocks instead of SISO sub-blocks.

The general circuit studied in this section is shown in Figure 4.4. The total circuit is a two-port. The input port of the circuit is excited by a source with a modulated signal and a reflection factor $\Gamma_{\text{in}}(j\omega_k)$. The output of the circuit is loaded by an output impedance with a reflection factor $\Gamma_{\text{out}}(j\omega_k)$.

The circuit contains N non-linear sub-circuits where each of these sub-circuits has p_n ports. The total amount of sub-circuit ports will be indicated with P

$$P = \sum_{n=1}^{N} p_n$$

The incident and reflected waves at the p^{th} port of the n^{th} sub-circuit are indicated as $A_{[n]p}(k)$ and $B_{[n]p}(k)$ respectively. They are gathered in two vectors:

$$\mathbf{B}_{[n]}(k) = \begin{bmatrix} B_{[n]1}(k) \\ \vdots \\ B_{[n]p_n}(k) \end{bmatrix} \qquad \mathbf{A}_{[n]}(k) = \begin{bmatrix} A_{[n]1}(k) \\ \vdots \\ A_{[n]p_n}(k) \end{bmatrix}$$

The relation between these two wave vectors is given by the S^{BLA}-parameters of the sub-circuit

$$\mathbf{B}_{[n]}(k) = \mathbf{S}^{\text{BLA}}_{\mathbf{A}_{[n]}\to\mathbf{B}_{[n]}}(j\omega_k)\,\mathbf{A}_{[n]}(k) + \mathbf{D}_{[n]}(k)$$

where the S^{BLA}-parameters are indicated with $\mathbf{S}^{\text{BLA}}_{\mathbf{A}_{[n]}\to\mathbf{B}_{[n]}}(j\omega_k) \in \mathbb{C}^{p_n\times p_n}$. The distortion introduced by the sub-circuit is a vector $\mathbf{D}_{[n]}(k) \in \mathbb{C}^{p_n\times 1}$.

The N sub-circuits are embedded in a linear package represented by a FRM $\mathbf{P}(j\omega_k) \in \mathbb{C}^{2P\times 2P}$.

The distortion at the output wave of the system is defined by considering the BLA from the reference multisine to the output wave B_t

$$B_t(k) = G^{\text{BLA}}_{R\to B_t}(j\omega_k)\,R(k) + D_t(k) \tag{4.4}$$

The goal of the DCA is to write the power in D_t as the sum of contributions from each of the sub-circuits.

Performing a DCA on the circuit level is very similar to the DCA on the system level with SISO sub-circuits. The three basic steps to perform a BLA-based DCA remain:

1. Determine the BLA of the non-linear sub-circuits ($\mathbf{S}^{\text{BLA}}_{\mathbf{A}_{[n]}\to\mathbf{B}_{[n]}}$)
2. Determine the distortion introduced by each sub-circuit ($\mathbf{D}_{[n]}$)
3. Refer the distortion of each non-linear sub-circuit to the output signal D_t

Step 1: Determine the BLA of each sub-circuit

The S^{BLA}-parameters of each sub-circuit can be determined using the experiments and simulations detailed in chapter 3. Determining these MIMO BLAs can be very time-consuming for large circuits. When the circuit is weakly non-linear, the BLAs can be approximated by its small-signal behaviour, so the small-signal S-parameters can be used to approximate the BLA.

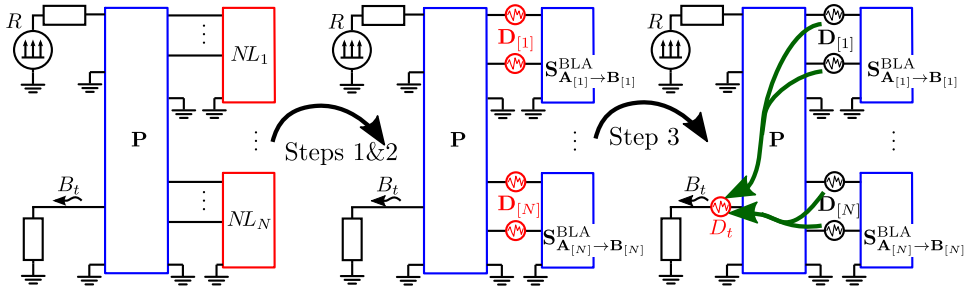

Figure 4.5.: Three-step procedure needed to perform a BLA-based DCA on the circuit level.

Step 2: Determine the distortion introduced by each stage

Just like in the system-level DCA, the distortion introduced by the sub-circuits can be correlated. To obtain an unbiased estimate of their covariance matrix, all the sub-circuits should be treated together. To this end, the $\mathbf{A}_{[n]}$ and $\mathbf{B}_{[n]}$ are gathered in two large vectors:

$$\mathbf{B}(k) = \begin{bmatrix} \mathbf{B}_{[1]}(k) \\ \vdots \\ \mathbf{B}_{[N]}(k) \end{bmatrix} \in \mathbb{C}^{P\times 1} \qquad \mathbf{A}(k) = \begin{bmatrix} \mathbf{A}_{[1]}(k) \\ \vdots \\ \mathbf{A}_{[N]}(k) \end{bmatrix} \in \mathbb{C}^{P\times 1}$$

The relation between $\mathbf{B}(k)$ and $\mathbf{A}(k)$ is now given by:

$$\mathbf{B}(k) = \mathbf{S}^{\mathrm{BLA}}_{\mathbf{A}\to\mathbf{B}}(j\omega_k)\,\mathbf{A}(k) + \mathbf{D}(k)$$

where $\mathbf{S}^{\mathrm{BLA}}_{\mathbf{A}\to\mathbf{B}}(j\omega_k) \in \mathbb{C}^{P\times P}$ is the block diagonal matrix which contains all BLAs of the sub-circuits:

$$\mathbf{S}^{\mathrm{BLA}}_{\mathbf{A}\to\mathbf{B}}(j\omega_k) = \begin{bmatrix} \mathbf{S}^{\mathrm{BLA}}_{\mathbf{A}_{[1]}\to\mathbf{B}_{[1]}}(j\omega_k) & \cdots & \mathbf{0} \\ \vdots & \ddots & \vdots \\ \mathbf{0} & \cdots & \mathbf{S}^{\mathrm{BLA}}_{\mathbf{A}_{[N]}\to\mathbf{B}_{[N]}}(j\omega_k) \end{bmatrix} \tag{4.5}$$

The vector of distortion sources $\mathbf{D}(k) \in \mathbb{C}^{P\times 1}$ is again noise-like, which can be characterised by its the covariance matrix $\mathbf{C_D} = \mathbb{E}\{\mathbf{D}\mathbf{D}^{\mathrm{H}}\}$.

Determining $\mathbf{C_D}$ is again done in a two-step procedure. First, the BLA from the reference multisine to the stacked output-input vector is used to obtain the

covariance matrix of the distortion at the output-input vector[1]:

$$\mathbf{D}_{\mathbf{Z}}^{\{m\}}(k) = \begin{bmatrix} \mathbf{B}^{\{m\}}(k) \\ \mathbf{A}^{\{m\}}(k) \end{bmatrix} - \begin{bmatrix} \mathbf{G}_{R\to\mathbf{B}}^{\mathrm{BLA}}(j\omega_k) \\ \mathbf{G}_{R\to\mathbf{A}}^{\mathrm{BLA}}(j\omega_k) \end{bmatrix} R^{\{m\}}(k)$$

$$\mathbf{C}_{\mathbf{D_Z}}(j\omega_k) = \mathbb{E}\left\{\mathbf{D}_{\mathbf{Z}}(k)\mathbf{D}_{\mathbf{Z}}^{\mathsf{H}}(k)\right\} \cong \frac{1}{M-1}\sum_{m=1}^{M} \mathbf{D}_{\mathbf{Z}}^{\{m\}}(k)\left(\mathbf{D}_{\mathbf{Z}}^{\{m\}}(k)\right)^{\mathsf{H}}$$

$\mathbf{C}_{\mathbf{D_Z}}(j\omega_k) \in \mathbb{C}^{2P\times 2P}$ is the covariance matrix of the distortion measured at all outputs and inputs of the sub-circuits. To obtain a full-rank estimate of $\mathbf{C}_{\mathbf{D_Z}}$, at least $2P$ phase realisations of the reference multisine must be simulated. The covariance matrix of the distortion sources $\mathbf{C_D}$ is finally obtained as

$$\mathbf{C}_{\mathbf{D}}(j\omega_k) = \begin{bmatrix} \mathbf{I}_N & -\mathbf{S}_{\mathbf{A}\to\mathbf{B}}^{\mathrm{BLA}}(j\omega_k) \end{bmatrix} \mathbf{C}_{\mathbf{D_Z}}(j\omega_k) \begin{bmatrix} \mathbf{I}_N & -\mathbf{S}_{\mathbf{A}\to\mathbf{B}}^{\mathrm{BLA}}(j\omega_k) \end{bmatrix}^{\mathsf{H}}$$

Step 3: Calculate the contributions to the output

In the third step of the DCA, the FRF from each of the distortion sources to the output wave of the total circuit needs to be calculated. This is done with an algorithm similar to the one described in [Dobr 89]. All S-matrices of the components in the circuit are gathered in a matrix $\mathbf{T}_{\mathrm{all}}(j\omega_k)$

$$\mathbf{T}_{\mathrm{all}}(j\omega_k) = \begin{bmatrix} \Gamma_{\mathrm{in}}(j\omega_k) & & & \\ & \Gamma_{\mathrm{out}}(j\omega_k) & & \\ & & \mathbf{P}(j\omega_k) & \\ & & & \mathbf{S}_{\mathbf{A}\to\mathbf{B}}^{\mathrm{BLA}}(j\omega_k) \end{bmatrix} \in \mathbb{C}^{(2P+4)\times(2P+4)}$$

This matrix expresses a set of equations which link a large vector of B-waves to a large vector of A-waves. A vector of generators $\mathbf{N}$ is added to obtain the following relation:

$$\mathbf{B}_{\mathrm{all}}(k) = \mathbf{T}_{\mathrm{all}}(j\omega_k)\mathbf{A}_{\mathrm{all}}(k) + \mathbf{N}(k)$$

Some of the waves in $\mathbf{A}_{\mathrm{all}}$ and $\mathbf{B}_{\mathrm{all}}$ are equal, because they are interconnected in the circuit. These equalities between the A and B-waves are expressed by an interconnection matrix $\mathbf{C}$

$$\mathbf{C} = \begin{bmatrix} \mathbf{0}_{2\times 2} & \mathbf{I}_{2\times 2} & & \\ \mathbf{I}_{2\times 2} & \mathbf{0}_{2\times 2} & & \\ & & \mathbf{0}_{P\times P} & \mathbf{I}_{P\times P} \\ & & \mathbf{I}_{P\times P} & \mathbf{0}_{P\times P} \end{bmatrix}$$

[1] When the small-signal S-parameters are used to approximate the BLA, the factor $1/M-1$ in the calculation of the covariance matrix should be replaced by a factor $1/M$

We can combine the previous expressions to obtain all the A-waves in the circuit as a function of the generators in the circuit.

$$\mathbf{A}_{\text{all}} = (\mathbf{C} - \mathbf{T}(j\omega_k))^{-1}\mathbf{N}(k) = \mathbf{W}^{-1}(j\omega_k)\mathbf{N}(k)$$

$\mathbf{W}(j\omega_k)$ is called the *connection scattering matrix* of the circuit [Dobr 89, Mona 74], its inverse contains the FRF from each of the possible generators in the circuit to all of the A-waves in the circuit. We want the FRFs from each of the distortion sources to the wave incident to the load of the circuit, which are the P last elements of the second row of $\mathbf{W}^{-1}$. This finally leads to the expression:

$$\mathbf{T}_{\text{out}}(j\omega_k) = \left[\mathbf{W}^{-1}(j\omega_k)\right]_{2,P+5..2P+4}$$

Like in the system-level DCA, $\mathbf{T}_{\text{out}}$ provides the link between the covariance matrix of distortion sources and the total distortion power at the output of the circuit:

$$\mathbb{E}\left\{D_t D_t^{\mathsf{H}}\right\}(k) = \mathbf{T}_{\text{out}}(j\omega_k)\,\mathbf{C}_{\mathbf{D}}(j\omega_k)\,\mathbf{T}_{\text{out}}^{\mathsf{H}}(j\omega_k)$$

This expression can be re-written as

$$\begin{aligned}\mathbb{E}\left\{D_t D_t^{\mathsf{H}}\right\}(k) = &\sum_{p=1}^{P}\left|T_{[p]}(j\omega_k)\right|^2\left[\mathbf{C}_{\mathbf{D}}(j\omega_k)\right]_{p,p}\\ &+\sum_{p=2}^{P}\sum_{q=1}^{p-1}2\Re\left\{T_{[p]}(j\omega_k)\,T_{[q]}^{\mathsf{H}}(j\omega_k)\left[\mathbf{C}_{\mathbf{D}}(j\omega_k)\right]_{p,q}\right\}\end{aligned}$$

The amount of distortion contributions in circuit-level simulations is determined by the amount of ports on the sub-circuits in the circuit. There are P direct contributions and $1/2P(P-1)$ correlation contributions. The amount of contributions can however easily be reduced by combining the contributions of each sub-circuit. A two-port sub-circuit, for example, will create 3 distortion contributions, two direct contributions and one correlation contribution which can be summed together to obtain a single contribution of the sub-circuit. The correlation contributions between two different sub-circuits can be combined in a similar way to obtain a single correlation contribution for the two sub-circuits. With all these combinations, the amount of distortion contributions in a circuit with N sub-circuits can be reduced to N direct contributions and $1/2N(N-1)$ correlation contributions.

If this amount of contributions is still too large for an easy interpretation of the results, the contributions of several sub-circuits can be combined into one contribution of a larger sub-circuit. It is a clear advantage that the BLA-based DCA can easily be applied hierarchically as this allows to zoom in selectively on the most contributing parts of the circuit, while leaving the other sub-circuits aggregated at a higher level of abstraction.

Example 4.3: DCA of a two-stage Miller Op-amp

We will demonstrate step-by-step how the circuit-level DCA can be used to determine the distortion contributions in an amplifier. Consider a low-frequency amplifier consisting of a two-stage Miller Operational Amplifier (op-amp) in an inverting feedback configuration with a gain of 4. The amplifier is loaded by a capacitance of 10pF.

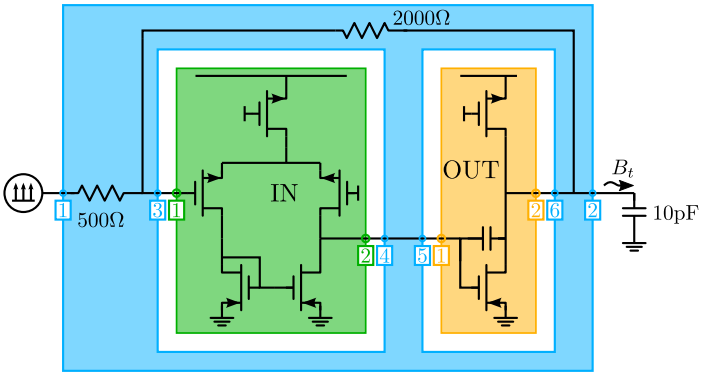

We will use the DCA to find out which of the two stages in the op-amp contributes most to the non-linear distortion at the output port of the amplifier. The two stages in the op-amp are considered as the sub-circuits in the DCA. They are indicated in red and blue in the schematic. Each sub-circuit has two-ports. The two-sub-circuits are embedded in a package which is indicated in green. Hence, the package contains 6 ports: two external ports and four internal ports connected to the two sub-circuits. The whole circuit is excited by a lowpass random-odd random-phase multisine with a frequency resolution of $f_{\text{res}} = 100\text{kHz}$ and $f_{\text{max}} = 10\text{MHz}$. The multisine source is a perfect voltage source and its rms voltage is set to 0.1V. The response of the amplifier to 100 different phase realisations of the multisine was obtained with Harmonic Balance (HB). The simulator settings were set using the guidelines explained in Appendix A. The spectrum of the output wave of the amplifier for some of the multisine realisations is shown below, a reference impedance of 50Ω was used to calculate the wave.

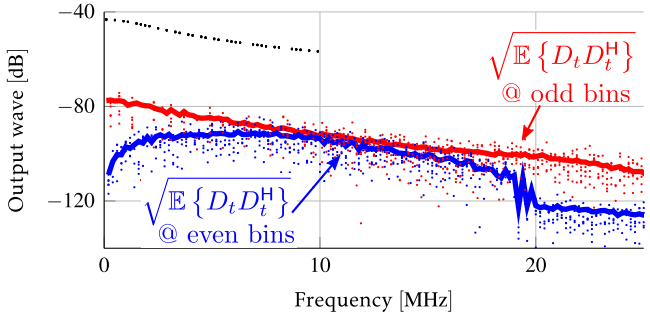

The frequency lines excited by the multisine are shown in black, the even frequency lines in blue and the non-excited frequency lines in red. The rms of the distortion in the output wave is shown with a red and blue line for the odd and even non-linear distortion respectively. The DCA will calculate the contributions of the two different stages to this output distortion. There will be 4 direct contributions and 6 correlation contributions.
A Miller op-amp in feedback can be considered as a weakly non-linear circuit, so the small-signal behaviour of the different circuits is used instead of the BLA to save simulation time. We will confirm later that this small-signal assumption holds. The small-signal Z-parameters for both sub-circuits are shown below.

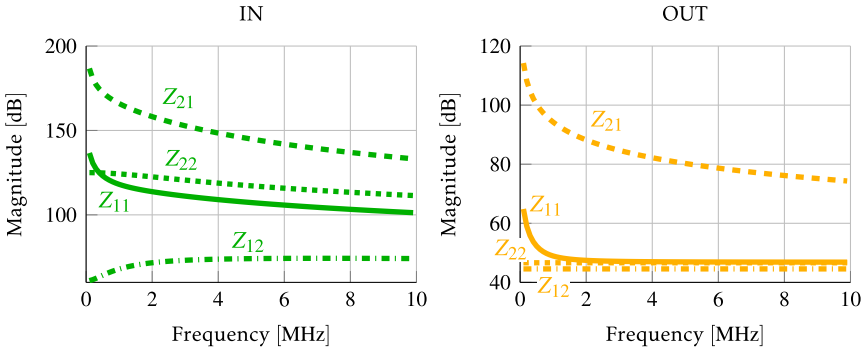

In the DCA, the S-parameters of the two stages were used, but the S-parameters don't provide a very interesting graph for these sub-circuits. The reference impedance for the S-parameters was also chosen 50Ω. The small-signal S-parameters of the sub-circuits are gathered into a block diagonal matrix which is to calculate the distortion covariance matrix $\mathbf{C_D}$.

In this circuit, the distortion covariance matrix is a 4×4 matrix for every frequency.
The S-matrix of the package around the two sub-circuits is given by

$$\mathbf{P}(j\omega_k) = \begin{bmatrix} 0.833 & 0.02 & 0.163 & 0 & 0 & 0.002 \\ 0.002 & -0.012 & 0.022 & 0 & 0 & 0.988 \\ 0.163 & 0.022 & 0.793 & 0 & 0 & 0.022 \\ 0 & 0 & 0 & 0 & 1 & 0 \\ 0 & 0 & 0 & 1 & 0 & 0 \\ 0.002 & 0.988 & 0.022 & 0 & 0 & -0.012 \end{bmatrix}$$

The port numbers are indicated on the schematic of the circuit shown above. The multisine source is an ideal voltage source, so it presents a perfect short to the circuit at the input. The output port of the circuit is loaded by a capacitor of 10pF. This gives the two following reflection factors at the input and output of the circuit

$$\Gamma_{\text{in}}(j\omega_k) = -1 \qquad \Gamma_{\text{out}}(j\omega_k) = \frac{1 - j\omega_k 50 \cdot 10\text{pF}}{1 + j\omega_k 50 \cdot 10\text{pF}}$$

The combination of the BLAs, the package and the loads allows to calculate the four FRFs from each distortion source to the output wave of the circuit. The four FRFs are shown below:

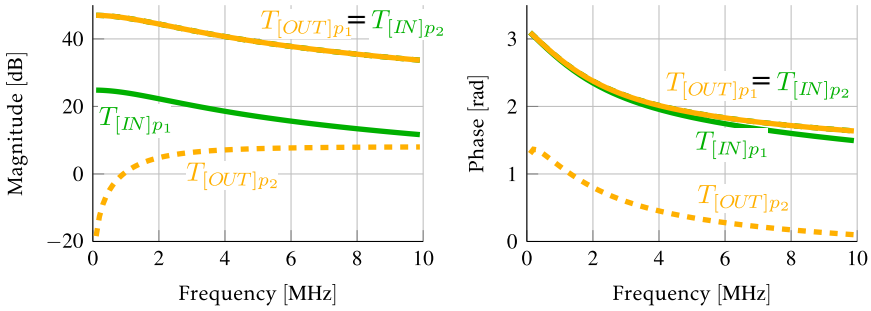

These FRFs are then used to calculate the 10 distortion contributions in the circuit. Showing all 10 contributions is difficult, so the contributions are combined into three large contributions: one direct contribution for the input stage ($C_{[IN]}$), one direct contribution for the output stage ($C_{[OUT]}$) and a single correlation contribution $C_{[IN,OUT]}$. These three contributions

are obtained as

$$
\begin{aligned}
C_{[IN]} &= C_{[IN_1]} + C_{[IN_2]} + 2\Re\left\{C_{[IN_1,IN_2]}\right\} \\
C_{[OUT]} &= C_{[OUT_1]} + C_{[OUT_2]} + 2\Re\left\{C_{[OUT_1,OUT_2]}\right\} \\
C_{[IN,OUT]} &= 2\Re\left\{C_{[IN_1,OUT_1]} + C_{[IN_2,OUT_1]} + C_{[IN_1,OUT_2]} + C_{[IN_2,OUT_2]}\right\}
\end{aligned}
$$

where $C_{[IN_1]}$ is, for example, the direct contribution due to the first port of the input stage of the op-amp.
An odd multisine was used as an excitation signal. Hence all the odd-order non-linear distortion generated by the circuit can be found at the odd frequency lines, while the even-order distortion is found at the even frequency lines. Due to this, two distinct sets of distortion contributions can be obtained: one for the even-order distortion and a second for the odd-order distortion.
The odd-order distortion contributions are shown below:

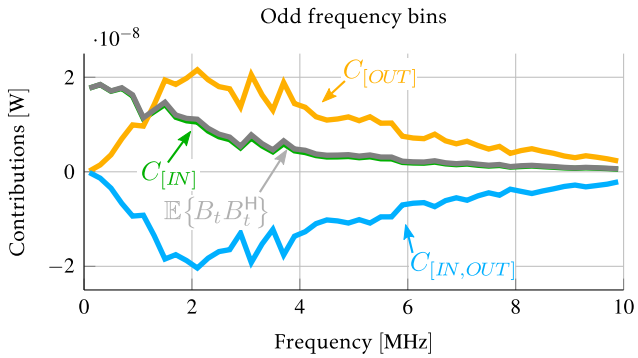

It can be concluded that the input stage determines the odd-order distortion level. The distortion introduced by the output stage is completely cancelled by the correlation contribution.
For the even-order non-linear distortion, the story is completely different. The distortion contributions to the even-order distortion at the output node are shown below:

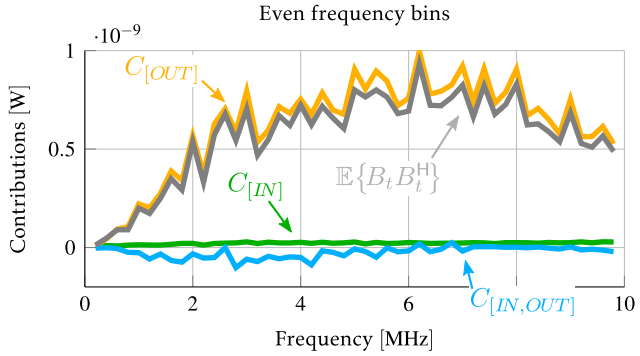

The output stage clearly dominates the even-order non-linear distortion, the input stage doesn't introduce a lot of even distortion, which is to be expected for a differential pair.
Finally, the validity of the small-signal assumption used in the DCA is verified. To do this, the small-signal FRF from the reference to the signals in the circuit is compared to the BLA. This BLA can be calculated easily, as it is a SIMO BLA. In this circuit, the largest difference was observed at the output wave of the second stage. Both the small-signal FRF $G^{\text{LIN}}_{R\to B_{[OUT]2}}$ and the BLA $G^{\text{BLA}}_{R\to B_{[OUT]2}}$ are plotted

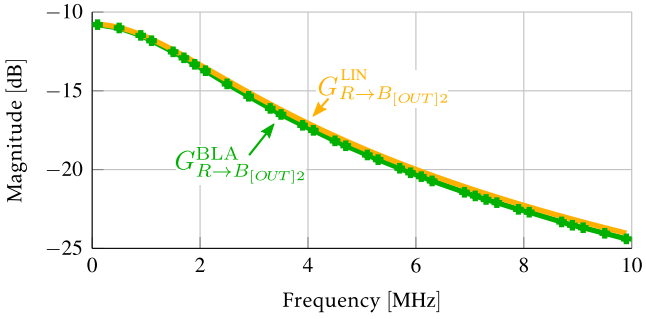

The compression of the amplifier is visible, but difference between the BLA and the small-signal FRF remains below 1dB, so the small-signal assumption is valid for this circuit.

Example 4.4: DCA of a Doherty power amplifier

The second circuit-level example that will be considered is a Doherty power amplifier found in the example library of Keysight's Advanced Design System (ADS). By performing the DCA of this amplifier, we demonstrate that the BLA-based DCA can also be used to determine the distortion contributions in a strongly non-linear circuit. The amplifier is built with two Freescale MRF8S21100H transistors for a center frequency of 2.14GHz.

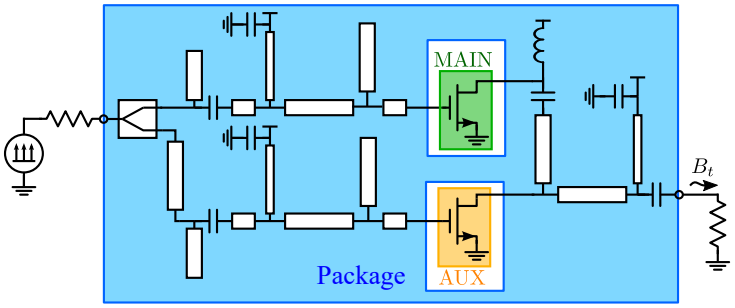

The main transistor is biased in class-AB with a quiescent current of 0.7A. The auxiliary transistor is biased deep in class-C with a quiescent current of 1mA.

The amplifier is excited by a multisine that excites 41 frequency bins in a band of 10MHz around 2.14GHz. The rms of the input multisine is 3V. The steady-state response of the circuit to the multisine excitation is obtained with a HB simulation configured as explained in Appendix A. The output wave around the center frequency is shown below

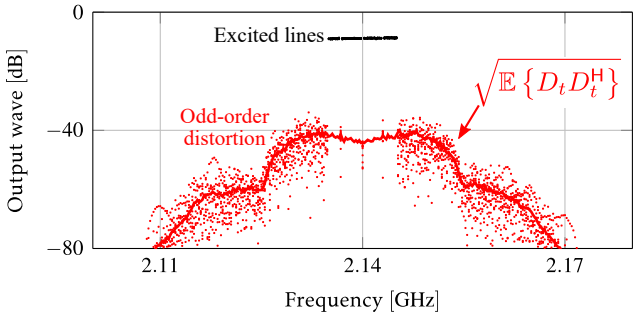

This circuit can be considered strongly non-linear, especially the auxiliary amplifier. To obtain the BLA of the two transistors in the circuit, the

techniques detailed in chapter 3 are used. A tickler multisine is added to the circuit at the output of the total amplifier. The added multisine is a current source which inserts an rms current of 1μA on frequency bins in between the frequencies of the main multisine. The S^{BLA}-parameters obtained for both the main and auxiliary amplifier are shown below:

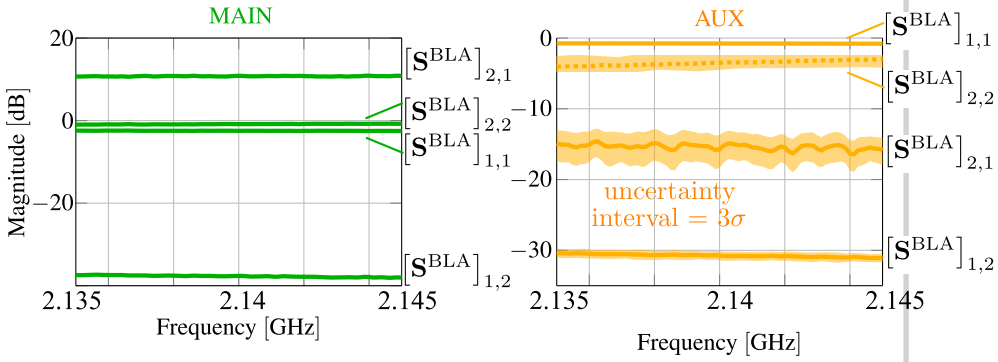

The S^{BLA}-parameters of the main amplifier do not deviate far from the small-signal S-parameters. For the auxiliary amplifier, a large difference is observed between the S^{BLA}-parameters and the small-signal amplifiers, which is to be expected for a transistor biased in class-C. With these two BLAs and the small-signal S-parameters of the package, we calculate the distortion contributions to the B_t wave of the circuit.
There are 10 distortion contributions in this circuit. Four direct contributions and 6 correlation contributions. The contributions due to the different ports in the circuit are combined in the following way:

$$
\begin{aligned}
C_{[MAIN]} &= C_{[MAIN_1]} + C_{[MAIN_2]} + 2\Re\left\{C_{[MAIN_1,MAIN_2]}\right\} \\
C_{[AUX]} &= C_{[AUX_1]} + C_{[AUX_2]} + 2\Re\left\{C_{[AUX_1,AUX_2]}\right\} \\
C_{[MAIN,AUX]} &= 2\Re\left\{C_{[MAIN_1,AUX_1]} + C_{[MAIN_1,AUX_2]} + C_{[MAIN_2,AUX_1]} + C_{[MAIN_2,AUX_2]}\right\}
\end{aligned}
$$

The resulting three distortion contributions are normalised with respect to the total distortion power in the input wave. The results are plotted below

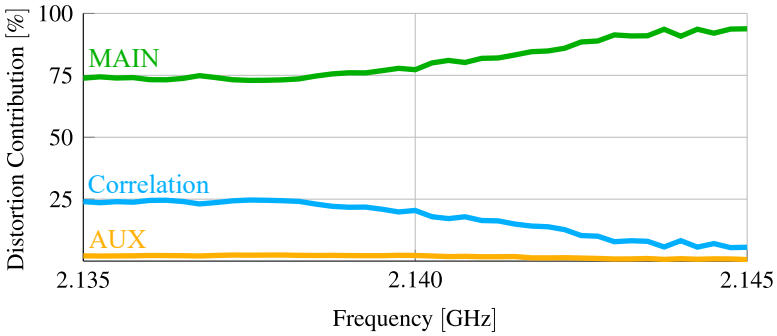

The dominant source of non-linear distortion is found to be the main transistor. This can be expected, as the auxiliary amplifier only kicks in for limited amounts of time in this Doherty configuration. A similar Doherty amplifier was analysed in [Aiki 12] with a DCA under two-tone excitation. It was concluded there that the auxiliary amplifier only contributes significantly to the distortion for very high amplitudes in the two-tone. With a modulated signal, like the multisines used in the BLA-based DCA, the peaks only occur from time to time, so its average contribution to the total distortion is low.

The information given by the BLA-based DCA is limited for the Doherty power amplifier, because only the signals around the carrier frequency are used here. Designers are also interested in how the low-frequency signals in the bias network are up-converted in-band through the second-order non-linearities [Aiki 11]. The current implementation of the DCA doesn't split the up-converted low-frequency signals from the high-frequency odd-order non-linear distortion appearing in-band. A more advanced BLA-based DCA can be implemented using the higher-order BLAs [Thor 11b]. This extension of the method is however considered to be outside of the scope of this thesis.

Example 4.5: DCA of a Gm-C filter

With this final example, we will demonstrate that the BLA-based DCA can also be used to analyse larger, hierarchical circuits. We reconsider the active filter from chapter 1. The filter is a fully differential Gm-C biquad [Kard 92] designed in a commercial 0.18μm CMOS technology. This circuit was designed by Dries Peumans, based on the master thesis of Stephane Bronckers. The circuit is shown below:

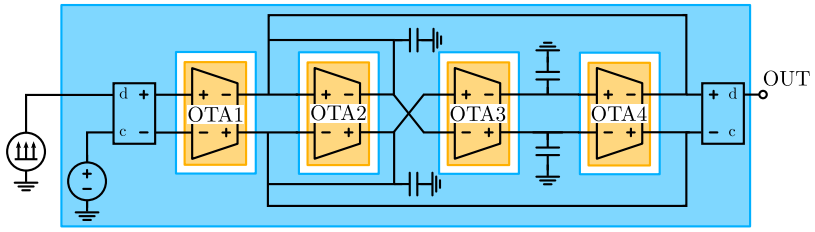

The biquad is configured to create a resonant pole pair at 10MHz. Perfect baluns were placed at the input and output of the biquad, to convert the signals into differential and common-mode signals. All Operational Transconductance Amplifiers (OTAs) are the same circuit, they are fully differential, so each OTA has 4 ports, 2 input ports and two output ports. The circuit of the OTAs circuit is shown below:

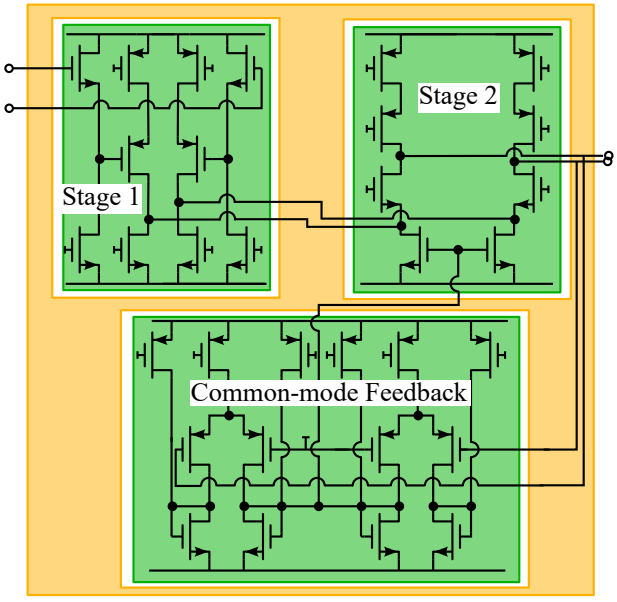

The OTA consists of an input stage (Stage 1) and a cascode stage (Stage 2) as shown in figure. The common-mode feedback in the transconductors is done actively and is considered as the third sub-block in the OTA.
The differential mode of the biquad is excited by full lowpass RPMs (all frequency lines are excited). The multisines have f_{res} =200kHz and f_{max} =100MHz. In a resonant system like this, the frequency resolution of the multisines should be chosen to have enough several lines in the resonance [Geer 13]. If, for example, only a single spectral line is placed in a sharp resonance, the PDF of the internal signals will tend to that of a sine wave, instead of the wanted Gaussian PDF. The wanted noise-like properties of the internal signals in the circuit then disappear, which is unwanted if the results are to be valid for Gaussian input signals. The rms of the multisines was set to 50mV and the steady-state response of the circuit to 50 different-phase multisines was obtained with HB. The HB simulator is configured as explained in Appendix A. The resulting spectrum at the differential output is shown below.

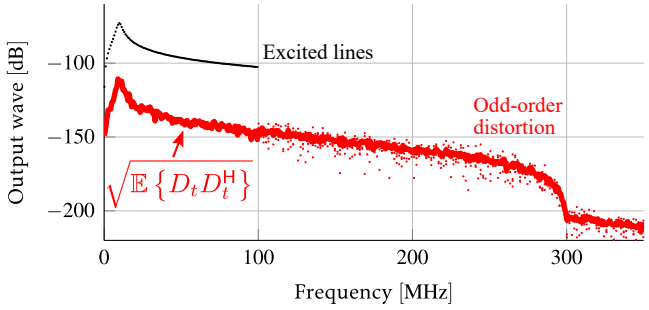

The distortion at the output lies 50dB below the signal level, so the circuit is behaving close to linear. No even-order contributions are present due to the differential nature and perfect symmetry in the simulations of the circuit. Note that the obtained odd-order distortion at the output shows a strong frequency dependence around the resonance.
The sub-circuits in this biquad are assumed to be weakly non-linear, so the 4-port S-parameters of each OTA were used in the DCA. This small-signal assumption was verified by comparing the frequency response from the input of the total circuit to each of the waves in the circuit with the corresponding BLAs. The largest difference was observed on the frequency response from the reference to the output waves of OTA4, but this difference

(shown in the figure below) is small enough to consider the small-signal assumption to be valid.

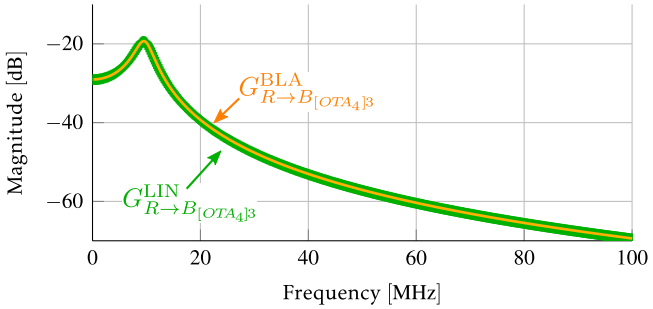

First, we apply the BLA-based DCA to calculate the distortion contributions of each OTA to the distortion in the output wave of the total circuit (B_t). There are four 4-port sub-circuits, which results in 120 distortion contributions of which 16 are direct distortion contributions. This number is clearly too large to be easily interpretable.
Additionally, due to the differential nature of the circuit, a lot of strong correlation between the distortion contributions is present. The contributions due to the two output signals of each OTA, for example, are very strongly correlated because the signals there only differ in sign. Having such a strong correlation and redundancy in the information returned by the DCA makes the results difficult to interpret. It is possible to transform the representation of each OTA to a mixed-mode representation [Ferr 06] to simplify the result [Coom 15]. Here we will just combine all contributions of each sub-circuit together in the same as we have done in the previous examples. When the contributions are combined only 10 contributions remain. We show the obtained contributions at 10MHz below

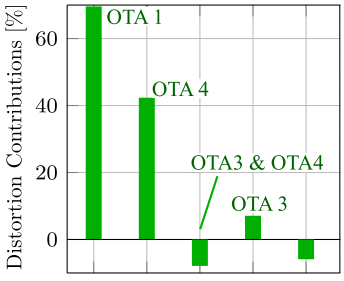

The first OTA is found to be the dominant source of distortion in the resonance peak of this circuit. The fourth OTA also introduces a considerable

contribution. To find out which part of the OTA is mainly responsible, the first and fourth OTA were split into three parts and the DCA was applied again. The obtained distortion contributions are shown below

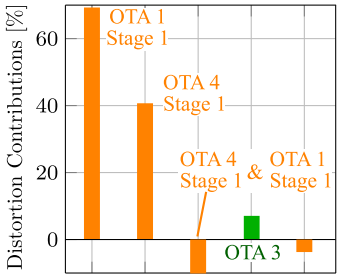

With this hierarchical application of the BLA-based DCA, it is found that the first stage of both OTAs 1 and 4 are the dominant contribution.
With this final example, we have demonstrated how the BLA-based DCA can be used in larger circuits and how it can be used hierarchically to zoom in on certain sub-circuits to determine the actual source of non-linear distortion.

Summary

In this chapter, we introduced the BLA-based Distortion Contribution Analysis (DCA) to determine the distortion contributions in an electronic circuit excited by a modulated signal. The proposed DCA combines the BLA with a noise analysis to calculate the distortion contributions.

A BLA-based DCA is a three-step procedure:

1. Determine the BLA of the non-linear sub-circuits
2. Determine the distortion introduced by each sub-circuit
3. Refer the distortion of each non-linear sub-circuit to the output signal

With these steps, we have shown that the power of the distortion added to the output signal can be written as the sum of direct contributions and correlation distortion contributions. The direct distortion contributions describe how each of the sub-circuits alone contributes to the total distortion while the correlation contributions represent the interaction between the distortion generated by two separate sub-circuits.

We have shown that this BLA-based DCA can be used to determine the distortion contributions in both circuit and system-level simulations. Through many

examples, we have shown that our DCA works for both weakly and strongly non-linear circuits and that can be applied hierarchically in larger circuits.

5. Local Stability Analysis

Stability analysis of non-linear systems operating under large-signal excitation is a topic I encountered as a side-track during my research. I was using Large-Signal Small-Signal (LSSS) *analyses to determine the BLA of of circuits when I found out that the* Harmonic Transfer Function (HTF) *can also be used to investigate the large-signal stability of amplifiers. This sparked my interest and led to a conference paper together with Francesco Ferranti and Ebrahim Louarroudi on the use of common-denominator modelling for stability analysis [Coom 16b].*

In a next step, the collaboration with Fabien Seyfert and Martine Olivi from INRIA, Sophia-Antipolis has led to a local stability analysis without the need to fit a rational model. The results of both collaborations are summarised in this chapter and in the upcoming publication [Coom 17b].

Stability analysis is an essential step in the design of active analog electronic circuits. An unstable circuit will generate spurious tones, which wastes energy, will introduce excessive distortion, will kill the overall performance of the circuit and might even lead to malfunction of the circuit. Instabilities hence have to be avoided at all costs.

Usually, a circuit designer focuses on meeting demands for the coverage of the frequency band in which the signals are present: the designer has to provide ample gain and synthesise proper input and output impedances in that band. The instabilities on the other hand usually occur outside the signal band, either at low frequencies in the biasing networks of the amplifier, or at high frequencies, where the reverse gain of the transistors increases compared to the forward gain. Designers need good simulation tools to be able to detect instabilities early in the design cycle to allow them to solve problems without the need to build or rebuild a prototype.

The issues with stability are becoming ever more challenging lately. The need for higher signal bandwidth in modern communication standards puts more strain on the biasing networks, and this increases the issues with stability at low frequencies [Crip 06]. The need for a better energy efficiency pushes devices more into their non-linear operating mode, which complicates the stability analysis at both high and low frequencies [Mull 67]. Finally, new circuit topologies which vary the bias voltages as a function of the signal properties, like envelope tracking amplifiers do, are known for their great benefits in performance but are also notorious for their stability issues [McCu 15].

In this chapter, we look into the local stability analysis of steady-state solutions of an electronic circuit. First, we show that the local stability analysis of a steady-state solution boils down to the stability of a linear system (Section 5.1). When the linear system obtained by linearisation of the circuit about its steady-state solution has poles in the complex right half-plane, said solution is unstable. Unfortunately, commercial simulators don't provide direct access to the poles of the linearised system, so they have to be obtained with a detour.

In the rest of the chapter, we look into two different methods to determine the stability of the linear system without direct access to the system poles. The first method (Section 5.3) uses a rational approximation to obtain the poles. This method is based on the state-of-the-art stability analysis method described in [Jugo 01] and [Mall 13].

Then, in Section 5.4, we propose an alternative method which can determine the stability of a linear system without a rational approximation. This method, which is based on projection instead of approximation, overcomes most of the issues which are encountered with the first proposed stability analysis method.

5.1. Local stability of a steady-state solution

In this first section, we define the basic concepts which will be used throughout the remainder of the chapter. The work in this first part is not new, local stability analysis of non-linear systems and circuits is a well-studied topic in literature. Much more information on local stability analysis of electronic circuits can be found in [Suar 02].

Consider a dynamic non-linear system driven by n_u generators $\mathbf{u}(t) \in \mathbb{R}^{n_u \times 1}$, has n_y outputs $\mathbf{y}(t) \in \mathbb{R}^{n_y \times 1}$ and a state vector[1] $\mathbf{x}(t) \in \mathbb{R}^{n_x \times 1}$ where n_x is the amount of

[1] The amount of states in this representation n_x is finite. This limits the circuit class we consider here to circuits which consists of lumped elements only. In circuits with transmission lines and delays,

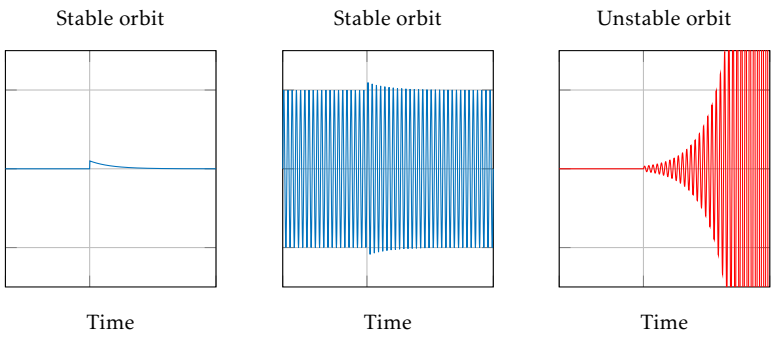

Figure 5.1.: When the steady-state solution is stable, it can recover from a small perturbation. The first and second plot show such stable solutions. In the first plot, the DC solution is perturbed, in the second plot, an oscillating solution is perturbed. In both cases, the circuit returns to the original solution, which indicates stability. The third plot shows the perturbation of an unstable DC solution. After the perturbation, the circuit shifts to an oscillating solution.

states. The behaviour of the system is then described by

$$\begin{cases} \dfrac{\partial \mathbf{x}(t)}{\partial t} & = \mathbf{f}(\mathbf{x}(t), \mathbf{u}(t)) \\ \mathbf{y}(t) & = \mathbf{g}(\mathbf{x}(t), \mathbf{u}(t)) \end{cases} \tag{5.1}$$

A steady-state solution of this system is either time-independent or periodic. A system can have many different steady-state solutions, some stable and others unstable. In this chapter, we will investigate the local stability of these steady-state solutions.

Definition A steady-state solution is locally stable when the linearised system about the solution is asymptotically stable i.e. it has no poles in the complex right half-plane or on the imaginary axis.

When the system is placed in an unstable steady-state solution and it is perturbed by an infinitely small perturbation, the system moves away from this steady-state solution to another solution. On the other hand, when the system is placed in a stable steady-state solution, it will return to the original solution after the perturbation. This behaviour is visualised in Figure 5.1.

the system becomes an infinite state system. We will show later in the chapter that the concepts obtained for finite state systems can be generalised to systems with transmission lines as well.

The steady-state solutions of an electronic circuit are easily obtained with the DC or Harmonic Balance (HB) simulator that is present in a commercial Computer-Aided Design (CAD) tool. There is however no guarantee that the obtained solution is stable, so a stability analysis needs to be performed on the obtained solution [Suar 15]. These stability analyses are the topic of this chapter. When the stability of the DC solution of a circuit is investigated, we will use the term *small-signal stability analysis*. The *large-signal stability analysis* investigates the stability of a periodic solution obtained with HB.

Small-signal stability

In a small-signal stability analysis, the stability of a DC solution or *equilibrium point* of the circuit is investigated. A circuit can have many possible DC solutions (although this is usually avoided by the designer) and each of the DC solutions can be either stable or unstable. The DC solution of an oscillator, for example, is made unstable on purpose. In amplifiers, the DC solution should be stable.

To obtain the DC solution, all input generators are set to a constant value. The DC simulator then finds a constant solution $\mathbf{x}^*$ of the circuit. When the system is placed in its DC solution, the system equations simplify to:

$$\begin{cases} \dfrac{\partial \mathbf{x}^*}{\partial t} & = \mathbf{f}(\mathbf{x}^*, \mathbf{u}) = 0 \\ \mathbf{y} & = \mathbf{g}(\mathbf{x}^*, \mathbf{u}) \end{cases}$$

where all signals $\mathbf{u}$, $\mathbf{y}$ and states $\mathbf{x}$ are now constant functions of time. To investigate the local stability of the solution, the circuit is linearised around this solution: infinitely small perturbations are introduced to the state vector ($\Delta_{\mathbf{x}}(t)$) and to the input vector ($\Delta_{\mathbf{u}}(t)$) and the response of the system to these perturbations is calculated:

$$\begin{cases} \dfrac{\partial \left(\mathbf{x}^* + \Delta_{\mathbf{x}}(t)\right)}{\partial t} & = \mathbf{f}\left(\mathbf{x}^* + \Delta_{\mathbf{x}}(t), \mathbf{u} + \Delta_{\mathbf{u}}(t)\right) \\ \mathbf{y}(t) + \Delta_{\mathbf{y}}(t) & = \mathbf{g}\left(\mathbf{x}^* + \Delta_{\mathbf{x}}(t), \mathbf{u} + \Delta_{\mathbf{u}}(t)\right) \end{cases}$$

$$\Rightarrow \begin{cases} \dfrac{\partial \Delta_{\mathbf{x}}(t)}{\partial t} & = \mathbf{A}\Delta_{\mathbf{x}}(t) + \mathbf{B}\Delta_{\mathbf{u}}(t) \\ \Delta_{\mathbf{y}}(t) & = \mathbf{C}\Delta_{\mathbf{x}}(t) + \mathbf{D}\Delta_{\mathbf{u}}(t) \end{cases} \tag{5.2}$$

where the **A**, **B**, **C** and **D** matrices are Jacobian matrices of the **f** and **g** functions with respect to the states and inputs

$$\mathbf{A} = \left.\frac{\partial \mathbf{f}(\mathbf{x},\mathbf{u})}{\partial \mathbf{x}}\right|_{\mathbf{x}^*,\mathbf{u}} \qquad \mathbf{B} = \left.\frac{\partial \mathbf{f}(\mathbf{x},\mathbf{u})}{\partial \mathbf{u}}\right|_{\mathbf{x}^*,\mathbf{u}}$$
$$\mathbf{C} = \left.\frac{\partial \mathbf{g}(\mathbf{x},\mathbf{u})}{\partial \mathbf{x}}\right|_{\mathbf{x}^*,\mathbf{u}} \qquad \mathbf{D} = \left.\frac{\partial \mathbf{g}(\mathbf{x},\mathbf{u})}{\partial \mathbf{u}}\right|_{\mathbf{x}^*,\mathbf{u}}$$

The local stability of the DC solution is now determined by the eigenvalues of the **A**-matrix [Khal 96, Suar 02]. If all eigenvalues of **A** are of multiplicity one and located in the complex left half-plane, the solution $\mathbf{x}^*$ is locally stable. If any of the eigenvalues lies in the complex right half-plane or on the imaginary axis, the solution is locally unstable.

Sadly enough it is not possible to get direct access to the **A**-matrix of a circuit in most commercial circuit simulators. Indirect methods are needed to check the stability of an equilibrium. These indirect methods to determine the stability will be discussed later. First, we take a look into how a circuit is linearised around a periodic steady state solution.

Large-Signal stability

In a large-signal stability analysis, the steady-state solution under investigation is periodic. These periodic steady-state solutions are encountered in simulations of oscillators and of circuits which are driven by a periodic signal. In oscillator simulations, the input generators $\mathbf{u}(t)$ are constant.

The periodic steady-state solution will be indicated with $\mathbf{x}^*(t)$. When the system is placed in $\mathbf{x}^*(t)$, the state equation equals:

$$\begin{cases} \dfrac{\partial \mathbf{x}^*(t)}{\partial t} & = \mathbf{f}(\mathbf{x}^*(t), \mathbf{u}(t)) \\ \mathbf{y}(t) & = \mathbf{g}(\mathbf{x}^*(t), \mathbf{u}(t)) \end{cases}$$

In simulations of high-frequency circuits, the Harmonic Balance (HB) simulator is often used to obtain the large-signal steady-state solution. A HB simulation is a frequency-domain method which returns the periodic steady-state solution of a circuit. To be able to do this, the user specifies the frequency grid for all signals and states in the circuit[2]. The possible solution is constrained to that frequency grid, which can result in the circuit being placed in an unstable steady-state solution [Suar 15]. For example, when an amplifier is driven by a generator

[2] More information about HB simulations can be found in Appendix A.

at frequency ω_{ex}, the HB simulation will find a steady-state solution which is periodic with the same frequency as the generator. This steady-state solution will be unstable when the amplifier wants to introduce spurious oscillations in addition to the response to the generator.

To simplify the argument, we will consider a single-frequency HB simulation only. The single user-provided frequency will determine the periodicity of all signals and states in the circuit, so $\mathbf{x}^*(t)$, $\mathbf{u}(t)$ and $\mathbf{y}(t)$ all have the same period. Like before, we can determine the stability of the steady-state solution by linearising the circuit around the steady-state solution by imposing infinitely small perturbations $\Delta_\mathbf{x}$ and $\Delta_\mathbf{u}$

$$\begin{cases} \dfrac{\partial\left(\mathbf{x}^*(t)+\Delta_\mathbf{x}(t)\right)}{\partial t} & = \mathbf{f}\left(\mathbf{x}^*(t)+\Delta_\mathbf{x}(t), \mathbf{u}(t)+\Delta_\mathbf{u}(t)\right) \\ \mathbf{y}(t)+\Delta_\mathbf{y}(t) & = \mathbf{g}\left(\mathbf{x}^*(t)+\Delta_\mathbf{x}(t), \mathbf{u}(t)+\Delta_\mathbf{u}(t)\right) \end{cases}$$
$$\Rightarrow \begin{cases} \dfrac{\partial \Delta_\mathbf{x}(t)}{\partial t} & = \mathbf{A}(t)\,\Delta_\mathbf{x}(t)+\mathbf{B}(t)\,\Delta_\mathbf{u}(t) \\ \Delta_\mathbf{y}(t) & = \mathbf{C}(t)\,\Delta_\mathbf{x}(t)+\mathbf{D}(t)\,\Delta_\mathbf{u}(t) \end{cases}$$

The time-varying matrices $\mathbf{A}(t)$, $\mathbf{B}(t)$, $\mathbf{C}(t)$ and $\mathbf{D}(t)$ have the same period as the signals and the states of the circuit and are given by:

$$\mathbf{A}(t) = \left.\frac{\partial \mathbf{f}(\mathbf{x},\mathbf{u})}{\partial \mathbf{x}}\right|_{\mathbf{x}^*(t),\mathbf{u}(t)} \qquad \mathbf{B}(t) = \left.\frac{\partial \mathbf{f}(\mathbf{x},\mathbf{u})}{\partial \mathbf{u}}\right|_{\mathbf{x}^*(t),\mathbf{u}(t)}$$
$$\mathbf{C}(t) = \left.\frac{\partial \mathbf{g}(\mathbf{x},\mathbf{u})}{\partial \mathbf{x}}\right|_{\mathbf{x}^*(t),\mathbf{u}(t)} \qquad \mathbf{D}(t) = \left.\frac{\partial \mathbf{g}(\mathbf{x},\mathbf{u})}{\partial \mathbf{u}}\right|_{\mathbf{x}^*(t),\mathbf{u}(t)}$$

The linear system obtained here is a Linear Time-Periodic (LTP) system. It has been shown that a similarity transformation can be performed on the state-space equations of an LTP system such that the **A**-matrix becomes time-invariant [Sand 05, Loua 14]. The eigenvalues of this time-invariant **A**-matrix determine the stability of the LTP system and with it, the local stability of the steady-state solution of the circuit [Moll 00]. If any of the eigenvalues lies in the complex right half-plane or on the imaginary axis, the steady-state solution is unstable.

In an oscillator, a periodic steady-state solution can be found when the input generators are all set to constant values. The time-invariant **A**-matrix of the linearised system around that steady-state solution will then have an eigenvalue in the origin of the complex plane [Suar 02]. According to our definition of stability, this solution is unstable, as it will not return to the original steady-state solution after a perturbation. It is possible to extend the definition of local stability such that this steady-state solution is considered stable, but this is outside of the scope of this work. We will not consider oscillators in the remainder of this chapter.

Similarly to what happened in the small-signal stability analysis, it is not possible here either to obtain direct information about the $\mathbf{A}(t)$ matrix in commercial simulators. Other techniques are therefore needed to determine the stability of the equilibrium.

5.2. Local stability analysis without access to the Jacobian

Without direct access to the **A**-matrix of the linearised system, the stability of a steady-state solution has to be determined in some other way. Over the years, many different techniques have been developed.

A first way to determine whether a steady-state solution is stable is to use a time-domain simulation. If the circuit returns to the original steady-state solution after a small perturbation, the solution is considered to be stable. In such a time-domain test, the initial state of the circuit needs to be chosen to be compatible with the steady-state solution obtained by a DC or HB simulation. Next, this state is perturbed slightly. If the circuit moves away from the initial orbit after the perturbation, it is unstable. The drawback of these time-domain techniques is that they can require very long simulations for the instability to express itself. Additionally, for high-frequency circuits, it is very hard to perform reliable time-domain simulations whenever transmission lines are included.

A second way to check for stability is to use open-loop methods. The feedback loop(s) in a circuit are then opened and the loop gain of each feedback loop is determined separately. Once the loop gain is known, classical control theory techniques can be applied to determine whether the loop is stable. When the loop is stable, gain and phase margins can be used to express how far from instability each feedback loop is. The open-loop methods are mostly used in low-frequency circuits [Tian 01]. In high frequency circuits, the loops in the circuit should be opened at the level of the intrinsic device present in each transistor [Jack 06, Suar 02]. Applying an open-loop method to high-frequency circuits therefore requires access to the internals of the transistor model, and this is not available in commercial simulators.

The third method to determine stability without access to the **A**-matrix is called *closed-loop stability analysis.* This is the method that we will study in the remainder of this chapter. In a closed-loop stability analysis, the Frequency Response Functions (FRFs) of the circuit taken from the perturbation generators to the outputs of the linearised system are determined. The poles of these FRFs are equal to the eigenvalues of the **A**-matrix as long as no pole-zero cancellations occur. By analys-

ing the FRFs of the linearised system, the stability of the steady-state solution can be determined without access to the **A**-matrix.

Small-signal closed-loop local stability analysis

When the non-linear system (5.1) is linearised around its DC solution as in (5.2), the FRFs from all perturbed input generators ($\Delta_{\mathbf{u}}$) to the measured output signals of the system ($\Delta_{\mathbf{y}}$) are gathered in a Frequency Response Matrix (FRM) given by

$$\mathbf{G}_{\Delta_{\mathbf{u}} \to \Delta_{\mathbf{y}}}(s) = \mathbf{C}\left(s\mathbf{I}_{n_x} - \mathbf{A}\right)^{-1}\mathbf{B} + \mathbf{D}$$

Written in a pole-residue format, this FRM can be expressed as

$$\mathbf{G}_{\Delta_{\mathbf{u}} \to \Delta_{\mathbf{y}}}(s) = \sum_{p=1}^{n_x} \frac{\mathbf{R}_p}{s - a_p} + \mathbf{D}$$

where a_p are the poles of the FRFs and $\mathbf{R}_p$ are the residues. The poles of the FRFs are equal to the eigenvalues of the **A**-matrix [Kail 80]. This means that the stability of an orbit can be determined by determining poles of the FRFs of the linearised system. Note that the above statement can only be made when the the unstable poles are observable. This means that the location of the perturbation generators should be chosen carefully. We will discuss the placement of the perturbation generators later. For now, we assume that all poles are observable.

Earlier, we ruled out circuits which contain distributed elements by assuming that the system (5.1) has only a finite number of states n_x. The good news is that the analysis of the FRFs can also be applied to determine the stability of such distributed circuits [Bara 14]. This holds even if the FRFs of a system with distributed elements are no longer rational functions, but more general functions of the following form [Bell 63, Part 97]:

$$G(s) = \frac{\sum_{p=0}^{N_1} a_p(s)\, e^{-\beta_p s}}{\sum_{l=0}^{N_2} b_l(s)\, e^{-\gamma_l s}} \tag{5.3}$$

where $0 = \beta_0 < \beta_1 < \ldots < \beta_{N_1}$ and $0 \leq \gamma_0 < \gamma_1 < \ldots < \gamma_{N_2}$; The $a_p(s)$ and $b_l(s)$ are polynomials in s. These functions have an infinite amount of poles in general. In the specific and practically relevant case that the finite bandwidth of active elements present in the circuit ensures that they become passive for all frequencies outside their bandwidth, the FRFs of the system only have a finite number of poles in the complex right half-plane [Bara 14]. As a consequence, the closed-loop stability analysis of circuits with distributed elements can still be performed analysing the FRFs of the linearised system.

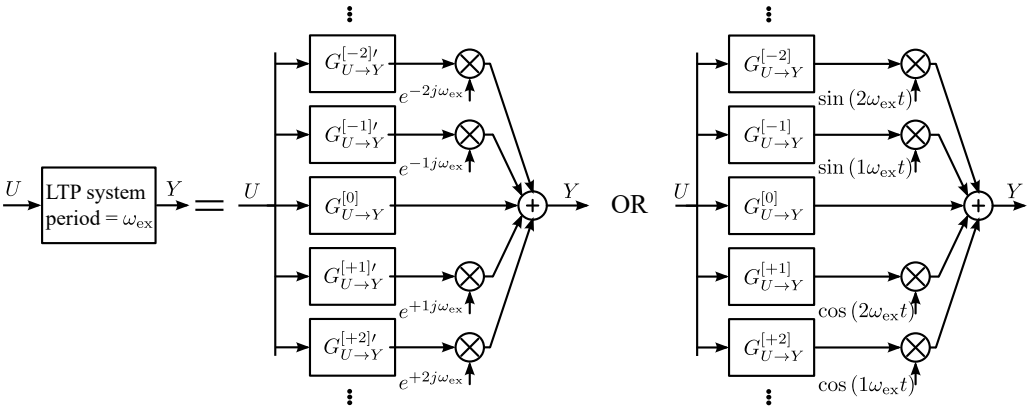

Figure 5.2.: A Linear Time-Periodic (LTP) system can be represented exactly by combination of an infinite series of LTI systems and ideal mixers. The LTI systems are called Harmonic Transfer Function (HTF) in this case. The signals which drive the mixers can be either sin and cos or complex exponentials.

Large-signal closed-loop local stability analysis

In analogy to the small-signal closed-loop stability analysis, the large-signal stability can also be determined analysing the FRFs of the linearised circuit. As we showed before, the linear system in the large-signal case becomes a Linear Time-Periodic (LTP) system. When a LTP system is excited by a single-tone small-signal perturbation at pulsation ω, the excitation will mix with the periodic variation of the system (at ω_{ex}) and create output contributions at frequencies $\omega + l\omega_{ex}$ where $l \in \mathbb{Z}$. The FRF obtained by division of the excitation at ω and the response at a frequency translated output at $\omega + l\omega_{ex}$ is called the Harmonic Transfer Function (HTF).

$$G^{[l]}_{\Delta_u \to \Delta_y}(j\omega) = \frac{\Delta_y(j\omega + lj\omega_{ex})}{\Delta_u(j\omega)}$$

The behaviour of the LTP system is exactly modelled by an infinite series of Harmonic Transfer Functions (HTFs) followed by ideal mixers as shown in Figure 5.2. The signals which drive the mixers in the representation can be chosen to be either sine and cosine functions or complex exponentials. When complex exponentials $e^{lj\omega_{ex}}$ are used as basis functions, we will indicate the HTF with a prime: $G^{[l]\prime}$. The HTFs with complex basis functions are not Hermitian as the associated time

signals are now complex.

$$G^{[l]\prime}_{\Delta_u\to\Delta_y}(j\omega) \neq \overline{G^{[l]\prime}_{\Delta_u\to\Delta_y}(-j\omega)}$$

When a $\sin(\cdot)$ and $\cos(\cdot)$ basis is used, the HTFs are Hermitian functions. We prefer to work with Hermitian functions to simplify the analysis later on. Whenever needed, the HTFs will be transformed from the exponential basis to the $\sin(\cdot)$ and $\cos(\cdot)$ basis using the following formula [Sand 05, Loua 14]:

$$G^{[l]}_{\Delta_u\to\Delta_y}(j\omega) = \frac{1}{2}\left[G^{[l]\prime}_{\Delta_u\to\Delta_y}(j\omega) + G^{[-l]\prime}_{\Delta_u\to\Delta_y}(j\omega)\right]$$
$$G^{[-l]}_{\Delta_u\to\Delta_y}(j\omega) = \frac{j}{2}\left[G^{[l]\prime}_{\Delta_u\to\Delta_y}(j\omega) - G^{[-l]\prime}_{\Delta_u\to\Delta_y}(j\omega)\right]$$

It is shown in the literature on LTP systems [Sand 05, Loua 14], that each HTFs can be modelled exactly as

$$G^{[l]}_{\Delta_u\to\Delta_y}(s) = \sum_{p=1}^{n_x}\sum_{c=-\infty}^{\infty}\frac{R_{p,c}}{s-(a_p - cj\omega_{\text{ex}})} + D_s \tag{5.4}$$

in this model, there are n_x base poles a_p which are equal to the eigenvalues of the time-invariant $\mathbf{A}$-matrix [Loua 14]. The base poles are repeated periodically on vertical lines in the complex plane with a spacing of ω_{ex}.

When distributed elements are present in the circuit under large-signal excitation, the above model (5.4) will not be able to exactly fit the HTFs of the linearisation around the periodic orbit. The correct form will be a generalisation of (5.3) to the periodic time-varying case. As far as we know, this generalisation has not yet been studied in great detail. In the remainder of this chapter, we will show that the proposed stability analyses return correct results, even in the large-signal case with distributed elements (Example 5.5), but future work is needed to show the limitations of the framework in this very general case.

Similarly to what happened in the small-signal case, the stability of the steady-state solution can be determined by analysing the location of the poles of the HTFs of the linearised system. Later on (in Sections 5.3 and 5.4) we will discuss two different methods to determine whether an FRF has poles in the right half-plane. The first method estimates a rational approximation to find the poles (Section 5.3). The second method projects the FRF onto bases of stable and unstable functions to check whether the FRF is analytic in the complex right half-plane or not, and leads to similar results without the need for a rational model. Because the stability analysis boils down to checking whether an FRF has poles in the right half-plane, the two methods can be used in both the small- and the large-signal local stability analysis. Before we looking into the methods themselves, we will summarise a method to determine the FRF of the linearised system using commercial circuit simulators.

Closed-loop local stability analysis of electronic circuits

In all commercial CAD tools, small-signal voltage and current sources are readily available to be included in the schematic diagram and perturb the steady-state solution obtained with a DC of HB simulation. The AC and Large-Signal Small-Signal (LSSS) simulations can then be used to determine the response of the linearised system in the neighbourhood of the DC and HB solutions respectively

When a small-signal voltage source is introduced as a perturbation source, a connection in the circuit needs to be split into two nodes and the small-signal voltage source can be connected in between the pre-existing and the new node. On the contrary, a small-signal current source can be connected in parallel to any circuit node. This eases automated modification of the circuit diagram significantly. The output signal used to obtain the FRF can then be any other voltage or current in the circuit.

The choice for the location of the perturbation source is very important: The unstable poles need to be observable in the obtained FRFs. It is advised to perturb as closely as possible to the active devices in the circuit [AMCA]. Determining many different FRFs minimises the risk of missing an unstable pole.

In this chapter, we will always use small-signal current sources to perturb the steady-state solution. They can be added easily to a circuit netlist without the need to introduce new nodes in the netlist. The output signal used to obtain the FRF will always be a voltage in the circuit. Measuring currents in the circuit requires adding current probes, which again introduces new nodes in the netlist. All FRFs analysed in this chapter are therefore impedances.

In a small-signal stability analysis, an AC simulation is used to determine the voltage response to the current perturbation(s) added to the circuit (Figure 5.3). The impedance is then determined in the classical way:

$$G_{\Delta_u \to \Delta_y}(j\omega) = Z_{mn}(j\omega) = \frac{V_m(j\omega)}{I_n(j\omega)}$$

where $I_n(j\omega)$ indicates the small-signal current injected into the selected node and $V_m(j\omega)$ is the voltage response to that current measured at a node in the circuit.

In a large-signal stability analysis a LSSS simulation is used to obtain the HTFs of the linearised circuit about a steady-state solution obtained with HB[3]. The HTFs of the circuit are then

$$G^{[l]}_{\Delta_u \to \Delta_y}(j\omega) = Z^{[l]}_{mn}(j\omega)(j\omega) = \frac{V_m(j\omega + l j\omega_{\text{ex}})}{I_n(j\omega)} \quad l \in \mathbb{Z}$$

[3]These LSSS simulations can be tricky to set up correctly. In appendix (B) the LSSS simulator of Advanced Design System (ADS) is studied in detail

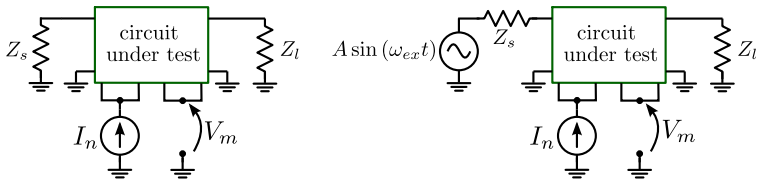

Figure 5.3.: The impedance presented by a circuit is determined by connecting a small-signal current source to a node in the circuit and by measuring the resulting voltage. In a large-signal stability analysis (right), the frequency-translated voltages are all measured.

where $I_n(j\omega)$ is the injected perturbation current. The LSSS simulation in ADS calculates the HTFs with exponential functions as signals which drive the mixers (as in Figure 5.2). They need to be transformed to the $\sin(\cdot)$ and $\cos(\cdot)$ basis to obtain real time signals and ensure that they are Hermitian functions.

5.3. Pole-zero estimation for Stability analysis

A first way to determine whether a FRF has poles in the complex right half-plane is to approximate the FRF by a a rational model first and next check whether any of the poles of the rational approximation ends up at the right side of the imaginary axis. This simple approach to closed-loop stability analysis was proposed originally in [Jugo 01]. The method based on rational approximation has been refined over the years [Ayll 08, Anak 10] and was patented [Mall 13]. The method has been applied to many different applications: to predict large-signal stability [Coll 04], to conduct a Monte-Carlo analysis [Coll 11], to predict the stability margins in power amplifiers [Oteg 12, Heij 16]. A commercial implementation of the method is available in the STAN tool of AMCAD engineering [AMCA].

Rational approximation for small-signal stability analysis of lumped circuits

The small-signal FRF of lumped circuits are perfectly described by rational functions. In this simple case, the rational approximation can easily be used to determine the local stability of the DC solution. We will show this in example 5.1 later in this section. Remember that all unstable poles of the linearised system have to be observable in the selected set of FRFs, and the model order of the rational approximation should be chosen correctly for the method to be reliable.

To ensure that the unstable poles in the circuit are observable, it is recommended to add a perturbation generator close to each of the transistors in the circuit

[AMCA]. This is especially important in amplifiers that can create odd-mode instabilities: this type of instability is unobservable at the input and output ports of the device [Jack 06].

The choice for the order of the rational approximation is also critical. When the model order is set too low, the poles in the approximation will not coincide with the poles of the linearised system. When the model order is set too high, the extra poles will appear somewhere in the complex plane. This can generate false positives for the stability analysis. A good model-order selection method is therefore key in a stability analysis method that is based on a rational approximation.

In the small-signal stability analysis of lumped circuits, the correct model order can easily be determined by increasing the order of the approximation until the difference between the FRF data and the rational approximation reaches the numerical precision. We will demonstrate this in example 5.1. When distributed elements are present in the circuit, this simple technique cannot be used because of the model errors introduced by the transmission lines.

Rational approximation for small-signal stability analysis of circuits with distributed elements As we have shown before, the FRFs of a circuit with distributed elements are no longer rational functions, but more general functions of the form (5.3). These functions can be well approximated by rational functions, but the obtained models are approximations only [Part 97]. The consequence of this property is that there is no guarantee that the poles of the rational approximation coincide with the poles of the underlying FRFs. Nevertheless, rational approximations are still used in practice to analyse the stability of distributed circuits [Anak 10, AMCA]. In the existing algorithms, the FRF data is cut in several frequency bands and low-order rational models are estimated on each band. If the low-order approximation does not produce a good fit, the frequency band is split again until a satisfactory fit can be obtained. When an unstable pole is detected in a band, the approximation is re-fitted around the obtained pole to determine whether the pole is a physical pole or a numerical artefact.

Rational approximation for Large-signal stability analysis For the large-signal stability analysis, we have shown that the FRFs of the linearised system are described as in equation (5.4). The underlying function contains a set of base poles and an infinite set of copies of these base poles located on vertical lines in the complex plane. Estimating this rational model with the constraint on the location of the poles in the complex plane from FRF data is a very hard problem [Loua 14] and the estimation algorithms that can fit this model are not widespread. The alternative is to use a normal rational model with a very high order. The location

of the poles is not guaranteed to satisfy the strong constraint imposed by (5.4), but it has been shown in literature that the approach can work in a stability analysis [Coll 04].

Example 5.1: Pole-zero stability analysis of a Low Noise Amplifier

To demonstrate how a pole-zero analysis can be used to determine the small-signal and large-signal stability of an electronic circuit, we will analyse an Low Noise Amplifier (LNA) from Infineon [Infi 07]. We will also determine whether it helps to model the rational approximations with a common-denominator, as this is not currently done in state-of-the art pole-zero stability analysis methods.
The ADS schematic used to simulate the LNA is shown below:

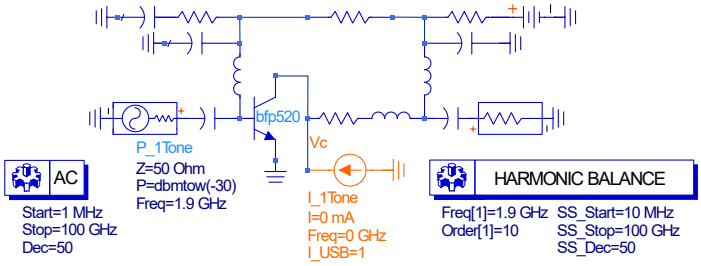

The circuit under test is stable, so any instability found is an artefact of a wrong pole estimation. We will use the Vector Fitting technique [Gust 99, Gust 06, Desc 08] with a weighted norm as our tool of choice to estimate the rational approximation of the FRFs, but any other algorithm to fit a rational approximation could be used here.

Small-signal stability analysis of the LNA To investigate the small-signal stability of the LNA, three small-signal current sources are connected to the circuit. One to collector of the transistor (indicated with c), a second one to the base of the transistor (b) and a third one to a node in the bias network of the circuit (a). In this way, 6 different impedances are obtained: Z_{cc}, Z_{bb}, Z_{aa}, Z_{cb}, Z_{bc}, and Z_{ac}.
The AC simulations are performed on a logarithmic frequency grid between 1MHz and 100GHz with 50 points per decade. The transition frequency f_T of the transistor used in the LNA is 45GHz, so the simulated frequency span covers the full range where the transistor can possibly generate oscillations.

The poles of the linearised system are now estimated twice. First only one FRF is given to the Vector Fitting algorithm. Then a common denominator model is estimated using the 6 different FRFs of the circuit. The order of the model is determined with a simple scan. The root mean square (rms) error of both estimated models as a function of the model order is shown below

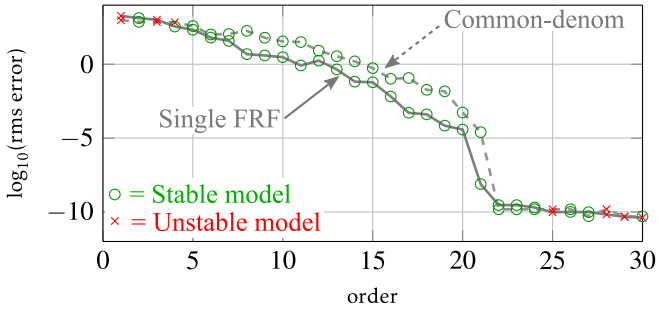

In both cases, the rms error of the models reaches numerical precision for a model order of 22 with a clear accuracy jump. A stable model is obtained for order 22, which allows us to conclude that the circuit is stable. Below and above the correct order, several falsely unstable models are obtained (indicated with ×). This result indicates that the common-denominator approach does not yield a significant improvement with respect to the pole-residue modelling from a single impedance FRF concerning stability analysis results. Of course, the latter result depends on the circuit and on the chosen node.

Large-signal stability analysis of the LNA The picture is completely different when the large-signal stability of the same LNA is investigated. A single-tone excitation at 1.9GHz is applied to the LNA and a HB simulation with an order of 10 is used to obtain the large-signal orbit and a small-signal current source is connected to the collector of the transistor. The small-signal excitation is swept in a LSSS simulation from 10MHz to 100GHz on a logarithmic frequency grid. Some of the obtained $Z_{mn}^{[l]}(j\omega)$ are shown below

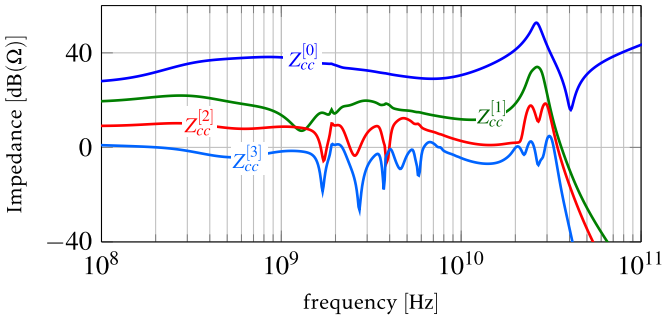

The higher-order harmonic transfer functions contain a lot more information about the location of the repeated poles in the system, so including them in the modelling algorithm enhances its robustness towards stability analysis results. It is clear from the plot that $Z_{cc}^{[0]}$ does not contain high dynamics around the higher-order copies of the system poles. The higher-order $Z_{cc}^{[l]}$ do show strong resonances at the frequencies associated with the copies. Due to this behaviour, the common-denominator estimation with multiple $Z_{cc}^{[l]}$ $l = -3,-2,-1,0,1,2,3$ together allows a more robust stability analysis with respect to the classic estimation performed on $Z_{cc}^{[0]}$ alone as shown below

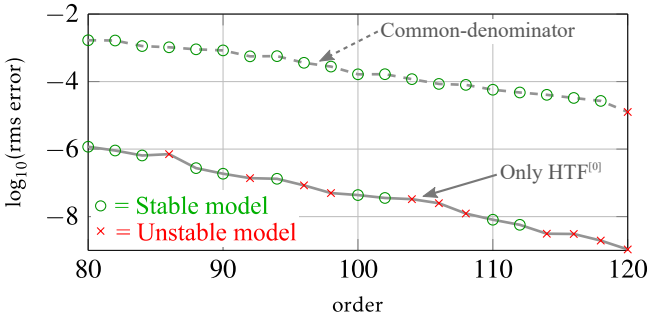

The first thing to notice here is that the model-orders needed to obtain a good fit are a lot higher than before. Also, the accuracy of the fit does not drop as sudden as before, which can be explained by the fact that an infinite amount of poles is needed to obtain a perfect fit in this case. The final thing to notice is that the classic approach generates many false-positives concerning the stability analysis during the scanning of the order. Instead, the common-denominator approach is more robust in this case.

From this basic example, we can conclude that using a rational approximation to perform a stability analysis may sound good on paper, but that, for large-signal stability analysis and for stability analysis of circuits with distributed elements, some extra tricks are needed to make it work reliably. In the following section, an alternative method to determine the stability of a FRF is proposed.

5.4. Stability analysis based on projection

The good news is that the fitting of a rational model can be avoided completely in a stability analysis however. Instead of working with a rational approximation to detect instability, we can split the FRF data into a stable and an unstable part using functional analysis.

This process can be explained intuitively as follows: The FRF $G(j\omega)$ can be written as the sum of a stable part G_{stable}, which is an analytic function in the complex right half-plane and an unstable part G_{unstable}, which is an analytic function in the left half-plane.

$$G(j\omega) = G_{\text{stable}}(j\omega) + G_{\text{unstable}}(j\omega)$$

Using an orthogonal basis with specific basis vectors for the stable and unstable part, we can determine the stable and unstable parts of the FRF by projecting the original FRF onto that basis [Oliv 13]. If a significant part of the original function appears at the basis functions that span the unstable part, then $G(j\omega)$ is found to be unstable. This projection can be performed without estimating a rational model, so the model-order selection problem is avoided completely. The difficulties with transmission lines are no longer present in this projection-based approach either.

Projecting onto the stable/unstable basis

We will, for now, assume that the FRF is a function in $L^2(j\mathbb{R})$, which are functions that are square integrable over the imaginary axis of the Laplace plane. This rules out impedances with poles placed on the imaginary axis, but includes FRFs of periodically varying systems and impedances resulting from circuits which contain transmission lines. The $L^2(j\mathbb{R})$ space can be partitioned into two subspaces: The Hardy space $H^2(\mathbb{C}^+)$ of functions analytic on the complex right half-plane and its orthogonal complement $H^2(\mathbb{C}^-)$

$$L^2(j\mathbb{R}) = H^2\left(\mathbb{C}^+\right) \oplus H^2\left(\mathbb{C}^-\right)$$

We can build a specific basis that spans the functions in $L^2(j\mathbb{R})$ [Part 97]. The basis function are denoted by B_b and are given by

$$B_b(s) = \sqrt{\frac{1}{\pi}} \frac{(1-s)^b}{(1+s)^{b+1}} \tag{5.5}$$

All basis functions with positive b span a basis for the stable functions, all basis functions with negative b span the unstable functions. When we have a FRF and

we want to know whether it originates from a stable orbit or not, all we have to do is to project the FRF onto the basis and see whether a part of the original function is projected onto the unstable basis. The projection of the FRF $G(j\omega)$ onto the basis functions boils down to calculating an inner product:

$$c_b = \langle G(j\omega), B_b(j\omega) \rangle = \int_{-\infty}^{\infty} G(j\omega)\overline{B_b(j\omega)}d\omega \tag{5.6}$$

Once the c_b coefficients are calculated, the stable and unstable parts of $G(j\omega)$ are easily recovered by calculating

$$G_{\text{stable}}(j\omega) = \sum_{b=0}^{\infty} c_b B_b(j\omega) \qquad G_{\text{unstable}}(j\omega) = \sum_{b=1}^{\infty} c_{-b} B_{-b}(j\omega) \tag{5.7}$$

To make calculations tractable, we will not calculate the inner product in (5.6) directly. We will first transform the FRF from the Laplace plane to the unit disc. This allows to use the Fast Fourier Transform (FFT) to perform the projection. This step is explained later.

Filtering to suppress edge effects

The inner product in (5.6) runs over all the frequencies while the FRF $G(j\omega)$ is only known over a certain frequency range $[f_{\min}, f_{\max}]$. To deal with the finite interval, the FRF is multiplied with a filtering function before the analysis:

$$G_{\text{f}}(j\omega) = G(j\omega)H(j\omega) \tag{5.8}$$

The filter $H(j\omega)$ is a high-order elliptic lowpass filter with its first transmission zero placed at $f_{\max}$. The order of the filter is chosen such that the transition to zero at its cut-off frequency is steep, but still smooth.

This filter will stabilise poles located closely to its cut-off frequency, so $f_{\max}$ should be chosen well beyond the maximum frequency at which the circuit can become unstable. $f_{\min}$ should be placed very close to DC. If $f_{\min}$ can't be close to DC, a bandpass filter should be used for $H(j\omega)$ instead. The smooth decay to zero of $G_{\text{f}}(j\omega)$ at the edges of the frequency interval will avoid instabilities to pop up due to the discontinuity of $G(j\omega)$.

Mapping onto the unit disc for the easy calculation of the coefficients

Working with the basis functions $B_b(j\omega)$ of equation (5.5) on the complex plane is troublesome from a numeric point of view. Performing the projection when

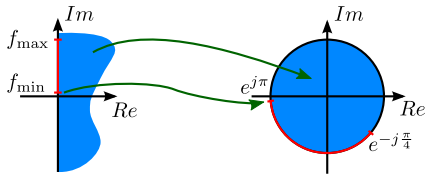

Figure 5.4.: Visual representation of the Möbius mapping used to transform the impedance data from the complex plane to the unit circle.

working on the unit circle yields numerically more stable results [Oliv 13]. The mapping from the Laplace plane to the unit circle is performed with the Möbius mapping visualised in Figure 5.4:

$$G_\mathrm{f}(s) \underset{\text{Möb}}{\longmapsto} G_\mathrm{f}^\mathrm{disc}(z) = \frac{1}{z-1} G_\mathrm{f}\left(\frac{z+1}{z-1} f_\mathrm{max}\left(1+\sqrt{2}\right)\right) \tag{5.9}$$

Our mapping of choice converts square integrable functions on the frequency axis into square integrable functions on the unit circle. Square integrable functions which are analytic on the right half-plane are mapped onto square integrable functions which are analytic inside the unit disc. The basis functions B_b map onto powers of z

$$B_b(s) \underset{\text{Möb}}{\longmapsto} B_b^\mathrm{disc}(z) = z^b$$

Projecting on this basis boils down to calculating the Fourier series of $G_\mathrm{f}^\mathrm{disc}\left(e^{j\theta}\right)$, with coefficients given by

$$c_k = \frac{1}{2\pi} \int_0^{2\pi} G_\mathrm{f}^\mathrm{disc}\left(e^{j\theta}\right) e^{-jk\theta} d\theta$$

This Fourier series can be calculated in a numerically efficient way using the FFT. The FFT requires that the θ-values are linearly spaced between 0 and 2π. Due to the mapping from the complex plane to the unit disc, the samples will not satisfy this constraint. A simple interpolation, with splines for example, can be used to obtain $G_\mathrm{f}^\mathrm{disc}$ on the θ-values required to perform the FFT. The interpolation can introduce artefacts in the unstable part if the FRF is not sampled on a sufficiently dense frequency grid. This will be shown to happen on an example later.

Summary of the projection method

The stable and unstable parts of a FRF are determined using the following steps:

1. Multiply the FRF with a high-order filter as in (5.8)
2. Transform the filtered FRF to the unit disc using (5.9)
3. Interpolate the transformed FRF to a linear grid and use the FFT to calculate the c_k coefficients
4. Reconstruct the stable and unstable part using (5.7)

When the obtained unstable part is significantly large compared to the stable part, the frequency response is considered unstable.

Obtaining the unstable poles

As was mentioned before, a circuit that contains transmission lines and active elements with a finite bandwidth can only have a finite number of unstable poles [Bara 14]. This means that most of the complexity of the frequency response will be projected onto the stable part, while the unstable part can easily be approximated by a low-order rational model to recover the unstable poles.

The "split-first, approximate later" approach proposed here is therefore more robust than the direct extraction of a rational model to recover the unstable poles. We do not have to deal with the modelling of the distributed effects of the circuit by a rational model.

Classic rational approximation tools can be used to approximate the unstable part and determine the unstable poles. When multiple frequency responses are analysed simultaneously, a common-denominator approximation is preferred. Vector fitting [Gust 99] has been used here, but other tools, like RARL2 [Marm] can also be used here.

Example 5.2: Random state-space system

As a first example, the stability analysis is applied to a random system of order 202 (generated with the rss function from Matlab). The test system has an unstable pole pair at 1Hz, as can be seen on its pole-zero map shown below. To introduce delay in the test system, a time delay of 2s is added to the system.

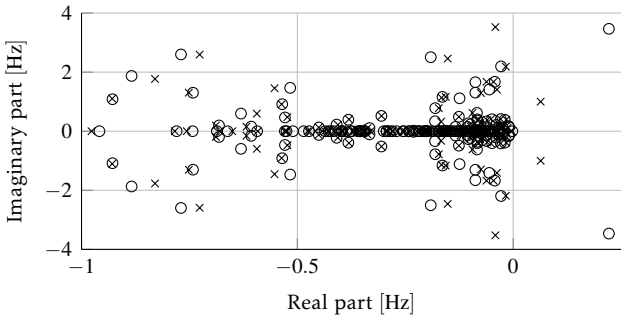

The FRF of the system is calculated at 1000 linearly spaced frequencies between 0Hz and 5Hz and is shown in green on the figure below.

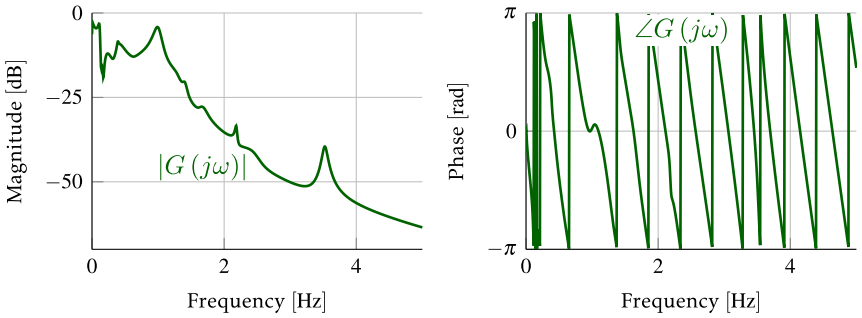

We will now apply the projection-based stability analysis to this FRF to determine whether the underlying system is stable or not.

Step 1: filtering To obtain a smooth transition to zero at the edge of the simulated frequency band, the FRF is filtered with a high-order elliptic lowpass filter. The order of the filter is set to 10 and an in-band ripple of 1dB was selected. The cutoff frequency of the filter is selected such that

the first transmission zero of the filter lies at 5Hz. The FRF of the obtained filter is shown below:

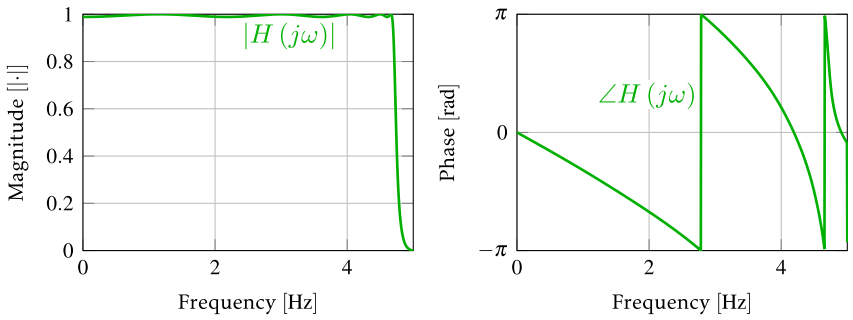

Step 2: Transform to the unit disc The filtered FRF is transformed to the unit disc using Möbius the transformation specified in (5.9). The mapping between the frequencies in the Laplace plane and the angle θ on the unit disc is given by

$$\theta = \Im\left\{\log\left(\frac{f/[f_{\max}(1+\sqrt{2})]+1}{f/[f_{\max}(1+\sqrt{2})]-1}\right)\right\}$$

DC is mapped to $\theta = \pi$ and $f_{\max}$ is mapped onto $7/4\pi$. The mapping is clearly non-linear, so the linear spacing of the frequencies is not preserved after transformation to the unit disc. The transformation is then completed by multiplying the data on the unit disc with the following factor

$$\frac{1}{e^{j\theta}-1}$$

Step 3: Calculate Fourier series To calculating the Fourier series of the transformed FRF with the FFT, a θ-grid with 2672 points linearly spaced between 0 and 2π is constructed. The values on the grid are then obtained as follows:

- For $\theta \in [\pi, 7/4\pi]$ the result of the Möbius transform is interpolated.
- The values for $\theta \in [1/4\pi, \pi[$ correspond to the negative frequencies on the complex plane, so the complex conjugate of the values between π and $7/4\pi$ is used.
- Remaining values are set to 0.

The magnitude of the FRF data sent to the FFT is shown on the plot below.

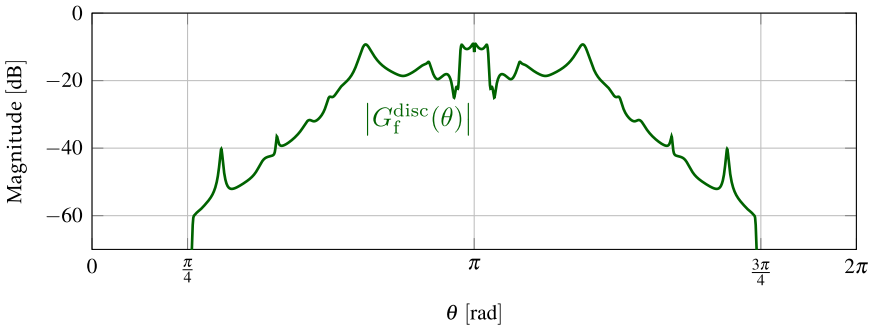

The obtained Fourier coefficients c_b are shown below.

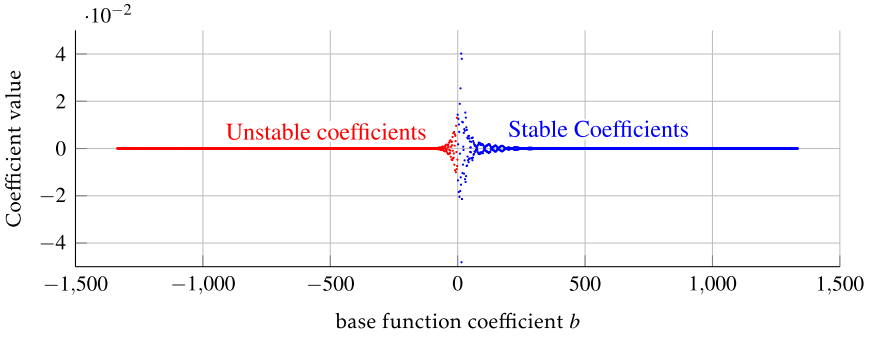

From these coefficients, we can already conclude that the FRF is unstable, because many coefficients with negative b-values are non-zero.

Step 4: Reconstruct the stable and unstable parts The reconstruction of the stable and unstable parts starting from the coefficients is performed without needing to calculate the sums in (5.7). To obtain the unstable part, all stable coefficients in the coefficient vector are set to zero and the Inverse Fast Fourier Transform (IFFT) is of the vector is calculated. The reconstructed unstable part is then still obtained on the unit disc. The inverse Möbius transform is then applied to transform it back to the complex plane. The same procedure is followed for the stable part, but now the unstable coefficients are set to zero before the IFFT. The reconstructed stable and unstable parts are now shown in red and blue on the figure below, together with the filtered impedance in green:

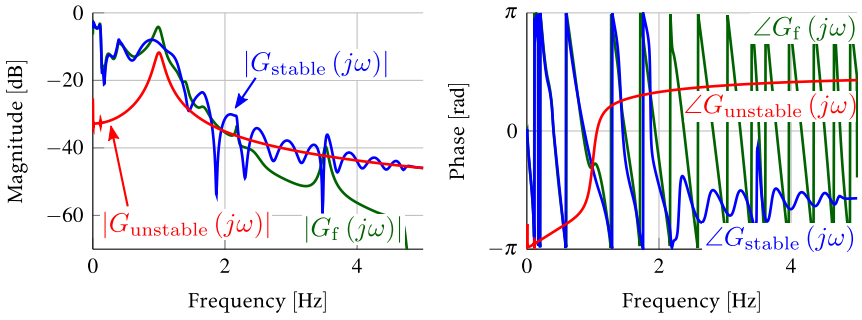

The obtained unstable part peaks at 1Hz: This matches the location of the unstable pole pair of the system. Note also that the obtained G_{unstable} has very simple shape: it is clearly a second-order system. Most of the complexity of the frequency response, including the delay, is projected onto the stable part. This observation supports the proposed approach of estimating a rational model only after projection. As is shown below, a good fit was obtained with a rational model that consisted of two unstable poles and a single zero. The two poles obtained with a rational approximation of G_{unstable} coincide exactly with the unstable poles that were introduced in the system.

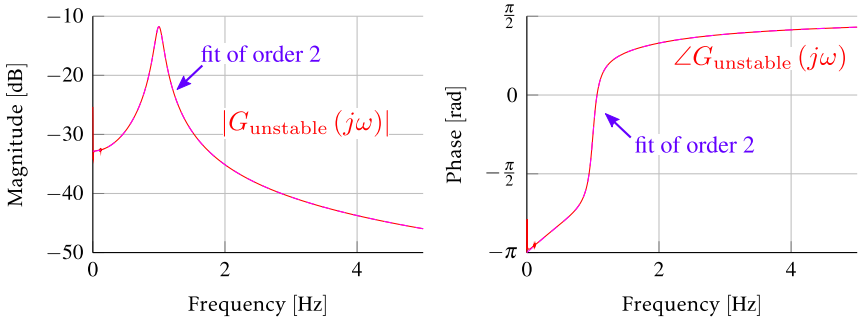

The filter of (5.8) can also be used in step 1 to "zoom" in on a certain frequency range of the frequency response and isolate a chosen resonance. In a second projection of the same frequency response data, a bandpass filter is used instead of a lowpass filter in the filtering step. The cutoff frequencies of the bandpass filter were 0.7Hz and 1.3Hz. The result of the "zoomed" projection is shown below:

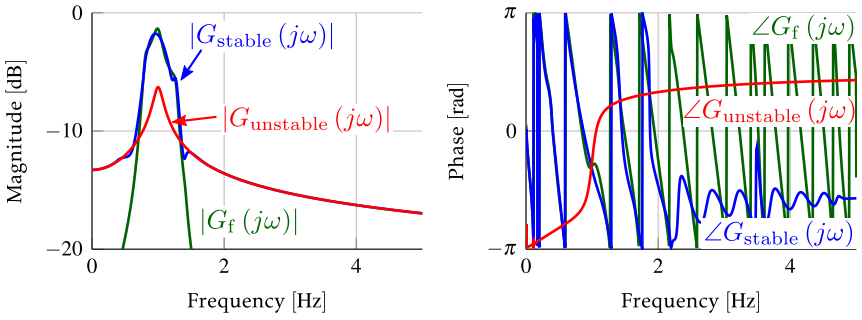
0
−10
−20
Magnitude [dB]
$|G_{\text{stable}}(j\omega)|$
$|G_{\text{unstable}}(j\omega)|$
$|G_{\text{f}}(j\omega)|$
0
2
4
Frequency [Hz]
π
0
−π
Phase [rad]
$\angle G_{\text{f}}(j\omega)$
$\angle G_{\text{unstable}}(j\omega)$
$\angle G_{\text{stable}}(j\omega)$
0
2
4
Frequency [Hz]

Example 5.3: Balanced Amplifier

As a second example we study the stability of the balanced amplifier. With this example, we will show that the projection-based analysis is also capable to detect the instability in simulations of real RF and microwave amplifiers. The ADS schematic of the amplifier is shown below:

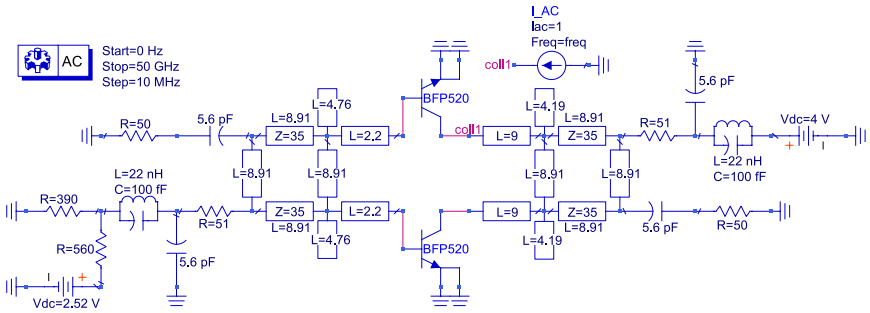

This example was built as a student project by Kurt Homan and Johan Nguyen for operation around 3.4GHz. Two BFP520 transistors were used to construct the amplifier. At measurement time, the design oscillated around 1.3GHz when terminated in 50Ω, so the circuit is a good candidate to verify the proposed method to find the instability in simulations.
The small-signal current source was connected to the collector of the top transistor. The BFP520 has a f_T of 45GHz, so the maximum frequency for the simulation was set to 50GHz. The impedance of the circuit at the test probe was determined starting from DC in 10MHz steps. The obtained impedance is shown below in green, the obtained stable and unstable parts are also shown in the same figure.

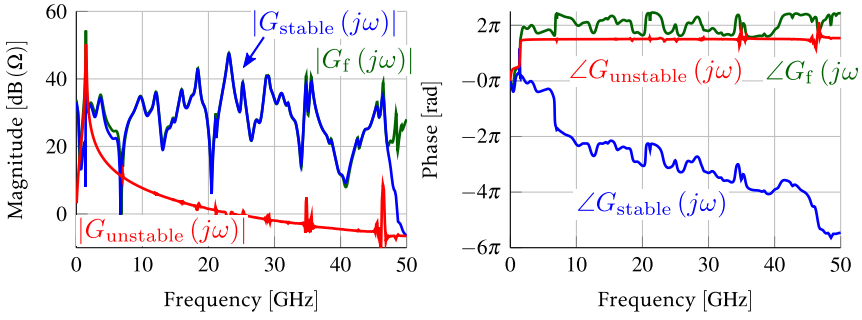

An instability around 1.3GHz is detected, but also some artefacts can be observed in the obtained unstable part at higher frequencies. These artefacts are due to the interpolation in step 3 of the stable/unstable projection.
To confirm that the artefacts are indeed artefacts caused by the interpolation, a second simulation was run, but now 1MHz steps were used instead of 10MHz.

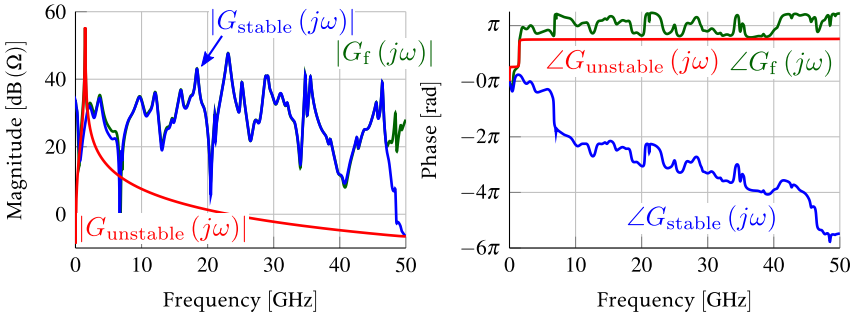

The stable/unstable projection of the denser frequency response data still predicts the instability around 1.3GHz, but the artefacts in the unstable part at higher frequencies are gone.
We have shown with this example that the projection-based can also detect the instability in real circuit examples. When the impedance is not sampled adequately dense, interpolation artefacts can appear in the unstable part. When a denser frequency grid is used however, the artefacts completely disappear.

Example 5.4: Low Noise Amplifier

In this third example, the small-signal stability of a stable LNA is analysed. The LNA is the same circuit as the one studied earlier with a pole-zero approximation in example 5.1. By studying a stable circuit, we can show the effects introduced by simulating the frequency responses on a finite frequency interval only.
The small-signal stability of the LNA is determined by analysing the impedance presented by the circuit at the collector of the transistor. The impedance was determined up to 10GHz and shown in green below. The result of the stable/unstable projection are plotted on the same figure.

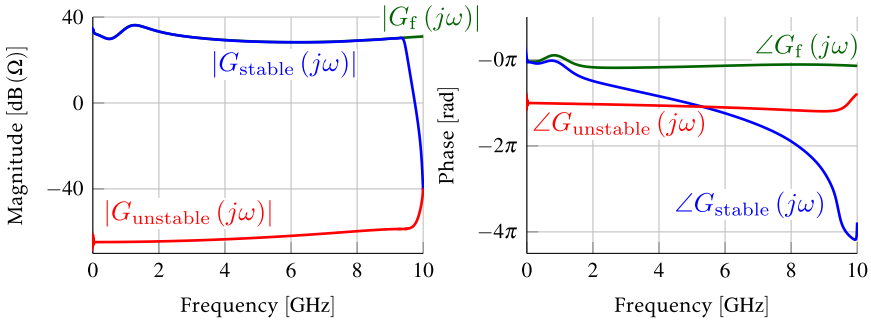

The obtained unstable part of the impedance is very small, but not zero due to the fact that the impedance was only simulated on a finite frequency interval. The filtering smoothens the transition to zero at the edge of the frequency interval, but its influence cannot be fully suppressed as is demonstrated by this example.

Example 5.5: R-L-Diode circuit

The final example shows that the stability analysis can also be used to determine the stability of orbits obtained with HB. We consider the R-L-diode circuit shown below:

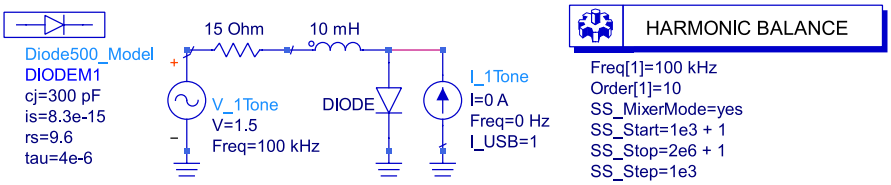

The circuit is based on [Azzo 83], but a realistic diode model was used to represent the diode in the circuit instead of the three equations provided in the original paper.

The circuit is excited by a single-tone voltage source with an amplitude V_{in} and a frequency of 100kHz. Because the diode has a transit-time of 4μs, the circuit generates period-doubling solutions for sufficiently high amplitudes V_{in}. For even higher V_{in}, the circuit will create chaotic solutions. To visualise this route to chaos, a bifurcation diagram is constructed using time-domain simulations in the same way as is described in [Azzo 83]: For every value of V_{in}, 1030 periods of 100kHz are simulated and the final 30 periods are sampled every $1/100\text{kHz}$. If the circuit solution is periodic with the same period as the input source, all 30 sampled points will fall on top of each-other. If a period-doubling occurs in the circuit, two different values will be obtained.

The obtained bifurcation diagram for our R-L-diode example is shown below:

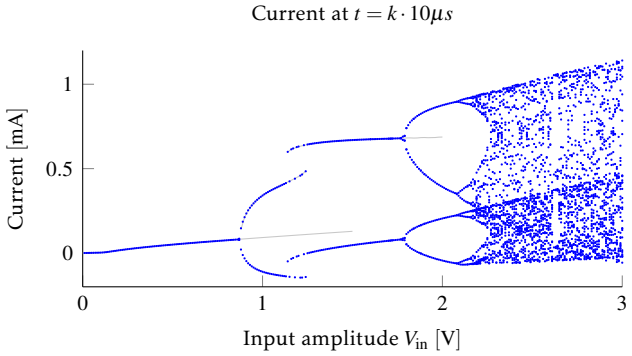

It is clear that a period-doubling occurs for V_{in} higher than 0.8V. Starting from 1.8V the period quadruples. For the highest input amplitudes, a chaotic solution is obtained.
If this R-L-diode circuit is simulated with HB, the circuit solution is constrained to harmonics of 100kHz. For input amplitudes higher than 0.8V, where the circuit wants to go to a period-doubling solution, the constrained HB solution will be locally unstable.
We run two HB simulations on this circuit. Both HB simulations have a base frequency of 100kHz and an order of 10. In the first simulation, V_{in} is set to 0.5V, which will result in a stable orbit. The second simulation has a V_{in} of 1.5V, which will cause the orbit to be unstable.
The frequency response of the linearised circuit around the HB solution is obtained with a LSSS simulation. The small-signal excitation was swept in both cases on a linear frequency grid starting from $(1\text{kHz}+1\text{Hz})$ up to $(2\text{MHz}+1\text{Hz})$ in 1kHz steps. The 1Hz was added to the start and stop values of the sweep to avoid overlap with the tones of the HB simulation. The obtained HTFs were combined then transformed to a sine and cosine basis to obtain Hermitian conjugate functions as was done before. $Z_{dd}^{[-1]}$ $Z_{dd}^{[0]}$ and $Z_{dd}^{[+1]}$ are then analysed with the stable/unstable projection method. The results for the HB solution obtained for $V_{\text{in}} = 0.5\text{V}$ are shown below:

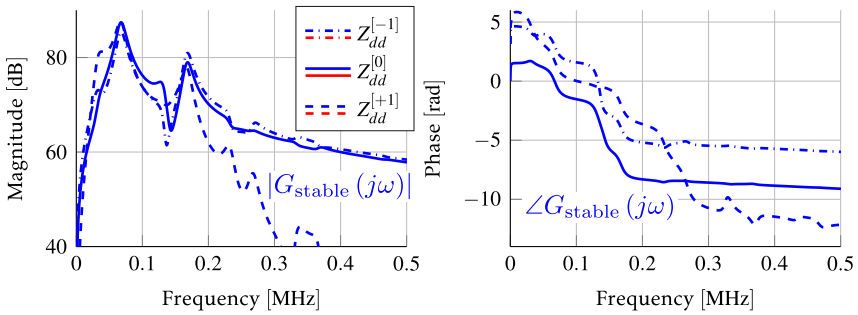

The obtained impedances are clearly stable: its unstable part is more than 70dB smaller than its stable part. The results of the stability analysis for for $V_{\text{in}} = 1.5\text{V}$ are shown next:

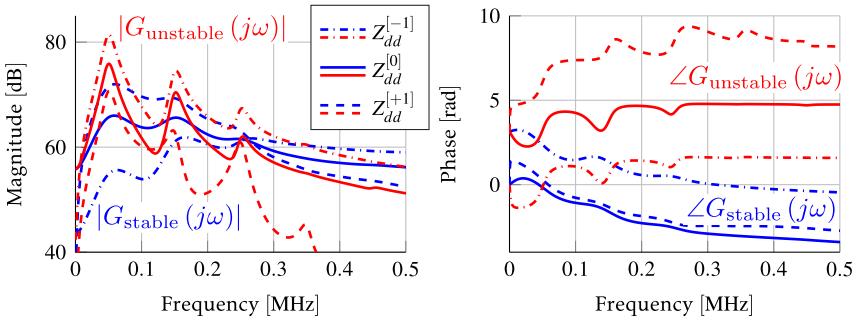

The solution is clearly unstable as the unstable part lies far above the stable part of the frequency response. Note that the lowest-frequency peak in the unstable part is located around 50kHz and that copies of the resonance are found at 150kHz, 250kHz,... This behaviour is to be expected and indicates that the circuit wants to go to a period-doubling solution.

Analysis of the period-doubled solution The system can be forced to the period-doubling solution by setting the base frequency of the HB simulation to 50kHz and by using a time-domain simulation to generate initial values for the HB simulator. Using this approach, we generated a period-doubled solution of the circuit for an input value of $V_{\text{in}} = 1.2\text{V}$. The obtained voltage across the diode for the period-doubled solution is shown in the figure below

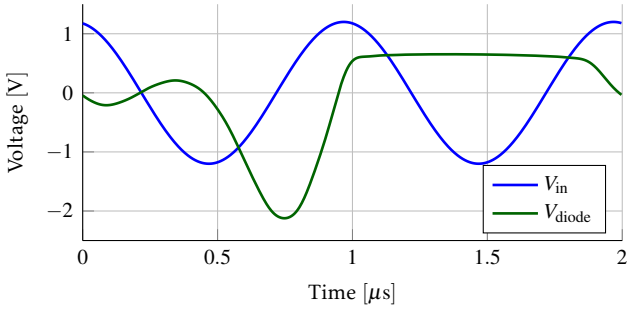

The results for the projection-based stability analysis around this period-doubled solution are shown below:

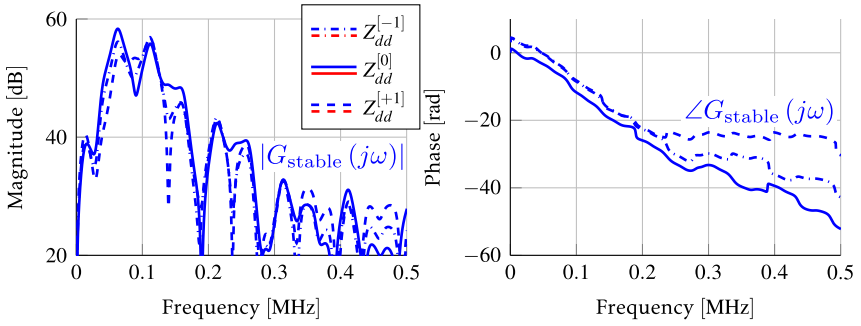

The period-doubled solution is found to be stable. The obtained unstable part is again about 70dB smaller than the stable part.

Conclusion

In this chapter, we have introduced an alternative method to determine the local stability of steady-state solutions of an electronic circuit. Commercial circuit simulators don't provide access to the Jacobian matrix of the circuit, so the local stability of a steady-state solution needs to be determined in some other way. In this chapter, we focused on closed-loop stability analysis where the FRF of the closed-loop system is analysed. When this FRF has poles in the complex right half-plane, the steady-state solution is locally unstable.

In state-of-the-art closed-loop stability analysis techniques rely on a rational approximation to determine whether the FRF has unstable poles. This method is shown to work well for lumped circuits, but struggles to analyse circuits which contain distributed elements.

We propose an alternative method based on functional projection instead of approximation. The projection-based method avoids many of the difficulties encountered in the state-of-the-art methods and is shown to effortlessly handle both lumped and distributed circuits. The projection-based method is applied to several examples to show that it is an effective way to determine the stability of both the DC and large-signal orbits.

6. Conclusions and Future work

In this final chapter of the thesis, we first summarise the results and detail the contributions made to both distortion analysis and stability analysis of analog electronic circuits. Then, we propose some possible further improvements and future research.

Distortion Contribution Analysis

In the first part of this thesis, we introduced a technique to determine the distortion contributions in a circuit excited by a modulated signal.

As was shown in chapter 1, classic methods to determine distortion will fail to accurately predict the performance of wideband electronic circuits under modulated excitation signals [De L 07]. It is therefore important to use the correct, modulated signals to get an accurate representation of the non-linear distortion introduced by the circuit.

Using a modulated signal in an already complicated circuit poses severe issues to keep the complexity of a distortion analysis in check. Some of the classic methods already return several hundreds of distortion contributions for a simple circuit under a single-tone excitation [Wamb 98]. Extending these classic methods to describe the distortion under modulated signals is a hopeless endeavour, which is why we opted for a completely different approach.

Our approach to analyse the distortion in a circuit under modulated signals is based on the Best Linear Approximation (BLA)[Pint 12]. As its name suggests, the BLA is an approximate linear model that best describes the response of a circuit or system to signals with a specified Power Spectral Density (PSD) and Probability Density Function (PDF). The BLA was introduced in chapters 2 and 3.

The BLA requires that the underlying system is a Period-In Same Period-Out (PISPO) system, but does not require it to be weakly non-linear. Hence, the results in this thesis are valid for both weakly and strongly non-linear circuits. To determine the BLA of a circuit or system in simulations, multisine signals are used instead of the real modulated signals. The multisines are shaped such that they have the same PSD and PDF as the modulated signals the circuit will encounter in its applications. Hence, the BLA and distortion obtained under multisine excitation will be a correct representation of the real-world performance of the circuit. The techniques to obtain the steady-state response of an electronic circuit to a multisine excitation were summarised in Appendix A.

In the BLA framework, the distortion is defined as “everything in the output not explained by the BLA". This distortion has noise-like properties when a modulated signal is used to excite the system. The distortion is then zero-mean and uncorrelated to the input signal. The power spectrum of the distortion added by the system is a smooth function of frequency. We have used these properties to combine the BLA with a noise analysis to calculate the distortion contributions in a circuit.

In chapter 4, we looked into the details of the BLA-based Distortion Contribution Analysis (DCA). We have shown that the distortion contributions in a circuit or system can be obtained with a three step procedure:

1. Determine the BLA of each sub-circuit.
2. Calculate the covariance matrix of all distortion sources at the output of the sub-circuits.
3. Refer each of the distortion contributions to the output of the total circuit.

The distortion contributions predict the contribution of each sub-circuit to the total distortion power seen at the output of the circuit. All contributions are real numbers. The distortion contributions were split in two classes: direct contributions, due to every sub-circuit, and correlation contributions, due to interaction between the distortion introduced by two sub-circuits. The direct contributions are always positive contributions to the total distortion power at the output of the circuit. The correlation contributions can be either positive or negative. A negative correlation contribution indicates that the distortion generated by one sub-circuit is cancelled by another. We found that it is very important to keep the correlation among the different distortion sources into account in the BLA-based DCA to obtain a correct result.

We applied the BLA-based DCA to determine the distortion contributions in several examples such as a low-frequency amplifier, a Doherty Power amplifier and a Gm-C biquad. Both weakly and strongly non-linear circuits were analysed. Some of the main advantages of the BLA-based that were demonstrated are the following

- The method can be applied hierarchically. When a sub-circuit consists of another set of sub-circuits, the BLA-based DCA can be used to zoom in on the sub-circuit. This allows the designer to limit the amount of distortion contributions in the circuit to a tractable amount.
- No special model or simulator access is required for the method to work. The BLA-based DCA can be used in a commercial simulator.
- The BLA-based DCA uses linear models and noise, two concepts designers are familiar with.
- The user of the BLA-based DCA is forced to work with the correct random excitation signals as it is impossible to define the BLA for such simple signals as two-tones.

To be able to perform the BLA-based DCA at the transistor level, we used the S^{BLA}-parameters to describe the behaviour of the sub-circuits. This is a Multiple-Input Multiple-Output (MIMO) representation. The BLA-based DCA is naturally extended to work with MIMO sub-circuits as was shown in chapter 4, but estimat-

ing the MIMO BLA of an electronic circuit in feedback is not easy. In chapter 3, we explained that, to be able to estimate the MIMO BLA, extra excitation signals need to be added to the circuit. These tickler signals are then placed on interleaved frequency grids to obtain an estimate of the S^{BLA}-parameters of the circuit.

Stability analysis

In the second part of the thesis, we shifted our attention from distortion analysis to the local stability analysis of electronic circuits. In a local stability analysis, the stability of the steady-state solutions of the circuit are investigated. These steady-state solutions can easily be obtained in a circuit simulator with a DC or Harmonic Balance (HB) simulation, but there is no guarantee that the obtained solution is stable.

The method analyses the impedance presented by the circuit to a small-signal perturbation source attached to the circuit. When this impedance has poles in the complex right half-plane, the circuit is unstable. State-of-the-art methods use a rational approximation to determine whether the impedance has poles in the right half-plane. These rational approximations work fine for the stability analysis of the DC solutions of lumped circuits, but they struggle to return reliable results in the case of circuits with transmission lines or in large-signal stability analysis.

We introduced a stability analysis method that avoids the use of a rational approximation. Instead, the impedance of the circuit is projected onto a basis of both stable and unstable functions. Stability analysis then boils down to checking whether any part of the impedance is projected onto the unstable basis functions. We showed that, when the impedance is transformed to the unit circle, the projection on the stable/unstable basis can be calculated with the Fast Fourier Transform (FFT), which makes the whole analysis very fast.

The projection-based stability analysis was successfully applied to determine the stability of several example circuits. The proposed method overcomes many of the issues encountered by the stability analysis based on rational approximations.

Proposals for future work

The proposed methods still have a lot of opportunities for improvement. Speed is the main issue here.

Speed-up the estimation of the BLA

In the current implementation of the DCA, a very large amount of time is spent acquiring enough phase realisations of the multisine(s) to obtain a good estimate of the BLA of the different sub circuits. There are many different techniques from system identification that can be used to reduce the amount of needed phase realisations.

Local modelling The first possible improvement is to use the Local Polynomial Method (LPM)[Pint 10a, Pint 10b]. The LPM uses the fact that the BLA is a smooth function of frequency to improve the quality of the estimate by fitting a local model in each of the frequency points.

Global modelling A second possibility is to go beyond local models and estimate a rational approximation on the complete obtained frequency response. This will reduce the variance on the BLA-estimate when it is done correctly. However, the model selection and validation will be a major issue.

Adding any of these methods to the DCA will increase the amount of user intervention that is needed to perform the DCA. The reason why these advanced techniques were not used was to demonstrate the bare minimum of user interaction needed to perform a BLA-based DCA.

Study what can be gained with model access

Throughout the thesis, it was assumed that no access to the internals of the transistor models was available. Although this is usually the case, it could be very interesting to investigate how the BLA-based DCA can be used with full access to the transistor models.

With access to the transistor models, the DCA could be used to predict which non-linearity inside of the transistor is adding the most non-linear distortion. Such information will only be useful in circuits that consist only of a handful of transistors, like Power Amplifiers (PAs), because the amount of distortion contributions will rise very quickly in more complicated circuits. In [Aiki 11], it is shown that such information can be used by a designer to improver the linearity of a PA.

An additional benefit of having full access to the transistor model is that the intrinsic device in the transistor often contains a perfect voltage or current controlled source. Estimating the BLA such a perfect source will be easier than estimating the S^{BLA}-parameters of the be full transistor. The estimation step in the DCA could be heavily simplified with model access. MIMO identification will still be required, but the problem of choosing the location for the tickler tones and determining their amplitude would be less outspoken.

Extend the representation for circuits with frequency translation

Throughout this thesis, we have always worked with circuits that have their input and output signals in the same frequency band. We have not studied circuits which are designed for frequency translation such as mixers. To determine the distortion contributions in a full transceiver, we need to be able to analyse mixers as well.

The BLA with frequency translation has been studied before. For mixers, the Best Mixer Approximation (BMA) has been developed [Vand 07, Vand 10]. Incorporating the BMA into the existing BLA-based DCA on the system level will not pose many issues. Including the BMA will be more difficult on the circuit level, because the MIMO extension of the BMA has not been developed yet.

The BLA with frequency translation will also improve the DCA in PAs. By adding the BMA, the distortion contributions due to the low-frequency dynamics in the power supply can be separated from the high-frequency non-linear distortion contributions. Preliminary research has been performed in that direction [Thor 11a, Thor 11b], but again, the MIMO extension of the proposed BLAextension has not been developed yet.

Extending the methods to mixed-signal applications

Besides systems with frequency translation, the second large class of circuits we cannot analyse yet with our BMA-based DCA are circuits which have their signals in both the digital and analog domain. With an extension to work in both the continuous- and discrete-time domains, the distortion introduced by Analog to Digital Convertors (ADCs) and Digital to Analog Convertors (DACs) can be analysed. [Bos 08] and [Vand 09] already show that the extension to mixed-signal applications is possible, but the details of the mixed-signal DCA, like the aliasing, will need to be looked into.

Besides ADCs and DACs, the mixed-signal BLA-based DCA could be used in the analysis of switched-capacitor circuits and in the analysis of pre-distorted power amplifiers. With a mixed-signal DCA, the analysis of many low-frequency control systems becomes possible. Applications that come to mind where non-linear distortion is critical are switching audio power amplifiers [Putz 03] and high-precision motor drives [Moha 03].

Improvements to the stability analysis

The final set of improvements that could be added to the work in this thesis are related to the stability analysis. The projection based approach is perfectly suited to detect an instability and to locate the unstable poles, but we have not looked into how this information could be used efficiently by the designer.

When an instability is encountered in the circuit, the designer wants to know what part of the circuit causes the unstable behaviour and how to resolve the problem. By analysing several different locations in the circuit, the location of the instability could be determined [Mori 16] and possibly resolved [Ayll 11].

When the circuit is stable, the current implementation of the method is not able to provide any information on how far from instability the circuit is located. By estimating the poles of the stable part, some of that information could be obtained. Estimating the poles of the stable part is a very difficult task however, due to the distributed elements present in the circuits.

When the stable and unstable poles of the circuit can be obtained, the stability as a function of one or more circuit parameters could be investigated by determining the trajectories of the circuit poles in the complex plane. The pole trajectories as a function of the amplitude of the excitation signal in a large-signal stability analysis are commonly used. Another interesting problem is to investigate the stability of a circuit a function of its load impedances.

A. Steady-state Simulation under multisine excitation

The simulation steps needed to obtain the steady-state response of an electronic circuit under a multisine excitation are detailed in this appendix.

The techniques detailed here are definitely not new, many people in the past have performed similar simulations. I mainly base the steps explained here on the research done by Ludwig De Locht [De L 07] and on tips and common-sense provided by Gerd Vandersteen. For the implementation in Advanced Design System (ADS)*, I worked together closely with Piet Bronders.*

Problem statement: Consider a simulation set-up of an electronic circuit and a given multisine excitation signal. The aim is to obtain the spectrum of the steady-state response of the circuit to the multisine excitation with commercial simulation tools.

The circuit under test assumed to be PISPO, which implies that it is a stable circuit that doesn't generate sub-harmonics or quasi-periodic solutions. The PISPO circuits only generate harmonics and intermodulation tones of its input signal.

Most electronic circuits will generate a large number (theoretically an infinite amount) of harmonics and intermodulation products due to feedback around the non-linear circuits or due to the non-polynomial non-linearities in the devices [Maas 88]. Infinity is not really a useful number to work with, so we define the non-linear order of the circuit א as the order of non-linearity needed to explain all harmonics and intermodulation products that lie significantly above the numeric noise floor.

The definition of the non-linear order of the circuit is unconventional, as it depends on properties that are not related to the circuit itself such as the amplitude level of the input signal, the numerical precision of the simulator and the simulation options. It is therefore rarely the case that א is known a-priori and several simulations have to be run to properly determine א. This leads to a chicken-or-egg problem where a correct simulation is needed to properly determine א, but א is needed to set-up a proper simulation. After a few iterations and with some common sense, it is usually possible to obtain a reasonable guess for the order א.

Example A.1: Determining the order ℵ of a circuit

As a simple example, we consider a non-linear resistor driven by a voltage source with an output impedance of 1Ω.

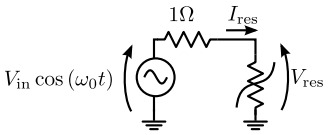

$$I_{\text{res}} = V_{\text{res}} + 0.1V_{\text{res}}^2 + 0.01V_{\text{res}}^3$$

The non-linear resistor has a polynomial voltage-current relationship of third order. The finite output impedance of the voltage source introduces feedback around the non-linear resistor, which will cause an infinite amount of harmonics originating from the circuit. We perform two simulations with an excessive non-linear order of 20 to show how ℵ is to be selected. The amplitude of the input generator is set first to 0.1V and then to 1V. The magnitude of the current below is plotted below:

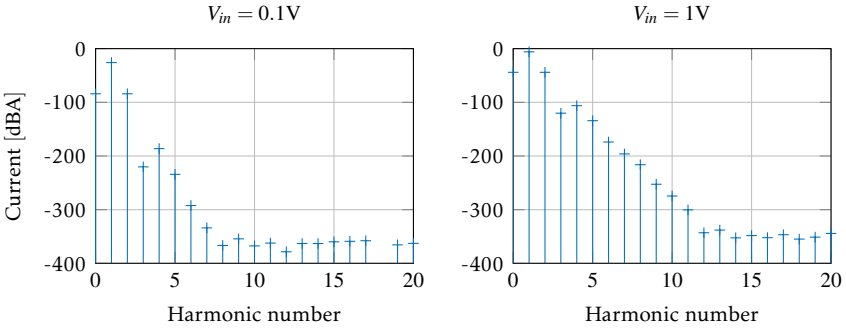

In the first case ($V_{\text{in}} = 0.1\text{V}$) the magnitude of the harmonics of the current lies below the numeric noise floor of −350dB starting from the harmonic number 8, so setting $\aleph = 8$ in this case seems the good option. When the input amplitude is raised to 1V, many more harmonics appear and ℵ should be set to 12.

Note that, in this purely static circuit, the harmonics alone can be used to determine the non-linear order. In a dynamic circuit, harmonics can be filtered, so also the intermodulation should be taken into account to obtain a proper choice for ℵ.

In this simple circuit, checking only one signal is sufficient. In a larger circuit, the amount of harmonics present in each signal differs, so many signals should be checked and the worst-case ℵ should be used.

A.1. Multisine source

Recall that a multisine is described by the following relation:

$$r(t) = \sum_{k=1}^{k_{\max}} A_k \sin(2\pi k f_{\text{res}} t + \phi_k) \tag{A.1}$$

A_k is the amplitude of the k^{th} component of the multisine, ϕ_k is the phase of the k^{th} component. Usually, the ϕ_k are chosen randomly from $[0, 2\pi[$. f_{res} is the base frequency of frequency resolution of the multisine. The period of the multisine is determined by $1/f_{\text{res}}$. The maximum frequency of the multisine $k_{\max} f_{\text{res}}$ will be denoted $f_{\max}$. We will make a difference between lowpass and bandpass multisines.

Bandpass multisines

In a bandpass multisine, the A_k are zero for all frequencies smaller than $f_{\min} = k_{\min} f_{\text{res}}$.

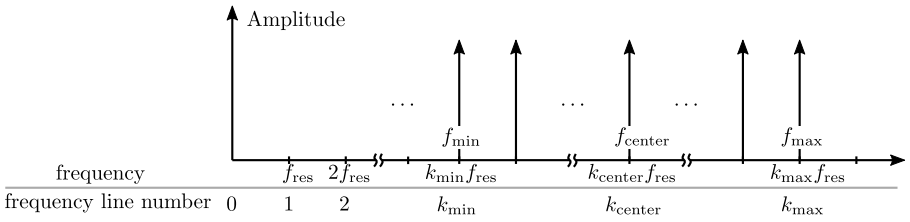

The bandwidth of the multisine $f_{\text{bandwidth}}$ is defined as $f_{\max} - f_{\min}$. The center frequency of the multisine is $f_{\text{center}} = 1/2(f_{\max} + f_{\min})$. To simplify simulating the multisine, we will always ensure that f_{center} is an integer multiple of f_{res}: $f_{\text{center}} = k_{\text{center}} f_{\text{res}}$. This means that $k_{\max} + k_{\min}$ has to be an even number. Due to this limitation, the amount of tones that can fall in the bandwidth of the bandpass multisine will always be an odd number. This amount of tones will be indicated with k_{tones} and it is equal to $k_{\max} - k_{\min} + 1$.

The spectral regrowth generated by a non-linear circuit excited by bandpass multisine will have the shape as shown in Figure A.1. The black area in the spectrum indicates the frequency band excited by the bandpass multisine. Odd order non-linear contributions are indicated in red, while even order contributions are shown in blue. The non-linear distortion appears in frequency bands around the harmonics of the center frequency. When the bandwidth is small enough and the spectral regrowth due to the non-linearity remains limited, no non-linear contributions are present in between the different bands. This property will be

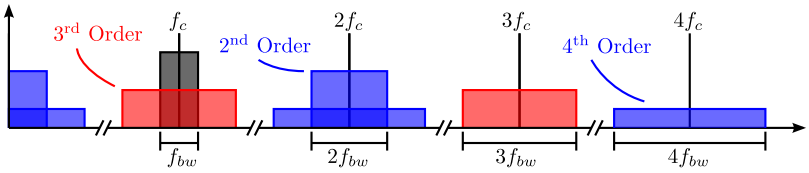

Figure A.1.: Response of a non-linear system with $\aleph = 4$ to a bandpass multisine.

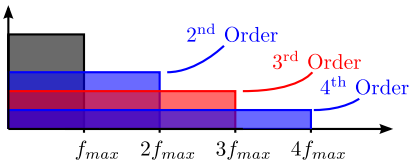

Figure A.2.: Response of a non-linear system with $\aleph = 4$ to a lowpass multisine. In both figures here, the black shaded area indicates the multisine frequency band. Odd-order distortion is shown in red, even-order distortion is shown in blue.

exploited in harmonic balance and envelope simulations. Even and odd non-linear contributions appear only around the even and odd harmonics of the center frequency respectively, so they are automatically separated in bandpass systems. The maximum bandwidth of non-linear contributions around the harmonics of the center frequency is $\aleph f_{\text{bandwidth}}$. The maximum frequency at which a non-linear contribution appears is $\aleph f_{\text{max}} = \aleph\,(f_{\text{center}} f_{\text{bandwidth}}/2)$.

Lowpass multisines

A lowpass multisine excites frequencies starting from DC, so $f_{\text{min}} = f_{\text{res}}$.

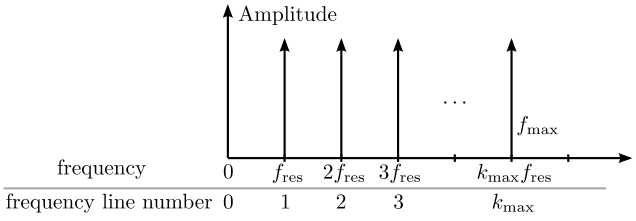

The distortion generated by a non-linear circuit as a response to a lowpass multisine is shown below:

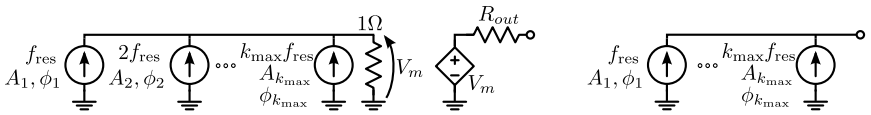

Figure A.3.: A multisine voltage source is shown on the left. On the right, a multisine current source is shown.

Again, the multisine is indicated in black, even-order distortion in blue and odd-order distortion in red. With a lowpass multisine as excitation signal, the even and odd non-linear contributions will overlap. Only exciting odd frequency bins in the multisine ($A_k = 0$ for all even k) allows to split the even and odd non-linear contributions: Even order non-linear distortion will be mapped on even frequency lines, while odd non-linear distortion will contribute on odd frequency lines. Note that DC should not be excited when applying the odd multisine excitation.

Multisine implementation in circuit simulation

In a circuit simulator, the multisine is best implemented with parallel current sources that inject their current in a 1Ω resistor, followed by a voltage controlled voltage source with the specified output impedance [De L 07]. If a multisine current source is required, only the parallel current sources should be added to the netlist. Both circuits are shown in Figure A.3.

Obtaining the response of a non-linear circuit to a multisine excitation can be done with many different simulators. The popular simulators are HB, Envelope, Transient and Periodic Steady-State (PSS) simulator. For the circuit-level simulations in this thesis, Keysight's ADS was used. In ADS, only the first three simulators are available, so these will be discussed further in this appendix. The PSS simulator can be considered as a special case of the transient simulation that imposes the periodicity of the initial and the final state, and it requires similar simulation settings than a transient simulation.

A.2. Transient simulators

In a transient analysis, the circuit behaviour is simulated at discrete time-steps. The user can control the start time (t_{start}), stop time (t_{stop}) and the time-step (t_{step}) used in the analysis. The continuous-time derivatives in the circuit have to be approximated in the discrete-time transient simulation. The way this approximation is performed is referred to as the integration method, which can be chosen by the user as well.

These 4 parameters (t_{start}, t_{stop}, t_{step} and the integration method) have to be set by the user. Once the time-domain waveforms are calculated by the simulator, they can be transformed to the frequency domain in a post-processing step.

Choosing the time-step

Both a fixed and variable time-step can be used in most commercially available transient simulators. Since we'd like to calculate the spectrum of the signals with the FFT, the time samples have to be equally spaced in time. This equal spacing is automatically obtained when a fixed time-step is used in the transient simulation. We will always use a fixed time-step in our time-domain simulations. If a variable time-step is used, the data can be interpolated to the fixed grid in time, but this will introduce interpolation errors. Alternatively, the simulator can be forced to simulate every time-point on an equally-spaced time-grid while the underlying time-step is still left free to take smaller steps when needed [Spec 03].

The fixed time step in a transient analysis is chosen such that the highest significant harmonic generated in the circuit can be represented in the simulation. The sample frequency f_{sample} should be at least $2 \aleph f_{max}$ to allow proper sampling of all harmonics without aliasing. To prevent spectral leakage when calculating the spectra using the FFT, the sample frequency should be chosen as an integer multiple of the frequency resolution.

It can happen that the corresponding time step $1/2 \aleph f_{max}$ cannot be represented by a finite amount of digits. An f_{sample} of 300kHz, for example, will result in a time-step t_{sample} of $3.33\ldots\mu$s. Rounding errors in the simulator can then introduce weird effects. Increasing f_{sample} to 400kHz yields a nicer t_{sample} of 2.5μs which can easily be written correctly to the netlist.

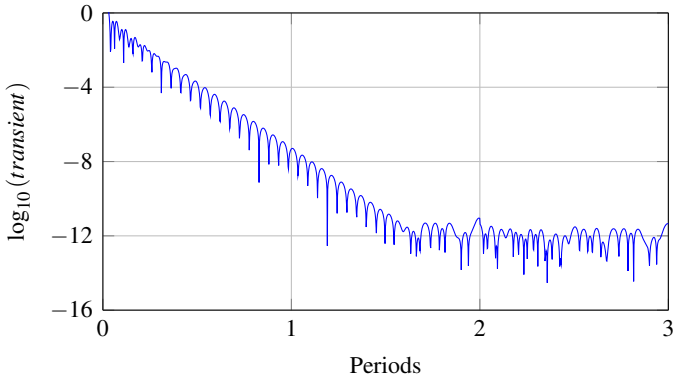

Figure A.4.: Result of subtracting the final period in a transient simulation from the previous ones. It is clear that the circuit reaches steady-state after 1.5 periods.

Choosing the start and stop-time

At least one period of the multisine should be simulated, so t_{stop} should be larger than $1/f_{\text{res}}$. Due to the initial conditions present in the circuit, a transient will be present in the signal. The simulation should be run long enough to allow the transient to damp out such that the circuit reaches steady-state. The length of the transient depends on the quality factors of possible resonances in the circuit, so it should be checked carefully whether transient is still present in the signals. This can be done by inspecting the obtained spectrum for leakage, or by subtracting the final period from the previous ones as is shown in Figure A.4. To create that figure, a transient simulation with 4 periods was run. The final period was subtracted from the three previous periods and the logarithm of the norm of the remainder of that subtraction is plotted. From such a plot, it can be concluded that the circuit reaches steady-state after 1.5 periods of the multisine, so t_{stop} should be set to 2.5 periods of the multisine.

The start time of the simulator t_{start} controls when the simulated points are returned to the user. Internally, the simulation starts always at $t = 0$, but to limit the amount of data stored to disc, the start time can be set. The transient from the initial conditions to steady-state contains a lot of information about the circuit behaviour, so our simulations always use $t_{\text{start}} = 0$.

Choosing the integration method

It is best to set the integration method of the transient analysis to trapezoidal [Kund 95]. Unlike other integration methods, trapezoidal integration doesn't introduce artificial damping into the circuit. Trapezoidal integration still introduces frequency warping in the circuit. With frequency warping, it is as if the circuit is being simulated at different frequencies as the ones specified in the multisine. The relation between the original frequencies and the warped frequencies is known and given by

$$f_{\text{warp}} = \frac{1}{\pi t_{\text{s}}} \tan\left(\pi f_{\text{original}} t_{\text{sample}}\right)$$

If, for example, a single tone at a frequency of 1GHz is applied to a bandpass filter and the whole circuit is simulated with a sample frequency of 4GHz, the original frequency is warped to 1.27GHz. If the bandpass filter has a narrow band around 1GHz, it can happen that the tone is filtered out, while it should not have been. To overcome this issue, a larger sample frequency should be used, or the warping should be taken into account properly on beforehand.

Transforming to the frequency domain

Once the simulation has been performed over several periods of the multisine with a fixed time-step, the last period of the time domain signals can be used to obtain the spectrum using the FFT. It is best to normalise the FFT such that the magnitude of a frequency line corresponds to the peak value of each corresponding tone in the spectrum.

To be able to compare the transient analysis results with the harmonic balance results, only the positive frequencies are saved, but are multiplied by 2 to maintain the power in the signal.

Example A.2: Transient simulation on a test circuit

The three different simulators discussed in this appendix will all be used to determine the steady-state response of a test circuit which is excited by a bandpass multisine. The used test circuit consists of a static non-linearity followed by a bandpass filter:

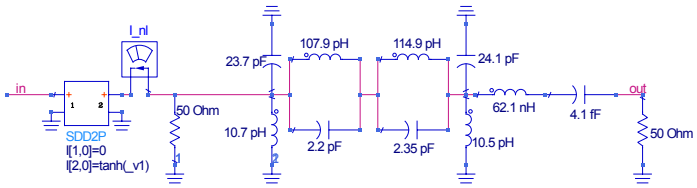

The static non-linear block is created with a Symbolically Defined Device (SDD) block from ADS. In an SDD block, the currents flowing into the ports can be specified as function of the voltage at the ports. In the configuration we used, no current flows into the input port of the SDD block while the output current is the $\tanh(\cdot)$ of the voltage at the first port. The bandpass filter is an elliptic bandpass filter with its center frequency around 10GHz and a bandwidth of 200MHz. Due to rounding errors in the components, the filter's frequency response deviates from the ideal elliptic frequency response, but this imperfection in the filter response matters little for the goal of this example. The inductors in the filter have been given a series resistance of 1pΩ to avoid simulation errors due to the loop of shorts created by the inductors in the filter.

The whole circuit is excited by a bandpass multisine connected to the *in* node of the circuit. The multisine has a frequency resolution of $f_{\text{res}} = 5\text{MHz}$ and a center frequency $f_{\text{center}} = 10\text{GHz}$. The multisine excites $T = 41$ frequencies in a 200MHz band around the center frequency, which results in $f_{\text{min}} = 9.9\text{GHz}$ and $f_{\text{max}} = 10.1\text{GHz}$. The root mean square (rms) voltage of the multisine is set to 0.2V and the multisine has a DC offset of 1V.

The non-linear order $\aleph$ of the circuit was set to 12, so a minimum sampling frequency of $2 \cdot 12 \cdot 10.1\text{GHz} = 242\text{GHz}$ is needed to be able to represent every harmonic up to the twelfth order in the circuit. This sampling frequency is rounded up to 250GHz to obtain a time-step t_{sample} of 4ps instead of the time step of 4.132...ps which corresponds to a sample frequency of 242GHz. 4 periods of the multisine were simulated to obtain the steady-state response of the circuit, so t_{stop} of the simulation was set to 800ns. To verify that the circuit is in steady-state, the different periods were compared

to the last period. The plot shown in Figure A.4 shows the result of the steady-state check obtained for this transient simulation.
With these settings, the transient simulator returns 200001 time samples for each of the measured signals. One period of the multisine corresponds to 50000 points. The last 50000 points in the waveforms were transformed to the frequency domain using the FFT. The result is shown below:

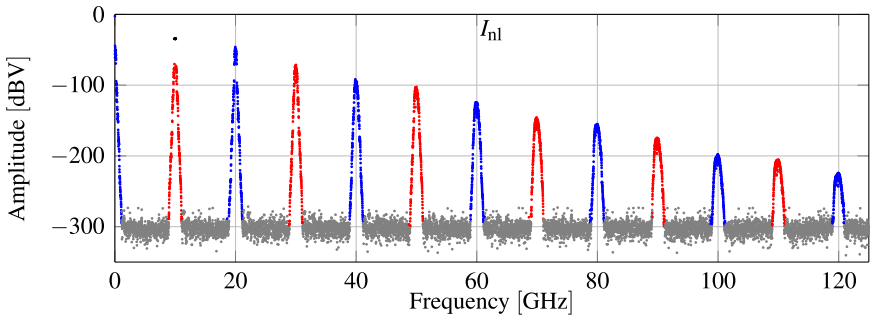

Looking at the harmonics in the spectrum of V_{int} indicates that the chosen $\aleph$ is still too low, although the error made at $\aleph = 12$ can be assumed low enough. Below, we show the output signal of the non-linear block and the output signal of the filter around the center frequency of the multisine:

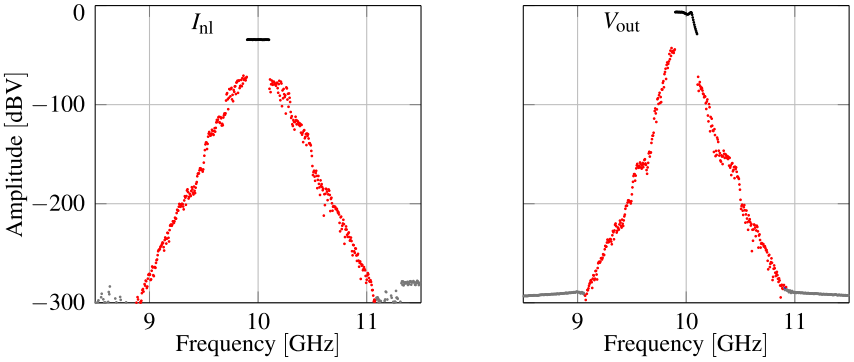

The steady-state spectrum of V_{out} contains some indications of the frequency warping effect: The multisine is placed in the middle of the passband of the filter, but the transient simulation indicates that its highest frequencies are filtered out.
Another way to visualise the frequency warping warping present in the transient simulator is by determining the Frequency Response Function (FRF) of the elliptic filter starting from the obtained steady-state

response. Once the steady-state spectra are calculated, calculating the frequency response of the filter boils down to a simple division in the frequency domain:

$$H_{\text{filter}}(j\omega_k) = \frac{V_{\text{out}}(k)}{I_{\text{nl}}(k)}$$

The results of this division are shown in green below. The FRF of the filter obtained with an AC simulation is shown with an orange dashed line.

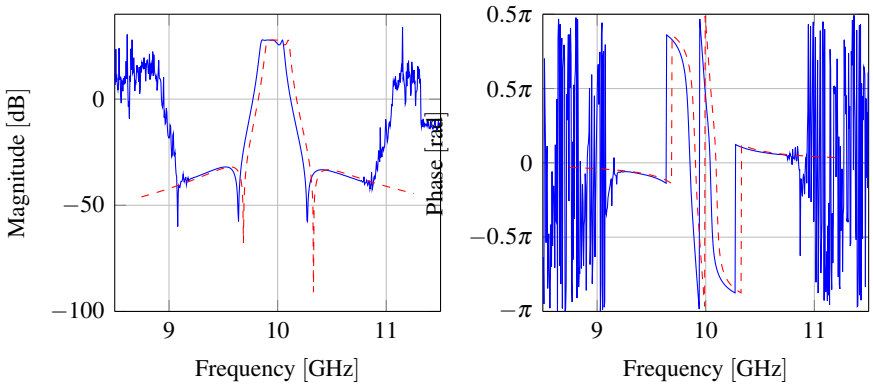

When the two FRFs are compared we can again see the frequency shift introduced by the transient simulation: the whole frequency response of the filter is shifted to higher frequencies due to the warping. The reason for the noisy estimate of the filter far away from the passband is due to the very low amplitude input signal at those frequencies. Outside of the frequency band excited by the multisine, the intermodulation distortion created by the non-linear block is used as input signal for the estimation of the filter frequency response.

A.3. Harmonic Balance simulators

The second simulator we consider is called Harmonic Balance (HB). In a HB simulation, the linear parts of the circuit are solved in the frequency domain. In the HB implementation of ADS, the response of the non-linear parts is obtained by simulation in the time-domain. The simulator then balances the responses of the linear and non-linear parts of the circuit such that the Kirchoff laws are satisfied at the interface between both the linear and non-linear parts [Maas 88]. For the HB simulation, it is assumed that all signals in the circuit are represented as a set of n base frequencies f_i with their harmonics and mixing frequencies:

$$z(t) = \sum_{k_1=-\infty}^{\infty} \cdots \sum_{k_n=-\infty}^{\infty} Z_{k_1 \ldots k_n} e^{j2\pi(k_1 f_1 + \ldots + k_n f_n)t} \tag{A.2}$$

The different base frequencies (f_i) have to be set by the user. In ADS, the amount of harmonics for each frequency is limited by its order, indicated here with O_{f_i}. The amount of mixing $|k_i + k_j|$ is limited by a parameter called *maximum mixing order.* This way of limiting the frequency grid is called *diamond truncation* [Pedr 03].

The HB simulator returns the steady-state response of the circuit in the frequency domain by retuning the different $Z_{k_1 \ldots k_n}$ phasors. No post-processing step is needed to calculate the spectra.

Setting the frequency grid

For a lowpass multisine, setting the HB frequency grid is easy: A single-frequency grid ($n = 1$) is used with frequency f_{res} and $O_{f_{\text{res}}} = \aleph k_{\max}$.

In a simulation with a bandpass multisine, the spectrum of the signals in the circuit is limited to bands around f_{center} of the multisine. When the spectral regrowth around the different harmonics of f_{center} starts overlapping a single-frequency grid with f_{res} and $O_{f_{\text{res}}} = \aleph k_{\max}$ should be used. When there is no overlap between the spectral regrowth around each harmonic of f_{center}, a two-frequency grid with base frequencies f_{res} and f_{center} is used to create a band of frequencies around each harmonic of f_{center}.

$O_{f_{\text{center}}}$ is set to $\aleph$ to generate every harmonic band of the multisine. When the maximum mixing order is not limited, the bandwidth around the m^{th} harmonic of f_{center} is $2f_{\text{res}}\left(O_{f_{\text{res}}} - m\right)$ due to the properties of the diamond truncation. When the order for f_{res} is set to $O_{f_{\text{res}}} = 1/2\,\aleph\,(k_{\text{tones}} + 1)$, a frequency grid is obtained that represents all the needed frequency lines around the $\aleph$ harmonics of f_{center}.

The final thing to take into consideration while setting the HB settings is the sequence in which the frequencies and orders are passed to the simulator: either

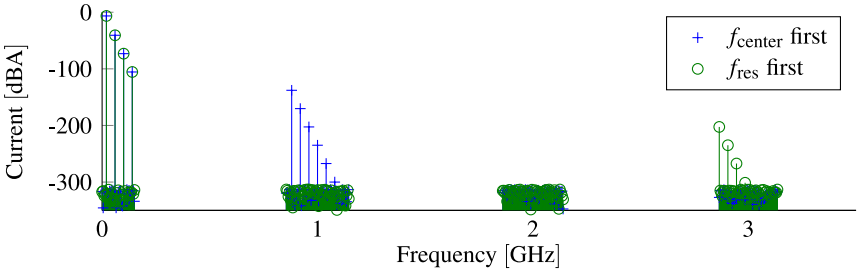

Figure A.5.: The order in which the frequencies are passed to the HB simulator influences the way tones alias from one frequency band to another.

f_{center} is passed first and then f_{res} or the other way round. The sequence of base frequencies doesn't make any difference for the obtained frequency grid, but changes how the signals are processed internally. During the HB simulation, the non-linear elements in the circuit are evaluated in the time domain. To go to the time-domain and back some form of multi-dimensional Discrete Fourier Transform (DFT) is used. One of the methods is to first map the different frequencies present in the HB simulation on a single frequency axis and transformed to a time-domain signal using a one-dimensional DFT. The obtained time-domain signal is then passed through the non-linearities in the circuit and then transformed back into the frequency domain. The combination of the mapping and the evaluation of the non-linearities in the time-domain can introduce spectral components in places that are not expected.

As an example for this effect, consider a static non-linear element excited by a single-tone excitation at 20MHz. This circuit is simulated with a HB frequency grid that contains two base frequencies: $f_{\text{res}} = 5\text{MHz}$ and $f_{\text{center}} = 1\text{GHz}$ with $O_{f_{\text{res}}} = 30$ and $O_{f_{\text{center}}} = 6$. In a first simulation, f_{res} was provided first to the simulator and f_{center} second. In a second simulation run, the order of the frequencies was changed. Both obtained spectra are shown in Figure A.5.

The first few harmonics of both simulations coincide. Once the harmonic becomes too high in frequency to be captured by the baseband frequency bins, they appear in another band. The frequency band in which these extra harmonics end up eventually is determined by the order in which the frequencies are provided to the simulator. When f_2 is provided first, the harmonics end up in the frequency band around 1GHz. When f_1 is provided first, the extra harmonics appear around the third harmonic of 1GHz.

We should note that the aliasing here occurs due to a very poor choice of $\aleph$ used in the simulation, so when a proper frequency grid is used, these strange aliased

tones will not be present in the frequency grids. During the initial simulations, where the non-linear order is still being selected, it can however be very confusing to encounter such aliased tones.

It is a personal preference to set to order of the frequencies in the harmonic balance simulation such that the aliasing just jumps a single harmonic (f_{center} first), as it is easier to debug such a simulation as the one where the aliased harmonics appear is a frequency band far from the one where they are being created.

Possible convergence issues in HB simulations

Once the frequencies and the orders in the HB simulation are set, there is not much left to do for the user of the simulation in normal circumstances. Internally, the HB simulation will run a non-linear optimisation routine to obtain its solution and one hopes that is converges quickly to a result.

In ADS, the user can choose the type of non-linear solver and influence the way the derivatives of the circuit equations are calculated to speed up the convergence at the risk of introducing errors in the simulation results. In Appendix B we closely look into how these settings affect the Large-Signal Small-Signal (LSSS) simulation results. For all multisine simulations in this thesis, the solver settings in HB simulations were set to the default values.

It can happen that the non-linear optimisation does not find the correct result, although this is quite rare in forced circuit simulations like the ones considered here. In simulations of autonomous circuits like oscillators, it happens more often that the wrong orbit is obtained. When convergence issues are encountered, the initial values for a HB simulation can be obtained from a transient simulation or from another HB simulation which is run on a simpler frequency grid. Additionally, if HB detects that it cannot find a solution due to very strongly non-linear behaviour of the circuit, the simulator will start a procedure called *source stepping*. Source stepping is a continuation technique [Suar 02]: The amplitude of all generators in the circuit is scaled down to decrease the non-linear behaviour of the circuit. When a HB solution is found for the tuned-down generators, it is used as initial value for the original HB simulation where the generators are running full-force. If the initial values obtained with the scaled generators is not good, more scaled-generator HB simulations are run until a good solution is found for the original problem.

If HB is source stepping for some phase realisations of the multisine, a little bit of Crest Factor (CF) optimisation usually solves the problem. CF optimisation should be done with great care though, as it changes the PDF of the multisines involved and influences the obtained BLA.

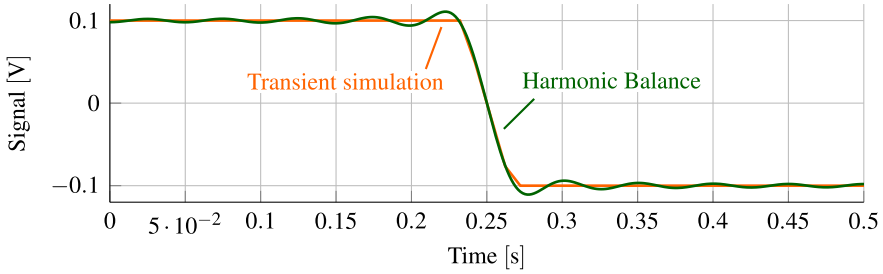

Figure A.6.: The Gibbs phenomenon is encountered when HB is used to simulate strongly non-linear behaviour, like a clipping non-linearity.

HB under switching and strongly non-linear behaviour

The HB simulator usually encounters problems when simulating circuits with very strongly non-linear behaviour, like clipping, switching or dead-zones. Another common source of convergence issues are models that are constructed by "glueing" functions together in a piecewise manner which creates discontinuities in the derivatives. These problems are mostly encountered in simulations of low-frequency circuits. For high-frequency circuits, usually the models are constructed with the HB simulator in mind and discontinuities in the models or its derivatives are avoided. Also, very abrupt clipping at these high frequencies is rare as the components used are not capable of generating the amount of harmonics required.

Many of the low-frequency transistor models on the other hand still contain discontinuities, as they are constructed only with time-domain simulations in mind. Discontinuities in the models usually introduce convergence issues in the HB simulations which are impossible to overcome without changing the transistor model.

Also, due to the very high gain in some of the low-frequency circuits, strongly non-linear behaviour can be encountered. When an operational amplifier, placed in feedback, reaches one of its supply rails abrupt clipping occurs, which is hard to capture in the frequency grids used in HB. As an example, we simulated a clipping non-linear element both with transient and HB. The result is shown in Figure A.6.

It is clear that the HB simulation struggles to represent the sudden discontinuity in the signal, while the transient simulation doesn't encounter any problem on the same circuit. The strong oscillations seen in the HB solution close to the discontinuity are due to the Gibbs phenomenon, which is encountered when a discontinuous signal is approximated by a Fourier series.

Example A.3: Harmonic Balance simulation of the test circuit

The same test set-up as in the previous example is now simulated using HB. Obtaining a result for this circuit is trivial for HB: there is no feedback in the circuit, so no non-linear optimisation steps are required to obtain the steady-state response. The static non-linear part of the circuit is evaluated in the time-domain and the obtained spectrum is passed through the elliptic filter by a simple multiplication in the frequency domain. The obtained solution will therefore be exact when the correct frequency grid is provided to the HB simulation.
The circuit is unchanged, so the same $\aleph = 12$ is used as before in the transient simulation. Because the used multisine is a bandpass multisine which excites $k_{\text{tones}} = 41$ tones around 10GHz which are spaced 5MHz apart, the HB simulator is given two frequencies $f_{\text{res}} = 5\text{MHz}$ and $f_{\text{center}} = 10\text{GHz}$ with orders $O_{f_{\text{res}}} = 252$ and $O_{f_{\text{center}}} = 12$ respectively. The maximum mixing order is set to $O_{f_{\text{res}}}$. This results in a spectrum that consists of 6157 frequencies. The obtained spectrum for the output of the non-linear block is shown below:

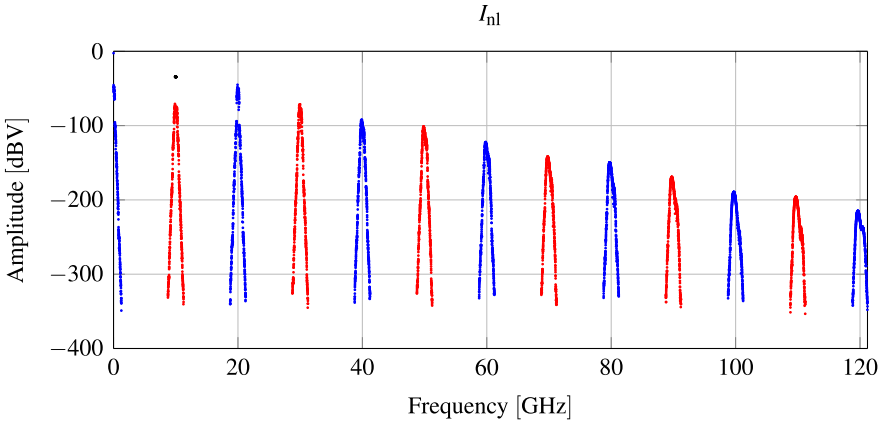

Note that the numeric noise floor in the HB simulations in ADS lies considerably lower than in the transient simulation. To be completely correct, a higher $\aleph$ should be used in this simulation, but the obtained error in this simulation is already so low that the added accuracy will be negligible. The spectra at the input and output of the elliptic filter, zoomed in around f_{center} are shown below:

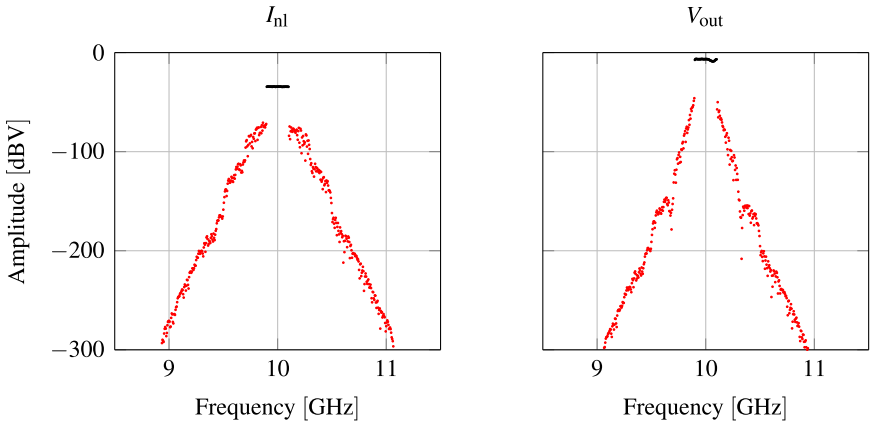

Again, these spectra are used to estimate the FRF of the elliptic filter. The obtained result is shown below

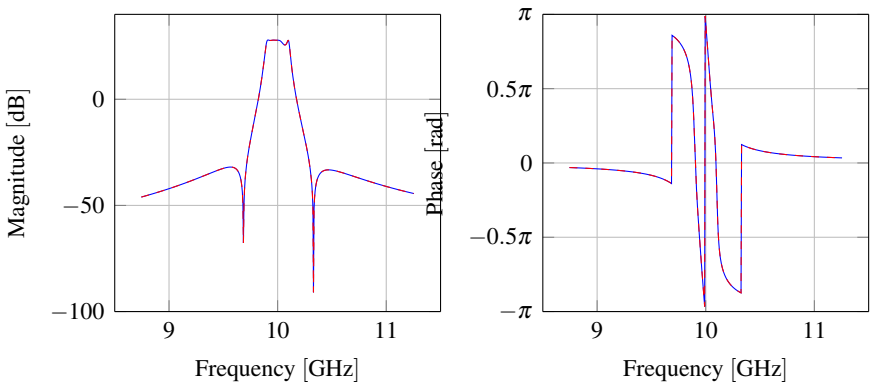

The FRF of the filter obtained with the HB coincides perfectly with the FRF obtained with an AC simulation. This is as expected, because the linear parts in the circuit are evaluated in the frequency domain during the HB simulation.

A.4. Envelope simulators

The final simulator we consider is the Envelope simulator. An envelope simulator combines the concepts of the HB simulation and transient simulation [**?**]. An envelope simulation is only useful for bandpass multisines, as it becomes equal to a transient simulation for low-pass multisines. In an envelope simulation, the internal signals in the circuit are represented as modulated harmonically related sine waves.

$$z(t) = \Re\left\{\sum_{k=0}^{N} z_k(t)\, e^{2\pi k f_{\text{center}} t}\right\} \tag{A.3}$$

each harmonic of the base frequency f_{center} is modulated with a complex time domain signal $z_k(t)$. The envelope simulation calculates the variation of the envelope $z_k(t)$ in the time domain, while the relation between the different harmonics is enforced using Harmonic Balance. This leads to two sets of simulation parameters in Envelope: f_{center} and $O_{f_{\text{center}}}$ for the underlying HB simulation and t_{stop}, t_{step} and the integration method for the time-domain part of the Envelope simulation.

Choosing the Envelope settings

The underlying HB simulation should be performed at the center frequency of the multisine f_c with an order equal to $\aleph$, the non-linear order of the circuit.

The time-step is determined using the bandwidth of the multisine. f_{sample} should be at least $\aleph f_{\text{bandwidth}}$ to allow correct sampling of all intermodulation products without aliasing. To prevent leakage, f_{sample} should be set to an integer multiple of f_{res}. Like in the transient simulation, f_{sample} is then increased such that the corresponding t_{sample} can be written down to the netlist with a finite number of digits. The current implementation of the envelope simulator in ADS only allows for a fixed time-step, but since the fixed time-step should be used anyway, this doesn't bother us much.

The stop time t_{stop} is determined in the same way as in the transient simulations. The circuit should reach steady-state, so several periods of the multisine are simulated and the difference to the final period is investigated.

Choosing the integration method

As in the transient simulation, a trapezoidal integration method is preferred to avoid artificial damping. When an Envelope simulation is run with a trapezoidal integration method in ADS, the circuit transients don't damp out after a few

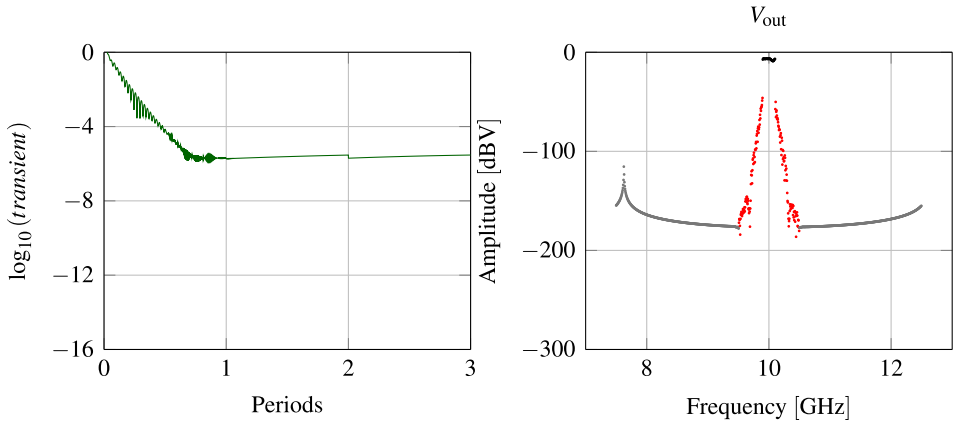

Figure A.7.: Envelope simulations on the test system reveal that a trapezoidal integration method introduces spurious oscillations. As a consequence, the circuit transient doesn't damp out fully and steady-state is not reached.

periods of the multisine and spurious oscillations appear in the circuit response. Both effects are shown in Figure A.7.

We choose to use Gear2 as an alternative integration method. When Gear2 is used, the problems disappear and the circuit reaches a steady-state. We'll have to accept the artificial damping introduced by these alternative integration methods.

Going to the Frequency domain

The envelope simulation returns the $z_k(t)$ for each of the harmonics $k = 0..\aleph$. The $z_k(t)$ are the complex time-domain signals with which each harmonic of the underlying HB simulation is modulated. In a post-processing step, the different time domain signals are transformed into the frequency domain and combined to obtain a single spectrum.

In a first step, the FFT of the last period of each of the $z_k(t)$ signals is calculated. Then, the DC bin of the signals is placed in the middle of the resulting vector using the fftshift function in Matlab. Finally, the DC bins of the different spectra are placed around their correct harmonic frequency. The base-band signal $z_0(t)$ is real-valued and has a symmetric spectrum. For $z_0(t)$ only the positive frequencies are saved in the result.

Example A.4: Envelope simulation of the test system

The same test set-up as in the previous examples of this appendix is now simulated using the envelope simulator.
The underlying HB simulation in the envelope simulation was given a frequency of 10GHz with an order equal to the non-linear order of the circuit $O_{f_{\text{center}}} = 12$. The minimum sampling frequency used in the envelope simulation is $\aleph f_{\text{bandwidth}} = 2.4\text{GHz}$. This is rounded up to 2.5GHz to obtain a round sampling time t_{sample} of 400ps.
4 periods of the multisine are simulated to allow the circuit to get into steady-state. This gives a stop time t_{stop} of 800ns. The steady-state condition was checked in the same way as is done in the transient simulations by subtracting the final period from the previous ones and by looking a the norm of the remaining signal. In an envelope simulation, this is done separately for each $z_k(t)$.
The envelope simulator returns 2000 complex time samples around every harmonic of the harmonic balance simulation, which corresponds to 26000 samples in total. The last 500 points of each time series are used to calculate the spectrum of the steady-state response. The reconstructed spectrum at the output of the non-linear element in the circuit is shown below

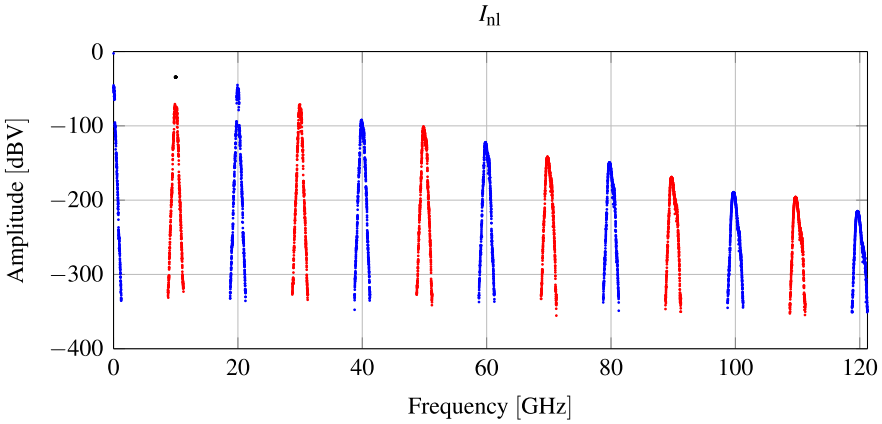

Like in the HB simulation, gaps are present in the spectrum, which results in reduced simulation time for these bandpass circuits and excitation signals compared to the transient simulation. The signals around f_{center} at the input and output of the filter are shown below:

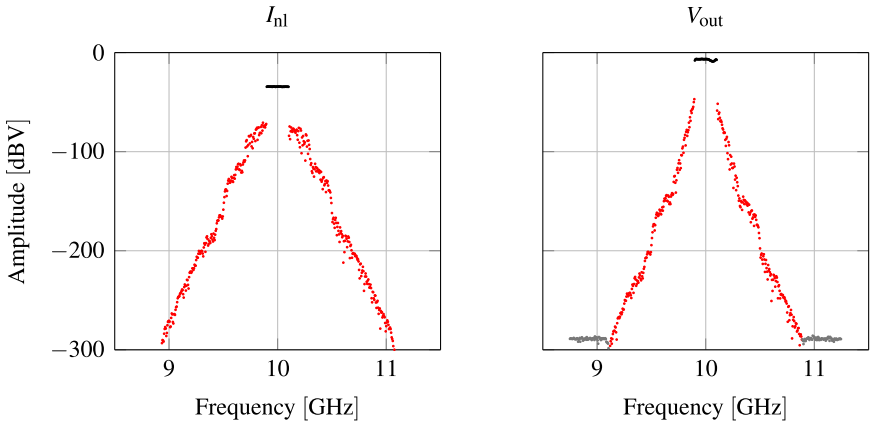

These signals are used to estimate the FRF of the elliptic filter like we did before with the spectra obtained with the transient and HB simulations:

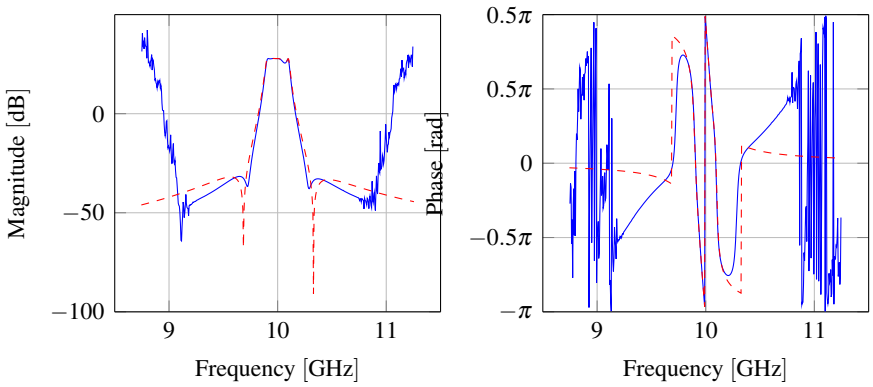

The artificial damping introduced by the Gear's integration method is clearly visible when the FRF of the filter is compared with its true FRF: the transmission zeros in the stop band of the elliptic filter are shifted from their location on the imaginary axis, which reduces their attenuation. Instead of warping the whole frequency axis, the warping in an envelope simulation is performed on a per-harmonic basis: the filter seems to be squeezed inwards around each harmonic of f_{center}.

B. Testing the Large-Signal Small-Signal simulator in ADS

Chapter 5 uses the Large-Signal Small-Signal (LSSS) simulator to determine the linearisation around a periodic orbit of a circuit. In this appendix, we verify the accuracy of the LSSS simulator in Advanced Design System (ADS). To do this, a test system with known frequency responses is simulated and the simulation results are compared to the exact expressions to discover the error level in the simulations.

We discover that the error made in the simulation is rather large when the default settings are used. By configuring the simulator correctly, a better result can be obtained. This work has been done with the help of Ebrahim Louarroudi.

A Large-Signal Small-Signal (LSSS) simulation calculates the linearised response around a periodic solution of a circuit to a small-signal excitation. A LSSS simulation is performed in two steps: First, an Harmonic Balance (HB) simulation is run to obtain the large-signal solution of the circuit to the external excitation[1]. In a second step, the linear response around the obtained solution is obtained using the Jacobian matrix of the final solution of the *HB* simulation.

In *Advanced Design System (ADS)*, the small-signal excitation is applied using a *V_1Tone* or *I_1Tone* component. Both components contain USB and LSB parameters that control the upper sideband and lower sideband small signal components. The USB and LSB components have a frequency relative to the frequency set in the 1Tone component. We will always work relative to DC, so the Freq parameter of the 1Tone components are set to 0Hz. The *V_1Tone* and *I_1Tone* components are shown below, together with the HB statement that performs the LSSS simulation:

[1] In case of an oscillator, the circuit doesn't need an external excitation, but the reasoning remains the same.

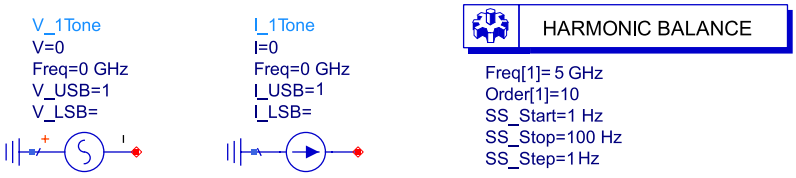

Figure B.1.: Small-signal sources and the HB statement which controls the LSSS simulation.

When the *V_1Tone* or *I_1Tone* components are configured as shown above, the LSSS will calculate the response of the periodically varying system to the following complex excitation signal:

$$i(t) = e^{j2\pi ft} \qquad v(t) = e^{j2\pi ft}$$

where the amplitude is infinitesimally small. The frequency f of the excitation signal is swept over the frequency range specified in the HB simulation. With the simulation settings above, the small-signal frequency f will be swept between 1Hz and 100Hz.

For this example, the HB base frequency is 5GHz with order 10. The LSSS will calculate the mixing with each tone in the HB simulation, which results in 21 contributions at the mixed frequencies $f + l\,(5\text{GHz})$ where $l = -10...10$.

Due to the way the response is calculated, the excitation frequency cannot be equal to any frequency in the large-signal simulation. This limitation can usually be resolved by adding a small frequency offset to the frequency grid of the small-signal simulation.

Testing the LSSS simulator

The linear system around a periodic solution is a Linear Time-Periodic (LTP) system. The behaviour of such a LTP system can be described perfectly by a infinite series of Frequency Response Functions (FRFs) called Harmonic Transfer Functions (HTFs) [Loua 14] (this was discussed in detail in Chapter 5). The HTF which describes the frequency response from the excitation frequency ω to a translated frequency $\omega + l\omega_{\text{ex}}$ will be denoted as $G^{[l]}_{U\to Y}(j\omega)$. ω_{ex} is used to indicate the pulsation of the LTP system.

To test the LSSS simulator, a periodically time-varying differential equation is implemented in ADS. The HTFs of such differential equations can also be calculated in Matlab using techniques described in [Loua 14]. By comparing the Matlab results to the results from ADS, we can get an indication of the error made in the simulator. The following periodically time-varying first order differential equation will be used:

$$\frac{dy(t)}{dt} + a(t)\,y(t) = u(t) \tag{B.1}$$

The time-variation $a(t)$ will be a random-phase multisine with a base pulsation of $\omega_{\text{ex}} = 2\pi f_{\text{res}} = 0.5\text{Hz}$. The multisine excites all tones up to $f_{\max} = 5\text{Hz}$. The amplitude of each tone in the multisine is set to 1 and random phases are used. A DC offset of 1 was added to the multisine as well. The resulting $a(t)$ signal is shown in Figure (B.2).

The implementation of this differential equation is done in ADS with a Symbolically Defined Device (SDD) block. The simulation set-up is shown in Figure (B.3). The SDD block in the schematic is configured such that the voltage at port 1 acts as the input signal $u(t)$ and the resulting current flowing into port 1 is the output signal $y(t)$. The control of the factor $a(t)$ is done through the second port of the SDD block. It is important to force a non-zero initial condition in that port, as setting the node to zero leads to errors in the simulation.

The whole circuit is simulated with a HB simulation with a base frequency of 0.5Hz which is given an order of 100. The LSSS was run on a logarithmic frequency grid going from 0.1Hz to 100Hz with 100 steps per decade. With these settings, ADS returns 201 HTFs sampled at 301 frequency points.

Calculating the HTFs in Matlab

For this simple differential equation, the HTFs can also be computed in Matlab using the methods described in [Loua 14]. To do so, first, we describe the time-variation of the $a(t)$-coefficient as a Fourier series:

$$a(t) = \sum_{k=-k_{\max}}^{k_{\max}} A_k e^{jk\omega_{\text{ex}}t}$$

To obtain the HTFs at a frequency f, we construct the following large matrix

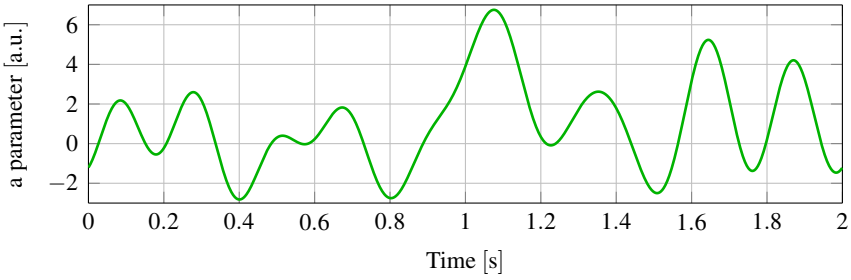

Figure B.2.: Values of the a parameter in the differential equation (B.1) as a function of time.

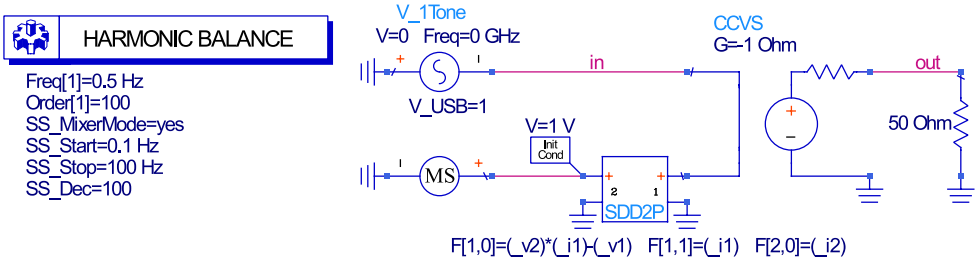

Figure B.3.: Simulation set-up in ADS to implement the time-varying differential equation (B.1)

$$\mathscr{A}(s)=\begin{bmatrix} \ddots & \ddots & \ddots & \ddots & \ddots & \ddots & \ddots \\ \ddots & A_0+s-2j\omega_{\text{ex}} & A_1 & A_2 & \ddots & \ddots & \ddots \\ \ddots & A_{-1} & A_0+s-j\omega_{\text{ex}} & A_1 & A_2 & \ddots & \ddots \\ \ddots & A_{-2} & A_{-1} & A_0+s & A_1 & A_2 & \ddots \\ \ddots & \ddots & A_{-2} & A_{-1} & A_0+s+j\omega_{\text{ex}} & A_1 & \ddots \\ \ddots & \ddots & \ddots & A_{-2} & A_{-1} & A_0+s+2j\omega_{\text{ex}} & \ddots \\ \ddots & \ddots & \ddots & \ddots & \ddots & \ddots & \ddots \end{bmatrix}$$

where $s = j2\pi f$. This $\mathscr{A}$-matrix is a band matrix. In our case, the multisine has 10 excited frequency lines, so the $\mathscr{A}$-matrix has 10 non-zero numbers above and below its diagonal. Every other number in the matrix is zero. Theoretically, the $\mathscr{A}$-matrix should be infinitely large, in practice, we will use a large square matrix of size $N \times N$. When N is significantly larger than the amount of HTFs that needs to be calculated, the error made by truncating $\mathscr{A}$ is limited [Loua 14]. We need to calculate 201 HTFs, so N was set to 401 to minimise errors.

The inverse of the $\mathscr{A}$-matrix is the Wereley matrix for this system [Loua 14, Were 91], which will be denoted as $\mathscr{G}(s)$

$$\mathscr{G}(s) = (\mathscr{A}(s))^{-1}$$

The Wereley matrix contains the HTFs of the circuit in the following arrangement:

$$\mathscr{G}(s) = \begin{bmatrix} \ddots & \ddots & \ddots & \ddots & \ddots \\ \ddots & G^{[-1]}(s-j\omega_{\text{ex}}) & \ddots & \ddots & \ddots \\ \ddots & G^{[0]}(s-j\omega_{\text{ex}}) & G^{[-1]}(s) & \ddots & \ddots \\ \ddots & G^{[+1]}(s-j\omega_{\text{ex}}) & G^{[0]}(s) & G^{[-1]}(s+j\omega_{\text{ex}}) & \ddots \\ \ddots & \ddots & G^{[+1]}(s) & G^{[0]}(s+j\omega_{\text{ex}}) & \ddots \\ \ddots & \ddots & \ddots & G^{[+1]}(s+j\omega_{\text{ex}}) & \ddots \\ \ddots & \ddots & \ddots & \ddots & \ddots \end{bmatrix}$$

so by selecting the right column out of $\mathscr{G}(s)$, the HTFs of the system are obtained.

Results of the comparison

The HTFs obtained with Matlab and ADS can now be compared. Below, we show $G^{[i]}$ for i between -40 and $+40$ in steps of 5. The HTFs obtained with Matlab are shown in light green, the HTFs obtained with ADS are shown with dark green dashed lines. The difference between both is shown in red.

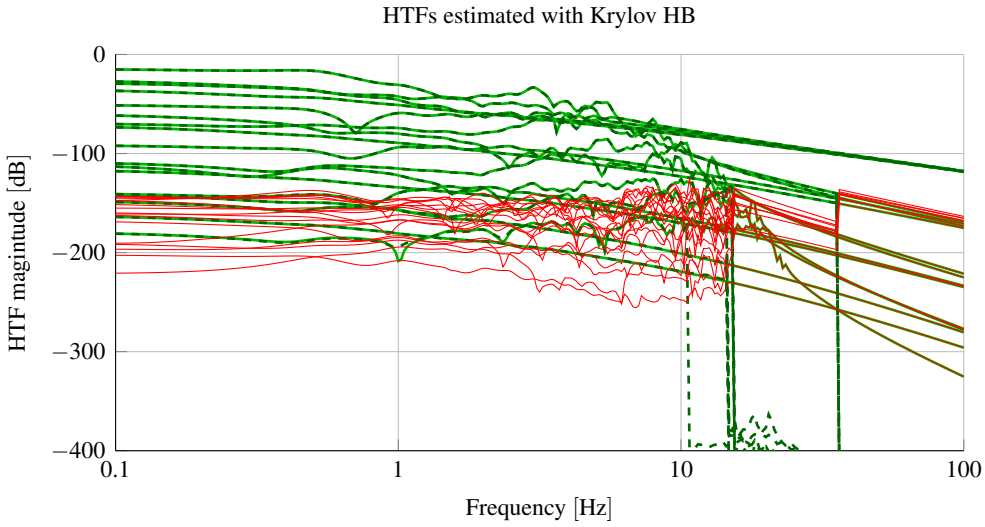

The error made in the analysis is small but not negligible. It is clear that some approximations are made in the default LSSS simulation of ADS. After some experimentation, we identified three parameters which influence the accuracy of the LSSS simulator:

Matrix Solver ADS defaults to using a Krylov method to perform matrix inversion in HB. This introduces significant errors in the LSSS simulation. When Krylov is disabled, a significant improvement in accuracy will be obtained, at the cost of a much longer simulation time and larger memory requirements.

Guard Threshold To increase sparseness in the matrices during the simulation, a Guard Threshold is used by default in ADS. Every value in the Jacobian matrix which is smaller than the Guard Threshold is set to zero. The small-signal behaviour of a circuit around its orbit is captured by this Jacobian matrix, so truncation in the Jacobian has a direct effect on the HTFs. The effect of the Guard Threshold is visible in the plot shown above: at higher frequencies, some of the HTFs jump to zero. To improve the accuracy of the LSSS simulation, the Guard Threshold is disabled by setting it to zero.

Samanskii constant To speed up convergence, the Jacobian matrix in HB is not re-calculated in every step of the optimisation routine, but the Jacobian matrix is re-used a few times. The amount of re-use is controlled by a parameter called the Samanskii constant. To guarantee that ADS re-calculates the Jacobian in the final step of the optimisation, the Samanskii constant is set to zero.

When the simulator is configured correctly, the following comparison is obtained:

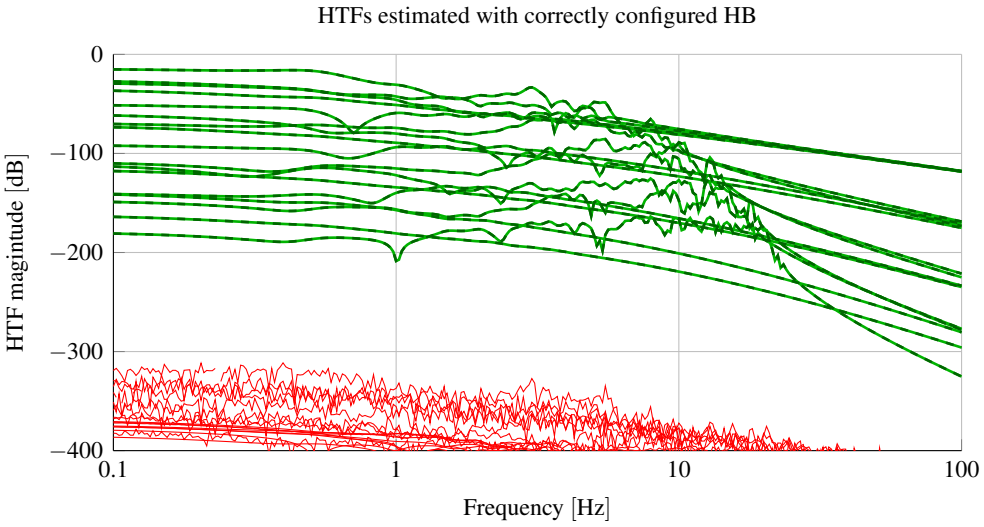

It is clear that the error made in the LSSS simulation of ADS is now determined by the numerical precision.

C. List of symbols

$\mathbb{N}$, $\mathbb{Z}$, $\mathbb{R}$ and $\mathbb{C}$	Natural, Integer, Real and Complex numbers
$\mathbb{C}^{N\times M}$	Set of $N \times M$ matrices filled with complex numbers
j	Imaginary unit $j = \sqrt{-1}$
$\lvert\cdot\rvert$	Norm of a complex number
$\Re\{\cdot\}$	Real part of a complex number
$\Im\{\cdot\}$	Imaginary part of a complex number
$\overline{X}$	Complex conjugate
x or X	Scalar
$\mathbf{x}$ or $\mathbf{X}$	Vector or matrix
$[\mathbf{X}]_{i,j}$	Element in the matrix $\mathbf{X}$ on the i^{th} column and j^{th} row.
$\mathbf{I}_N$	Identity matrix of size N
$\mathbf{0}_{N\times M}$	Matrix of size $N \times M$ filled with zeroes
$\mathbf{X}^{\mathrm{T}}$	Matrix transpose
$\mathrm{vec}(\mathbf{X})$	The vec operator stacks the columns of a matrix $\mathbf{X}$ on top of each-other. In $\mathbf{X}$ is an $M \times N$ matrix, $\mathrm{vec}(\mathbf{X})$ is a column vector of length MN.
$\otimes$	Kronecker product
$\mathbf{X}^{\mathsf{H}}$	Hermitian. The hermitian is the complex conjugate of the transpose of a matrix
$\mathbb{E}\{\cdot\}$	Expected value of a number
$x(t)$	A signal in the time domain
$X(k)$	A signal in the frequency domain at frequency bin k. The signal is measured in steady-state.
$\mathbf{X}(k)$	A vector of signals all evaluated at frequency bin k
$(j\omega_k)$	Index used to indicate a frequency corresponding to frequency bin k on a function that is continuous

Frequency Response Functions

$G^{\text{LIN}}_{X\to Y}(j\omega_k)$	Small-signal frequency response from signal X to signal Y
$G^{\text{BLA}}_{X\to Y}(j\omega_k)$	Single-Input Single-Output (SISO) Best Linear Approximation (BLA) from signal X to signal Y.
$\mathbf{G}^{\text{BLA}}_{X\to \mathbf{Y}}(j\omega_k)$	Single-Input Multiple-Output (SIMO)BLA from signal X to vector of signals $\mathbf{Y}$
$\mathbf{G}^{\text{BLA}}_{\mathbf{X}\to \mathbf{Y}}(j\omega_k)$	Multiple-Input Multiple-Output (MIMO) BLA from vector of signals $\mathbf{X}$ to vector of signals $\mathbf{Y}$
$\mathbf{C}_{\text{vec}(\mathbf{G}^{\text{BLA}}_{\mathbf{X}\to\mathbf{Y}})}(j\omega_k)$	Covariance matrix which expresses the uncertainty on the BLA-estimate. When the BLA has n_u inputs and n_y outputs, the size of this covariance matrix is $n_u n_y \times n_u n_y$.

System-level signals

$r(t)$ or $R(k)$	Reference signal
$u(t)$ or $U(k)$	Input signal of the system under test
$y(t)$ or $Y(k)$	Output of the system under test
$d(t)$ or $D(k)$	Distortion introduced by the system under test
$\mathbf{M}$	Feedback dynamics
$\mathbf{E}$	Generator dynamics
$\mathbf{O}$	Output dynamics

Circuit level signals

$V(k)$	Voltage in a circuit, The voltage signal is measured in steady-state and transformed to the frequency domain
$I(k)$	Current measured in a circuit
$Z(j\omega_k)$	Impedance of an element
$A(k)$	Incident wave
$B(k)$	Reflected wave
$\Gamma(j\omega_k)$	Reflection factor
$\mathbf{S}^{\text{LIN}}_{\mathbf{A}\to\mathbf{B}}(j\omega_k)$	S-parameters which describe the circuit with incident waves $\mathbf{A}$ and reflected waves $\mathbf{B}$. $\mathbf{S}$-matrices are always square matrices.
$\mathbf{S}^{\text{BLA}}_{\mathbf{A}\to\mathbf{B}}(j\omega_k)$	S^{BLA}-parameters of the circuit with incident waves $\mathbf{A}$ and reflected waves $\mathbf{B}$
$\mathbf{D}(k)$	Distortion introduced by the circuit. When the circuit has N ports, $\mathbf{D}(k)$ is a column vector of length N
$\mathbf{C}_{\mathbf{D}}(k)$	Covariance matrix of the distortion vector
$\mathbf{P}$	Package of the circuit
$\mathbf{L}$	Load of the circuit

Variables related to multisines

f_{res}	Frequency resolution of the multisine
A_k	Amplitude of the k^{th} frequency bin of the multisine
ϕ_{k}	Phase of the k^{th} frequency bin of a phase realisation the multisine
f_{min} and k_{min}	Minimum excited frequency of the multisine. $k_{\text{min}} = f_{\text{min}}/f_{\text{res}}$ indicates the corresponding frequency bin for f_{min}
f_{max} and k_{max}	Maximum excited frequency of the multisine. $k_{\text{max}} = f_{\text{max}}/f_{\text{res}}$ indicates the corresponding frequency bin for f_{max}
f_{center} and k_{center}	Center frequency of the excited band of the multisine. $k_{\text{center}} = f_{\text{center}}/f_{\text{res}}$ indicates the corresponding frequency bin for f_{center}
$f_{\text{bandwidth}}$	Bandwidth of the bandpass multisine: $f_{\text{bandwidth}} = f_{\text{max}} - f_{\text{min}}$

Symbols related to simulations

$\aleph$	Order of non-linearity of the circuit
t_{sample}	Sample time used in time domain simulations
f_{sample}	Sample frequency used in time domain simulations
t_{stop}	Stop time used in time domain simulations

Symbols related to stability analysis

ω_{ex}	Base pulsation of a periodic time-varying circuit.
$Z_{mn}^{[l]}(j\omega)$	Trans-impedance between nodes m and n in the circuit. $l \in \mathbb{Z}$ indicates the frequency translation $l\omega_{\text{ex}}$ in the impedance. The trans-impedances are written in a sine and cosine basis such that they are Hermitian functions.
$L^2(j\mathbb{R})$	Set of functions that are square integrable on the imaginary axis

Colors used to plot spectra

Black	Excited frequency lines of a spectrum
Red	Odd-order non-linear distortion
Blue	Even-order non-linear distortion
Magenta	A mix between odd and even-order non-linear distortion
Grey	Other frequency lines which normally contain only numerical noise

D. List of Publications

Journal publication

[Coom 13] A. Cooman, G. Vandersteen, and Y. Rolain. "Finding the dominant source of distortion in two-stage op-amps". *Analog Integrated Circuits and Signal Processing*, Vol. 78, No. 1, pp. 153–163, January 2013.

Workshop

[Vand 14] G. Vandersteen, and A. Cooman. "Nonlinear distortion analysis of circuits and systems". Tutorial 11 at the *2014 International Symposium on Circuits and Systems (ISCAS 2014)*, Melbourne, Australia, June 1, 2014

Journal publications under review

[Scho 17] M. Schoukens, J. Hammenecker, and A. Cooman. "Obtaining the Pre- Inverse of a Power Amplifier using Iterative Learning Control". Submitted to the *IEEE transactions on Microwave Theory and Techniques*

[Coom 17b] A. Cooman, F. Seyfert, M. Olivi, S. Chevillard, and L. Baratchart. "Model-Free Closed-Loop Stability Analysis: A Linear Functional Approach". Submitted to the *IEEE transactions on Microwave Theory and Techniques*

[Coom 17a] A. Cooman, P. Bronders, D. Peumans, G. Vandersteen, and Y. Rolain. "Distortion Contribution Analysis with the Best Linear Approximation". Submitted to the *IEEE Transactions on Circuits and Systems I: Regular Papers*, 2017.

Conference publications

[Coom 12] A. Cooman, E. Geerardyn, G. Vandersteen, and Y. Rolain. "Determining the Dominant Nonlinear Contributions in a multistage Op-amp in a Feedback Configuration". In: *Proceedings of the 2012 International Conference on Synthesis, Modeling, Analysis and Simulation Methods and Applications to Circuit Design (SMACD)*, september 2012.

[Coom 14] A. Cooman and G. Vandersteen. "Distortion Contribution Analysis by combining the Best Linear Approximation and noise analysis". In: *Proceedings of the 2014 International Symposium on Circuits and Systems (ISCAS 2014)*, pp. 2772 – 2775, 2014.

[Coom 15] A. Cooman and G. Vandersteen. "Wideband Distortion Contribution Analysis of Analog Circuits with Differential Signalling". In: *Proceedings of the 2015 International Conference on Synthesis, Modeling, Analysis and Simulation Methods and Applications to Circuit Design (SMACD)*, 2015.

[Coom 16a] A. Cooman, P. Bronders, and G. Vandersteen. "Distortion Contribution Analysis of strongly non-linear analog circuits". In: *Proceedings of the 2016 International Conference on Synthesis, Modeling, Analysis and Simulation Methods and Applications to Circuit Design (SMACD)*, 2016.

[Peum 16] D. Peumans, A. Cooman, and G. Vandersteen. "Analysis of Phase-Locked Loops using the Best Linear Approximation". In: *Proceedings of the 2016 International Conference on Synthesis, Modeling, Analysis and Simulation Methods and Applications to Circuit Design (SMACD)*, 2016.

[Coom 16b] A. Cooman, F. Ferranti, E. Louarroudi, Y. Rolain, and G. Vandersteen. "Common-denominator modelling for stability analysis of electronic circuits". In: *Proceedings of the 11th European Microwave Integrated Circuits Conference*, 2016.

Bibliography

[Aiki 05] J. Aikio and T. Rahkonen. "Detailed distortion analysis technique based on simulated large-signal voltage and current spectra". *IEEE Transactions on Microwave Theory and Techniques*, Vol. 53, No. 10, pp. 3057–3066, Oct 2005.

[Aiki 09] J. Aikio and T. Rahkonen. "A Comprehensive Analysis of AM-AM and AM-PM Conversion in an LDMOS RF Power Amplifier". *IEEE Transactions on Microwave Theory and Techniques*, Vol. 57, No. 2, pp. 262–270, Feb 2009.

[Aiki 11] J. P. Aikio and T. Rahkonen. "Utilization of distortion contribution analysis". In: *Circuit Theory and Design (ECCTD), 2011 20th European Conference on*, pp. 701–704, Aug 2011.

[Aiki 12] J. P. Aikio. "Distortion contribution analysis of an LDMOS Doherty power amplifier". In: *Proceeding of the Workshop on Integrated Nonlinear Microwave and Millimetre-Wave Circuits (INMMIC)*, pp. 1–3, Sept 2012.

[AMCA] AMCAD engineering. *STAN tool - Stability Analysis*.

[Anak 10] A. Anakabe, N. Ayllon, J. Collantes, A. Mallet, G. Soubercaze-Pun, and K. Narendra. "Automatic pole-zero identification for multivariable large-signal stability analysis of RF and microwave circuits". In: *Proceedings of the 2010 European Microwave Conference (EuMC)*, pp. 477–480, Sept 2010.

[Ayll 08] N. Ayllon, A. Anakabe, J. M. Collantes, G. Soubercaze-Pun, and S. Forestier. "Sensitivity enhancement in pole-zero identification based stability analysis of microwave circuits". In: *Proceedings of the Integrated Nonlinear Microwave and Millimeter Wave Circuits Workshop*, pp. 75–78, November 2008.

[Ayll 11] N. Ayllon, J. M. Collantes, A. Anakabe, I. Lizarraga, G. Soubercaze-Pun, and S. Forestier. "Systematic Approach to the Stabilization of Multitransistor Circuits". *IEEE Transactions on Microwave Theory and Techniques*, Vol. 59, No. 8, pp. 2073–2082, Aug 2011.

[Azzo 83] A. Azzouz, R. Duhr, and M. Hasler. "Transition to chaos in a simple nonlinear circuit driven by a sinusoidal voltage source". *IEEE Transactions on Circuits and Systems*, Vol. 30, No. 12, pp. 913–914, Dec 1983.

[Bara 14] L. Baratchart, S. Chevillard, and F. Seyfert. "On Transfer Functions Realizable with Active Electronic Components". Tech. Rep., Inria Sophia Antipolis, 2014. [Research Report] RR-8659 available on hal-01098616.

[Bell 63] R. Bellman and K. Cooke. *Differential-Difference Equations*. Academic Press, New York, 1963.

[Bos 08] L. Bos, G. Vandersteen, Y. Rolain, and R. Pintelon. "Analysis and Modelling of Mixed-Data Systems with Frequency Translation using Multisine Excitations". In: *Proceedings of the 2008 Instrumentation and Measurement Technology Conference (IMTC 2008)*, pp. 542 –546, may 2008.

[Brew 78] J. Brewer. "Kronecker products and matrix calculus in system theory". *IEEE Transactions on Circuits and Systems*, Vol. 25, No. 9, pp. 772–781, Sep 1978.

[Bron 08] S. Bronckers, G. Vandersteen, J. Borremans, K. Vandermot, G. Van der Plas, and Y. Rolain. "Advanced nonlinearity analysis of a 6 GHz wideband receiver". In: *Proceedings of the 2008 Instrumentation and Measurement Technology Conference (IMTC 2008)*, pp. 1340 –1343, may 2008.

[Cann 06a] S. O. Cannizzaro, G. Palumbo, and S. Pennisi. "Distortion Analysis of Miller-Compensated Three-Stage Amplifiers". *IEEE Transactions on Circuits and Systems I: Regular Papers*, Vol. 53, No. 5, pp. 961–976, May 2006.

[Cann 06b] S. Cannizzaro, G. Palumbo, and S. Pennisi. "Effects of nonlinear feedback in the frequency domain". *Circuits and Systems I: Regular Papers, IEEE Transactions on*, Vol. 53, No. 2, pp. 225 – 234, feb. 2006.

[Coll 04] J. Collantes, I. Lizarraga, A. Anakabe, and J. Jugo. "Stability verification of microwave circuits through Floquet multiplier analysis". In: *Proceedings of the 2004 IEEE Asia-Pacific Conference on Circuits and Systems*, pp. 997–1000 vol.2, Dec 2004.

[Coll 11] J. Collantes, N. Otegi, A. Anakabe, N. Ayllon, A. Mallet, and G. Soubercaze-Pun. "Monte-Carlo stability analysis of microwave amplifiers". In: *Proceedings of the 2011 IEEE 12th Annual Wireless and Microwave Technology Conference (WAMICON)*, pp. 1–6, April 2011.

[Coom 12] A. Cooman, E. Geerardyn, G. Vandersteen, and Y. Rolain. "Determining the Dominant Nonlinear Contributions in a multistage Op-amp in a Feedback Configuration". In: *Proceedings of the 2012 International Conference on Synthesis, Modeling, Analysis and Simulation Methods and Applications to Circuit Design (SMACD)*, september 2012.

[Coom 13] A. Cooman, G. Vandersteen, and Y. Rolain. "Finding the dominant source of distortion in two-stage op-amps". *Analog Integrated Circuits and Signal Processing*, Vol. 78, No. 1, pp. 153–163, Januari 2013.

[Coom 14] A. Cooman and G. Vandersteen. "Distortion Contribution Analysis by combining the Best Linear Approximation and noise analysis". In: *Proceedings of the 2014 International Symposium on Circuits and Systems (ISCAS 2014)*, pp. 2772 – 2775, 2014.

[Coom 15] A. Cooman and G. Vandersteen. "Wideband Distortion Contribution Analysis of Analog Circuits with Differential Signalling". In: *Proceedings of the 2015 International Conference on Synthesis, Modeling, Analysis and Simulation Methods and Applications to Circuit Design (SMACD)*, 2015.

[Coom 16a] A. Cooman, P. Bronders, and G. Vandersteen. "Distortion Contribution Analysis of strongly non-linear analog circuits". In: *Proceedings of the 2016 International Conference on Synthesis, Modeling, Analysis and Simulation Methods and Applications to Circuit Design (SMACD)*, 2016.

[Coom 16b] A. Cooman, F. Ferranti, E. Louarroudi, Y. Rolain, and G. Vandersteen. "Common-denominator modelling for stability analysis of electronic circuits". In: *Proceedings of the 2016 European Microwave Integrated Circuits Conference (EuMIC)*, 2016.

[Coom 17a] A. Cooman, P. Bronders, D. Peumans, G. Vandersteen, and Y. Rolain. "Distortion Contribution Analysis with the Best Linear Approximation". *Submitted to the IEEE Transactions on Circuits and Systems I: Regular Papers*, 2017.

[Coom 17b] A. Cooman, F. Seyfert, M. Olivi, S. Chevillard, and L. Baratchart. "Model-Free Closed-Loop Stability Analysis: A Linear Functional Approach". *Submitted to the IEEE Transactions on Microwave Theory and Techniques*, 2017.

[Cran 98] J. Craninckx and M. Steyaert. *Wireless CMOS Frequency Synthesizer Design*. Kluwer Academic Publishers, 1998.

[Crip 06] S. Cripps. *RF power Amplifiers for Wireless Communications, second edition*. Artech House, 2006.

[De L 04] L. De Locht, G. Vandersteen, P. Wambacq, Y. Rolain, R. Pintelon, J. Schoukens, and S. Donnay. "Identifying the main nonlinear contributions: use of multisine excitations during circuit design". In: *Proceedings of the 64th ARFTG Conference*, pp. 75–84, Dec 2004.

[De L 06] L. De Locht, Y. Rolain, and G. Vandersteen. "Designing power amplifiers? Use good excitation signals". In: *Proceedings of the 67th ARFTG Conference*, pp. 211–213, June 2006.

[De L 07] L. De Locht. *Measuring, modeling and realization of high-frequency amplifiers*. PhD thesis, Vrije Universiteit Brussel (VUB), 2007.

[Desc 08] D. Deschrijver, M. Mrozowski, T. Dhaene, and D. De Zutter. "Macromodeling of Multiport Systems Using a Fast Implementation of the Vector Fitting Method". *Microwave and Wireless Components Letters, IEEE*, Vol. 18, No. 6, pp. 383–385, June 2008.

[Dobr 03] P. Dobrovolny, G. Vandersteen, P. Wambacq, and S. Donnay. "Analysis and compact behavioral modeling of nonlinear distortion in analog communication circuits". *IEEE Transactions on Computer-Aided Design of Integrated Circuits and Systems*, Vol. 22, No. 9, pp. 1215–1227, Sept 2003.

[Dobr 89] J. A. Dobrowolski. "A CAD-oriented method for noise figure computation of two-ports with any internal topology". *Microwave Theory and Techniques, IEEE Transactions on*, Vol. 37, No. 1, pp. 15–20, Jan 1989.

[Engb 95] J. Engberg and T. Larsen. *Noise Theory of Linear and Nonlinear Circuits*. John Wiley & Sons, Inc, 1995.

[Enqv 05] M. Enqvist. *Linear Models of Nonlinear Systems*. PhD thesis, Linkoping universitet, 2005.

[Ferr 06] A. Ferrero and M. Pirola. "Generalized mixed-mode S-parameters". *IEEE Transactions on Microwave Theory and Techniques*, Vol. 54, No. 1, pp. 458–463, Jan 2006.

[Geer 13] E. Geerardyn, Y. Rolain, and J. Schoukens. "Design of Quasi-Logarithmic Multisine Excitations for Robust Broad Frequency Band Measurements". *IEEE Transactions on Instrumentation and Measurement*, Vol. 62, No. 5, pp. 1364–1372, May 2013.

[Ghan 09] F. M. Ghannouchi and O. Hammi. "Behavioral modeling and predistortion". *IEEE Microwave Magazine*, Vol. 10, No. 7, pp. 52–64, Dec 2009.

[Groe 94] G. Groenewold and W. J. Lubbers. "Systematic distortion analysis for MOSFET integrators with use of a new MOSFET model". *IEEE Transactions on Circuits and Systems II: Analog and Digital Signal Processing*, Vol. 41, No. 9, pp. 569–580, Sep 1994.

[Gust 06] B. Gustavsen. "Improving the pole relocating properties of vector fitting". *IEEE Transactions on Power Delivery*, Vol. 21, No. 3, pp. 1587–1592, July 2006.

[Gust 99] B. Gustavsen and A. Semlyen. "Rational approximation of frequency domain responses by vector fitting". *IEEE Transactions on Power Delivery*, Vol. 14, No. 3, pp. 1052–1061, Jul 1999.

[Heij 16] M. van Heijningen, A. de Hek, F. van Vliet, and S. Dellier. "Stability Analysis and Demonstration of an X-band GaN Power Amplifier MMIC". In: *Proceedings of the 11th European Microwave Integrated Circuits Conference*, 2016.

[Hern 03] B. Hernes and T. Saether. *Design Criteria for Low Distortion in Feedback Opamp Circuits*. Kluwer, 2003.

[Hern 05] B. Hernes and W. Sansen. "Distortion in Single-, Two- and Three-Stage Amplifiers". *IEEE Transactions on Circuits and Systems I: Regular Papers*, Vol. 52, No. 5, pp. 846–856, May 2005.

[Infi 07] Infineon. "Application note No. 051; SIEGET45 Low noise amplifier with BFP520 transistor at 1.9GHz". Tech. Rep., 2007.

[Jack 06] R. Jackson. "Rollett proviso in the stability of linear microwave circuits-a tutorial". *IEEE Transactions on Microwave Theory and Techniques*, Vol. 54, No. 3, pp. 993–1000, March 2006.

[Jugo 01] J. Jugo, J. Portilla, A. Anakabe, A. Suarez, and J. Collantes. "Closed-loop stability analysis of microwave amplifiers". *Electronics Letters*, Vol. 37, No. 4, pp. 226–228, Feb 2001.

[Kail 80] T. Kailath. *Linear Systems*. Prentice Hall, 1980.

[Kard 92] J. E. Kardontchik. *Introduction to the design of transconductor-capacitor filters*. Kluwer Academic Publishers Group, 1992.

[Khal 96] H. K. Khalil. *Nonlinear Systems*. Prentice Hall, 2 Ed., 1996.

[Kund 95] K. S. Kundert. *The Designer's Guide to Spice and Spectre*. Kluwer Academic Publishers, 1995.

[Kuro 65] K. Kurokawa. "Power Waves and the Scattering Matrix". *IEEE Transactions on Microwave Theory and Techniques*, Vol. 13, No. 2, pp. 194–202, Mar 1965.

[Li 03] P. Li and L. T. Pileggi. "Efficient per-nonlinearity distortion analysis for analog and RF circuits". *IEEE Transactions on Computer-Aided Design of Integrated Circuits and Systems*, Vol. 22, No. 10, pp. 1297–1309, Oct 2003.

[Loua 14] E. Louarroudi. *Frequency Domain Measurement and Identification of Weakly Nonlinear Time-Periodic Systems*. PhD thesis, Vrije Universiteit Brussel (VUB), 2014.

[Maas 86] S. A. Maas. *Microwave Mixers*. Artech House, 1986.

[Maas 88] S. A. Maas. *Nonlinear Microwave Circuits*. IEEE Press, 1988.

[Mall 13] I. Mallet, A. Ankabe, G. Soubercaze-Pun, and J.-M. Collantes. "Automation of the zero-pole identification methods for the stab analysis of microwave active circuits". Patent, 2013.

[Mark 92] R. B. Marks and D. F. Williams. "A general waveguide circuit theory". *Journal of Research-National Institute of Standards and Technology*, Vol. 97, pp. 533–533, 1992.

[Marm] J.-P. Marmorat and M. Olivi. "RARL2: a Matlab based software for H2 rational approximation".

[McCu 15] E. McCune. *Dynamic Power Supply Transmitters*. Cambridge University Press, 2015.

[Moha 03] N. Mohan, T. M. Undeland, and W. P. Robbins. *Power Electronics, Converters, Applications and Design*. John Wiley & Sons, 2003.

[Moll 00] E. Mollerstedt and B. Bernhardsson. "Out of control because of harmonics-an analysis of the harmonic response of an inverter locomotive". *Control Systems, IEEE*, Vol. 20, No. 4, pp. 70 –81, aug. 2000.

[Mona 74] V. Monaco and P. Tiberio. "Computer-Aided Analysis of Microwave Circuits". *Microwave Theory and Techniques, IEEE Transactions on*, Vol. 22, No. 3, pp. 249–263, Mar 1974.

[Mori 16] L. Mori, A. Anakabe, I. Lizarraga, N. Otegi, J. M. Collantes, V. Armengaud, and G. Soubercaze-Pun. "Stability analysis of multistage power amplifiers using Multiple-Input Multiple-Output identification". In: *Poceedings of the 2016 IEEE MTT-S International Microwave Symposium (IMS)*, pp. 1–4, May 2016.

[Mull 67] O. Muller and W. G. Figel. "Stability problems in transistor power amplifiers". *Proceedings of the IEEE*, Vol. 55, No. 8, pp. 1458–1466, Aug 1967.

[Nara 67] S. Narayanan. "Transistor distortion analysis using volterra series representation". *The Bell System Technical Journal*, Vol. 46, No. 5, pp. 991–1024, May 1967.

[Oliv 13] M. Olivi, F. Seyfert, and J.-P. Marmorat. "Identification of microwave filters by analytic and rational H2 approximation". *Automatica*, Vol. 49, Februari 2013.

[Oteg 12] N. Otegi, A. Anakabe, J. Pelaz, J. Collantes, and G. Soubercaze-Pun. "Experimental Characterization of Stability Margins in Microwave Amplifiers". *IEEE Transactions on Microwave Theory and Techniques*, Vol. 60, No. 12, pp. 4145–4156, Dec 2012.

[Pact 07] S. A. Pactitis. *Active Filters Theory and Design*. CRC Press, 2007.

[Palu 03] G. Palumbo and S. Pennisi. "High-frequency harmonic distortion in feedback amplifiers: analysis and applications". *IEEE Transactions on Circuits and Systems I: Fundamental Theory and Applications*, Vol. 50, No. 3, pp. 328 – 340, March 2003.

[Part 97] J. R. Partington. *Interpolation, Identification, and Sampling*. Oxford University Press, 1997.

[Pedr 03] J. Pedro and N. Carvalho. *Intermodulation Distortion in Microwave and Wireless Circuits*. Artech House, 2003.

[Peum 16] D. Peumans, A. Cooman, and G. Vandersteen. "Analysis of Phase-Locked Loops using the Best Linear Approximation". In: *Proceedings of the 2016 International Conference on Synthesis, Modeling, Analysis and Simulation Methods and Applications to Circuit Design (SMACD)*, pp. 1–4, June 2016.

[Pint 10a] R. Pintelon, J. Schoukens, G. Vandersteen, and K. Barbé. "Estimation of nonparametric noise and FRF models for multivariable systems Part I: Theory". *Mechanical Systems and Signal Processing*, Vol. 24, No. 3, pp. 573 – 595, 2010.

[Pint 10b] R. Pintelon, J. Schoukens, G. Vandersteen, and K. Barbé. "Estimation of nonparametric noise and FRF models for multivariable systems-Part II: Extensions, applications". *Mechanical Systems and Signal Processing*, Vol. 24, No. 3, pp. 596 – 616, 2010.

[Pint 11] R. Pintelon, G. Vandersteen, J. Schoukens, and Y. Rolain. "Improved (non-)parametric identification of dynamic systems excited by peri-

odic signals The multivariate case". *Mechanical Systems and Signal Processing*, Vol. 25, pp. 2892 – 2922, 2011.

[Pint 12] R. Pintelon and J. Schoukens. *System Identification a frequency domain approach*. John Wiley & Sons, Inc., 2 Ed., 2012.

[Pint 13] R. Pintelon and J. Schoukens. "FRF Measurement of Nonlinear Systems Operating in Closed Loop". *IEEE Transactions on Instrumentation and Measurement*, Vol. 62, No. 5, pp. 1334–1345, May 2013.

[Putz 03] B. Putzeys. "Digital Audio's Final Frontier". *IEEE Spectrum*, March 2003.

[Rive 09] D. E. Rivera, H. Lee, H. D. Mittelmann, and M. W. Braun. "Constrained multisine input signals for plant-friendly identification of chemical process systems". *Journal of Proc*, Vol. 19, No. 4, pp. 623–635, April 2009.

[Rola 13] Y. Rolain, G. Vandersteen, and M. Schoukens. *Modern RF and Microwave Measurement Techniques*, Chap. 12 Vector network analysis for nonlinear systems, pp. 309 – 344. Cambridge University Press, 2013.

[Sand 05] H. Sandberg, E. Mollerstedt, and Bernhardsson. "Frequency-domain analysis of linear time-periodic systems". *IEEE Transactions on Automatic Control*, Vol. 50, No. 12, pp. 1971 – 1983, dec. 2005.

[Sche 80] M. Schetsen. *The Volterra and Wiener Theories of Nonlinear Systems*. Wiley and Sons, 1980.

[Scho 09] J. Schoukens and R. Pintelon. "Estimation of Nonparametric Noise Models for Linear Dynamic Systems". *IEEE Transactions on Instrumentation and Measurement*, Vol. 58, No. 8, pp. 2468–2474, Aug 2009.

[Scho 17] M. Schoukens, J. Hammenecker, and A. Cooman. "Obtaining the Pre-Inverse of a Power Amplifier using Iterative Learning Control". *Submitted to the IEEE transactions on Microwave Theory and Techniques*, 2017.

[Scho 98] J. Schoukens and T. Dobrowiecki. "Design of broadband excitation signals with a user imposed power spectrum and amplitude distribution". In: *Proceedings of the 1998 Instrumentation and Measurement Technology Conference (IMTC 98)*, pp. 1002–1005 vol.2, May 1998.

[Spec 03] *Spectre Circuit Simulator Reference*. Cadence, product version 5.0 Ed., September 2003.

[Suar 02] A. Suarez and R. Quere. *Stability analysis of nonlinear microwave circuits*. Artech House, 2002.

[Suar 15] A. Suarez. "Check the Stability: Stability Analysis Methods for Microwave Circuits". *Microwave Magazine, IEEE*, Vol. 16, No. 5, pp. 69–90, June 2015.

[Thor 11a] M. Thorsell, K. Anderson, G. Pailloncy, and Y. Rolain. "Using the Best Linear Approximation to Model the Nonlinear Behavior of Supply Modulated Amplifiers". In: *Proceedings of the 6th European Microwave Integrated Circuits Conference*, 2011.

[Thor 11b] M. Thorsell, K. Andersson, G. Pailloncy, and Y. Rolain. "Extending the Best Linear Approximation to Characterize the Nonlinear Distortion in GaN HEMTs". *IEEE Transactions on Microwave Theory and Techniques*, Vol. 59, No. 12, pp. 3087–3094, Dec 2011.

[Tian 01] M. Tian, V. Visvanathan, J. Hantgan, and K. Kundert. "Striving for small-signal stability". *IEEE Circuits and Devices Magazine*, Vol. 17, No. 1, pp. 31–41, January 2001.

[Vand 07] K. Vandermot, W. Van Moer, Y. Rolain, and R. Pintelon. "Extending the Best Linear Approximation for Frequency Translating Systems: The Best Mixer Approximation". In: *Instrumentation and Measurement Technology Conference Proceedings, 2007. IMTC 2007. IEEE*, pp. 1 –6, may 2007.

[Vand 09] G. Vandersteen and L. De Locht. "Qualification and quantification of the nonlinear distortions in discrete-time sigma-delta ADCs". In: *Proceedings of the European Conference on Circuit Theory and Design (ECCTD)*, pp. 759–762, Aug 2009.

[Vand 10] K. Vandermot. *Best Linearized models for RF systems*. PhD thesis, Vrije Universiteit Brussel (VUB), 2010.

[Vand 14] G. Vandersteen and A. Cooman. "Nonlinear distortion analysis of circuits and systems". Tutorial at the 2014 International Symposium on Circuits and Systems (ISCAS 2014), june 2014.

[Vanh 00] K. Vanhoenacker, T. Dobrowiecki, and J. Schoukens. "Design of multisine excitations to characterize the nonlinear distortions during FRF-measurements". In: *Proceedings of the 17th IEEE Instrumentation and Measurement Technology Conference (IMTC)*, pp. 1254–1259 vol.3, 2000.

[Verb 99] J. Verbeeck, R. Pintelon, and P. Lataire. "Identification of synchronous machine parameters using a multiple input multiple output approach". *IEEE Transactions on Energy Conversion*, Vol. 14, No. 4, pp. 909–917, Dec 1999.

[Wamb 98] P. Wambacq and W. Sansen. *Distortion Analysis of Analog Integrated Circuits*. Kluwer, 1998.

[Wamb 99] P. Wambacq, G. G. E. Gielen, P. R. Kinget, and W. Sansen. "High-frequency distortion analysis of analog integrated circuits". *IEEE Transactions on Circuits and Systems II: Analog and Digital Signal Processing*, Vol. 46, No. 3, pp. 335–345, Mar 1999.

[Were 91] N. M. Wereley. *Analysis and control of linear periodically time varying systems*. PhD thesis, Massachusets Institute of Technology (MIT), 1991.

Acknowledgements

Doing a PhD was a lot of fun. Messing around with electronics and simulators is a great way to spend four years, especially when it all happens at the VUB.

Research is teamwork and I was part of a great team. Without the expertise of the following people, this thesis would not have been. I would like to thank Gerd, Rik and Yves for always being there to answer questions. Thanks to Ebrahim, Francesco, Maarten, Egon, Piet and Dries for helping me with the dirty details of the science, the programming and the writing. All this cannot be done without the excellent technical support provided by Sven, Ann and Johan.

For the part on stability analysis I would like to thank Fabien, Martine, Laurent and Sylvain for the invitation to France and for the fruitful collaboration.

Thanks to the members of my jury for evaluating my work and providing constructive feedback to improve my thesis. And I would also like to thank Lennert Gavel for helping me with the lay-out of this thesis.

I would like to thank my friends and colleagues. Hannes, Maral, Matthias, Evy, Freddie, Nils, Wesley, Maarten and Glenn for great times in Brussels. Io and the gang for great times in Aalst. Ariane en Nick for great times in Ghent. Karsten and Joerie for letting me win in squash every time. The people of the PhD network for the nice events we were able to organise. And my colleagues Alexander, Anna, Evy, Georgios, Gabriel, Jean, Jan, Johan, John, Jos, Leo, Mark and Philippe for making ELEC great (again).

Finally I would like to thank my family. Mama, Papa, Meter, Moeke en Vake for dealing with my surprise visits. Tante V, tante Sophie, Io, Seb en Vita for being awesome.

DISTORTION ANALYSIS OF ANALOG ELECTRONIC CIRCUITS USING MODULATED SIGNALS

Reducing non-linear distortion in modern analog electronic circuits is key to obtaining correct performance. Lower supply voltages, higher bandwidth and the need for higher energy efficiency are making the design of circuits with low distortion very challenging, so designers need good tools to analyse their circuit's performance. Classical distortion analyses predict the distortion contributions for weakly non-linear circuits excited by single-tone and two-tone signals. In their application, the analog circuits are used with modulated signals for which the distortion obtained with one and two-tone test is not representative at all.

Author | ***Adam Cooman***
Promotor | ***Gerd Vandersteen***

In this thesis, the distortion analysis of electronic circuits is performed using modulated signals which resemble the signals the circuit will encounter in its application. The distortion analysis is performed by combining the concepts of the Best Linear Approximation with a noise analysis. In this way, a distortion analysis is obtained that predicts the distortion contributions under modulated excitation and that can handle both weakly and strongly non-linear electronic circuits.

Additionally to the non-linear distortion analysis, a local stability analysis of electronic circuits is considered in this PhD thesis.